BENDING AND SHEAR LOAD RATING OF AN ARCH RING BRIDGE

By

Henry Díaz Alvarez

A thesis submitted in partial fulfillment of the requirements for the degree of

MASTER OF SCIENCE

IN

CIVIL ENGINEERING

UNIVERSITY OF PUERTO RICO
MAYAGÜEZ CAMPUS
2011

Approved by:

Luis E. Suárez, Ph.D. President, Graduate Committee	Date
Ricardo Ramos, Ph.D. Member, Graduate Committee	Date
Genock Portela, Ph.D. Member, Graduate Committee	Date
Darrell Hajek, Ph.D. Representative of the Graduate School	Date
Ismael Pagán Trinidad, M.S.C.E Director of Civil Engineering and Surveying Department	Date

ABSTRACT

This MS thesis entails an analytical study of the structural behavior of a concrete arch beam from the Lahontan Dam Spillway Bridge located in the city on Fallon, NV. This comes as a necessity from the U.S. Army Corps of Engineers specifically the Sacramento District due to the unknown capacity of the existing bridge. This project focuses on the load rating calculations for the bridge using two different methods of evaluation. The bridge was rated using the American Association of State Highway and Transportation Officials (AASHTO) standards which include the Load Factor Rating (LFR) and the Load Resistance Factor Rating (LRFR) methods.

The bridge is 97 years old and consists of five continuous spans that have three cast-in-place reinforced concrete arch beams. The exterior beams have a stem width of half the size of the interior beam, therefore both beam types were evaluated for this study. At the time of this study the bridge had been closed for almost two years due to its uncertain structural conditions. Structural cracks were present on several locations along the bridge. Since the structural capacity of the bridge was unknown, it was necessary to perform a live load analysis with the intention of determining its safe live load carrying capacity.

A finite element model (FEM) was developed to study in detail the performance of the arch beams under different load scenarios. The two structural parameters chosen for evaluation were the capacity under flexion and capacity under shear. The rating factors (RF) results for both design HS20-44 and HL93 notional vehicles were less than unity. Load rating results under the AASHTO legal loads, Type 3, Type 3S2 and Type 3-3 showed that the bridge requires a limit weight posting sign.

RESUMEN

Esta investigación trata sobre el estudio analítico del comportamiento estructural de vigas de concreto con forma de arco en el puente conocido como "Lahontan Spillway" el cual está ubicado en la ciudad de Fallon, Nevada. La motivación de este estudio se fundamenta en la necesidad por parte del cuerpo de Ingenieros de los Estados Unidos específicamente del distrito de Sacramento, en establecer la capacidad de carga del puente con vigas en forma de arco. Este proyecto se enfoca en los cálculos de los factores de calificación utilizando los métodos de evaluación "Load Factor Rating" (LFR) y el "Load Resistance Factor Rating" (LRFR). Ambos métodos son regidos por la agencia "American Association of State Highway and Transportation Officials" (AASHTO).

El puente tiene 97 años y consiste de cinco tramos continuos los cuales constan de tres vigas de hormigón reforzado con forma de arco. Las vigas exteriores tienen distinta área transversal que la viga interior, por lo que ambas vigas fueron estudiadas. Al momento del análisis, el puente llevaba cerrado al tráfico por un período de dos años debido a la condición estructural incierta. Fue necesario desarrollar un análisis de carga viva para determinar la carga máxima de servicio sobre el puente.

Un modelo de elementos finitos fue desarrollado para poder estudiar el comportamiento de este tipo de vigas bajo distintos escenarios de carga. Los dos parámetros estructurales evaluados fueron la capacidad en flexión y en cortante. Los resultados del estudio usando los vehículos de diseño HS20-44 y HL 93 produjeron factores de calificación menores de uno, lo cual confirma la podre condición estructural del puente. Debido a esto se realizó un nuevo análisis de calificación donde se utilizaron los vehículos legales, Tipo 3, Tipo

3S2 y el Tipo 3-3. Resultados provenientes de estos tres vehículos establecieron que el puente requiere un letrero el cual establezca el límite de capacidad.

To God

To my parents:
Henry Díaz Flores and María L. Álvarez

To my sister, Leslie M.

To my son, Eriam Yael

To my wife, Mariely

ACKNOWLEDGEMENTS

During the development of my graduate studies in the University of Puerto Rico several persons and institutions collaborated directly and indirectly with my research. Without their support it would have been impossible for me to finish this work. That is why I wish to dedicate this section to recognize their support.

I would like to thank all the members of my graduate committee, Dr. Luis E. Suárez, Dr. Ricardo Ramos, and Dr. Genock Portela for all their help and support throughout my career at the University. Thanks to all for all their continuous advice and encouragement through this important part of my life. All the lessons learned from you all, as an engineer and as a person, will last forever.

Thanks to the Engineer Research and Development Center (ERDC) for giving me the opportunity of working on this research project. Special thanks to Dr. Mihan McKenna, Mr. Terry R. Stanton and Mr. Gerardo Velázquez for their collaboration and support.

Last but not least, I would also like to thank my father Henry Díaz Flores, my mother María L. Alvarez, my wife Mariely Mejías, and my son Eriam Y. Díaz for they love and support, and for always being there for me whenever I needed them.

Finally, I want to thank God for always blessing me during my life.

TABLE OF CONTENTS

ABSTRACT ii

RESUMEN iii

ACKNOWLEDGEMENTS v

TABLE OF CONTENTS vi

LIST OF FIGURES ix

LIST OF TABLES xi

LIST OF APPENDICES xii

1 INTRODUCTION 1

1.1 Problem Statement 1
1.2 Related Studies 4
1.3 Research Objectives 7
1.4 Methodology 8
1.4.1 Capacity of the Arch Beams 8
1.4.2 Finite Element Model 9
1.4.3 Bridge Load Rating 10
1.5 Thesis Organization 11

2 DESCRIPTION OF THE STRUCTURAL SYSTEM 12

2.1 Bridge Inspection Report Logistic 12
2.2 General Description of the Lahontan Dam Bridge 13
2.3 Bridge Inspection Results 17
2.4 Exterior Beam Description 20
2.5 Interior Beam Description 22
2.6 Abutment and Piers Description 23

3 DESCRIPTION OF LOAD RATING METHODS 24

3.1 Introduction 24
3.2 Load Factor Rating (LFR) 27
3.3 Load and Resistance Factor Rating (LRFR) 28
3.4 Distribution Factors 31
3.5 Dynamic Impact Factors 34

4 ANALYSIS OF THE ARCH BEAMS 36

4.1 Introduction 36
4.2 Finite Element Model Considerations 36
4.2.1 Dead Load Effects 37
4.2.2 Superimposed Dead Load (SDL) Effects 37
4.3 Live Loads (LL) Demands 40
4.3.1 Live Load LFR and LRFD Analysis 41
4.3.2 Live Load Analysis Using Legal Loads 43
4.3.3 Live Load Moment and Shear from the SAp2000 ® model 45

5 NOMINAL RESISTANCE OF THE ARCH BEAM SECTIONS 52

5.1 Introduction 52
5.2 Flexural Resistance of a Concrete Arch Beam 53
5.3 Shear Resistance of the Concrete Arch Beam 58
5.3.1 LRF Shear Capacity 59
5.3.2 LRFR Shear Capacity 61

6 LOAD RATING RESULTS 63

6.1 Introduction 63
6.2 Design Level Rating Results 63
6.2.1 LFR Moment Rating Factor 64
6.2.2 LFR Shear Rating Factor 65
6.2.3 LRFR Moment Rating Factor 65
6.2.4 LRFR Shear Rating Factor 67
6.2.5 Discussion of the Results 68
6.3 Legal Loads Rating Results 69
6.3.1 LFR Moment Rating Factors 70
6.3.2 LRFR Moment Rating Factors 72
6.3.3 Discussion of the results 73
6.4 Limit weight of the bridge 74

7 PARAMETRIC STUDY: FRAME ELEMENT vs. FINITE ELEMENT 78

7.1 Introduction 78
7.2 Frame Section Properties 79
7.3 Case I: Statically determinate beam 80
7.3.1 Beam with varying depth and uniform centroid 81
7.3.2 Beam with varying depth and non -uniform centroid 82
7.3.3 Discussion of results of the statically determinate beam model 83
7.4 Case II: Statically indeterminate beam 84
7.4.1 Beam with varying depth and uniform centroid 84
7.4.2 Beam with varying depth and non-uniform centroid 85
7.4.3 Discussion of results of the statically indeterminate beam model 87

7.5 Shell Elements 88
7.6 Parametric Study Analysis 90

8 CONCLUSIONS AND RECOMMENDATIONS 92

8.1 Summary 92
8.2 Conclusions 93
8.3 Recommendations for Future Work 95

REFERENCES 96

APPENDIX A LIVE LOAD DESCRIPTIONS 99

APPENDIX B BRIDGE RAILING CALCULATIONS 105

APPENDIX C FLEXURE AND SHEAR CAPACITY 106

APPENDIX D RATING FACTOR EXAMPLE 129

APPENDIX E BRIDGE DESIGN DRAWINGS 154

LIST OF FIGURES

Figures **Page**

Figure 1.1.1 View of concrete arch beams looking from bay 6 3
Figure 2.2.1 Aerial view of the Lahontan Bridge 13
Figure 2.2.2 Elevation view of the north bridge 14
Figure 2.2.3 Longitudinal view of the north bridge approach 14
Figure 2.2.4 Elevation view of bridge 15
Figure 2.2.5 Schematic sketch of the bridge 15
Figure 2.2.6 Typical bridge cross section 16
Figure 2.2.7 Bridge plan view 16
Figure 2.3.1 Longitudinal crack in right approach roadway 17
Figure 2.3.2 Spalling of deck joint above north approach 17
Figure 2.3.3 Crack in railing post near right approach (upstream side of deck) 18
Figure 2.3.4 Horizontal crack in upstream face of downstream beam 19
Figure 2.3.5 Spalling at bottom of downstream beam 19
Figure 2.3.6 Erosion of concrete at upstream nose of Pier 2 20
Figure 2.3.7 Horizontal crack at top of Pier 4 20
Figure 2.4.1 Exterior beam cross-section at the edge 22
Figure 2.5.1 Interior beam cross-section at the edge 23
Figure 3.4.1 Distribution factor for the exterior beam 33
Figure 3.4.2 Distribution factor for the interior beam 33
Figure 4.2.1 Locations for calculation of moments, shear and capacity 37
Figure 4.2.2 Stress distribution due to DL and SDL 38
Figure 4.2.3 Maximum negative moment at the edge section of the exterior beam due to DL+SDL 39
Figure 4.2.4 Maximum positive moment at the mid-span section, exterior beam due to DL+SDL 39
Figure 4.3.1 FEM of the exterior arch beam with the lane path 41
Figure 4.3.2 Design truck HS20-44 (adapted from AASHTO, 2004) 42
Figure 4.3.3 LRFD tandem loading 43
Figure 4.3.4 Legal Load Type 3 43
Figure 4.3.5 Legal Load Type 3S2 43
Figure 4.3.6 Legal Load Type 3-3 44
Figure 4.3.7 Deform shape of the arch beam due to HS20-44 loading 44
Figure 4.3.8 HS20-44 Configuration used on the FEM of SAP2000® 45
Figure 4.3.9. Maximum bending moment at the edge section of exterior beam for HS20-44 loading 46
Figure 4.3.10 Maximum bending moment at the mid-span of exterior beam from HS20-44 loading 46
Figure 4.3.11 Vehicles bending moment demand in the exterior arch beam, LFR 48
Figure 4.3.12 Vehicles bending moment demand in the interior arch beam, LFR 48
Figure 4.3.13 Vehicles shear force demand in the exterior arch beam, LFR 49
Figure 4.3.14 Vehicles shear force demand in the interior arch beam, LFR 49

Figure 4.3.15 Vehicles bending moment demand in the exterior arch beam, LRFR 50
Figure 4.3.16 Vehicles bending moment demand in the interior arch beam, LRFR 50
Figure 4.3.17 Vehicles shear force demand in the exterior arch beam, LRFR 51
Figure 4.3.18 Vehicles shear force demand in the interior arch beam, LRFR 51
Figure 5.2.1 Exterior beam 53
Figure 5.2.2 Interior beam 53
Figure 5.2.3 Geometry of the doubly reinforced T-section 54
Figure 5.2.4 Stress and strain distribution on T beam 55
Figure 5.2.5 Tensile steel centroid location (Y) 57
Figure 5.2.6 Nominal Flexural Strength for interior and exterior arch beam 58
Figure 5.3.1 Shear strength for exterior and interior arch beam using the LFR 61
Figure 5.3.2 Shear strength for exterior and interior arch beam using the LRFR method 62
Figure 6.2.1 Flexural RF summary due to the HS20-44 loading 64
Figure 6.2.2 Shear RF summary due to the HS20-44 loading 65
Figure 6.2.3 Flexural RF summary due to the HL-93 loading 67
Figure 6.2.4 Shear RF summary due to the HL-93 loading 68
Figure 6.3.1 Flexural RF summary for the exterior beam due to the Legal Load loading for the LFR method 71
Figure 6.3.2 Flexural RF summary for the interior beam due to the Legal Load loading for the LFR method 71
Figure 6.3.3 Flexural RF summary for the exterior beam due to the Legal Load loading, LRFR 72
Figure 6.3.4 Flexural RF summary for the interior beam due to the Legal Load loading, LRFR 73
Figure 7.2.1 Model of the simple supported beam 79
Figure 7.3.1 Extruded view of the beam with uniform centroid 81
Figure 7.3.2 Deformed shape due to DL for a beam with uniform centroid 81
Figure 7.3.3 Moment diagram (k-ft) due to self weight for beam with uniform centroid 82
Figure 7.3.4 Shear diagram (kip) due to self weight for beam with uniform centroid 82
Figure 7.3.5 Extruded view of the beam with non-uniform centroid 82
Figure 7.3.6 Deformed shape due to DL for a section with non-uniform centroid 83
Figure 7.3.7 Moment diagram (k-ft) due to self weight for beam with non-uniform centroid 83
Figure 7.3.8 Shear diagram (kip) due to self weight for beam with non-uniform centroid 83
Figure 7.4.1 Fixed-ends beam with a uniform centroid 85
Figure 7.4.2 Deflection due to DL for the fixed-ends beam with uniform centroid 85
Figure 7.4.3 Moment diagram (k-ft) due to DL for the fixed-ends beam with uniform centroid 85
Figure 7.4.4 Shear diagram (kip) due to DL for the fixed-ends beam with uniform centroid 85
Figure 7.4.5 Fixed-ends beam with a non-uniform centroid 86
Figure 7.4.6 Displacement due to DL for the beam with fixed-ends and non-uniform centroid 86
Figure 7.4.7 Moment diagram (k-ft) due to DL for the beam with fixed-ends and non-uniform centroid 87

Figure 7.4.8 Shear diagram (kip) due to DL for the beam with fixed-ends and non-uniform centroid.. 87
Figure 7.5.1 Shell element model 88
Figure 7.5.2 Beam deflection due self weight 89
Figure 7.5.3 Negative moment on the FEM of the fixed-ends beam................................ 89
Figure 7.5.4 Positive moment on the FEM of the fixed-ends beam 90
Figure 7.5.5 Stress distribution for a rectangular beam 90

LIST OF TABLES

Tables **Page**

Table 3.1.1 LRFR flow chart from the AASHTO MCE LRFR (AASHTO, 2003).......... 26
Table 3.3.1 Condition factor (from AASHTO, 2003) 30
Table 3.3.2 System factor (from AASHTO, 2003).. 30
Table 3.3.3 Limit States and Load Factors for Load Rating (AASHTO, 2004)............... 31
Table 4.2.1 Summary of bending moment and shear force of the exterior beam due to dead load and superimposed dead load.. 40
Table 4.2.2 Summary of bending moment and shear force of the interior beam due to dead load and superimposed dead load.. 40
Table 6.2.1 LRFR Load Factors for Strength I (from AASHTO, 2003) 66
Table 6.4.1 Summary of LFR and LRFR load rating results for the exterior beam 74
Table 6.4.2 Legal Load limit weight (Inventory) 75
Table 7.2.1 Frame Section Properties.. 79
Table 7.3.1 Summary of the response - Statically determinate beam models 84
Table 7.4.1 Summary of the response - Statically indeterminate beam models 88
Table 7.5.1 Shell element model.. 89
Table 7.6.1 Frame elements vs. Shell elements 91

LIST OF APPENDICES

Appendixes **Page**

APPENDIX A LIVE LOAD DESCRIPTIONS 99

APPENDIX B BRIDGE RAILING CALCULATIONS 105

APPENDIX C FLEXURE AND SHEAR CAPACITY 106

APPENDIX D RATING FACTOR EXAMPLE 129

APPENDIX E BRIDGE DESIGN DRAWINGS 154

1 INTRODUCTION

1.1 Problem Statement

The strength and capacity of bridge superstructures, which are found in an extensive array of systems with diverse structural behavior and materials composition, under heavy truck loading, has long been of concern to state and federal Departments of Transportation. The problems posed by old bridges subjected to new loadings have been highlighted by recent bridge failures, most notably the collapse of the I-35W Mississippi River Bridge in Minnesota on August 1st 2007 (Accident Report NTSB/HAR-08/03). Changes in vehicles loading is a common problem observed in transportation systems where dead and live loads change drastically during the lifetime of the structure. This is one reason it is imperative to evaluate the actual condition of bridges. Therefore, understanding of the mechanics and performance of bridges during on-site inspections becomes an important tool for analysis and rating evaluations. Based on this idea, the American Association of State Highway and Transportation Officials (AASHTO) has prepared guidelines and standards to provide minimum requirements for national transportation systems such as bridges.

The purpose of a bridge inspection is to document the current condition of the bridge, determine the degree of wear and deterioration, and recommend repairs or other needed services. Federal requirements for bridge inspection, documented in the National Bridge Inspection Standards (NBIS), mandate that public agencies inspect and report on all public bridges, vehicle-carrying structures with a centerline length of 20 *ft* or greater.

According to the Federal Highway Administration (FHWA), the intent of the NBIS is to maintain a 24 month interval as the normal inspection frequency for routine inspection. Bridges which have been determined to be deficient in condition or load capacity require more frequent inspection. Additionally, bridges with special features may require additional inspections of those specific features. Such additional inspections might include underwater inspection of submerged structural components. The objective of this study is to investigate the load capacity of a spillway bridge constructed with three concrete arch hunched beams approximately 97 years ago.

The bridge which is the object of this study forms part of the Lahontan Dam. The Lahontan Dam is an earthfill embankment structure on the Carson River located approximately 45 miles northeast of Carson City, Nevada and 16 miles west of Fallon, Nevada. A detailed description of the bridge's surroundings is provided in the next chapter. There are two spillways, one near each abutment. There are two bridges that span across each spillway located within the embankment. Each spillway consists of a 250-foot-long uncontrolled concrete overflow crest. Four bridge piers and two abutments divide each spillway crest into five bays, each approximately 50 *ft* wide. Each bridge is 260.22 *ft* long and has five continuous spans with a single lane. Currently all traffic is restricted due to the unknown existing safe load carrying capacity of the bridge. The superstructure consists of three concrete arch beams (ribs) supported by concrete piers and abutments (see Figure 1.1.1). The bridges were constructed in 1914 and the available bridge design drawings are included in Appendix D.


Figure 1.1.1 View of concrete arch beams looking from bay 6

To identify the arch behavior and determine the safe live load that the bridge can carry a load rating was performed. The bridge live load capacity was determined using current AASHTO load rating procedures and standardized design vehicular loadings.

Two different rating procedures were used on this study; the first one consisted of the Load Factor Rating *(*LFR) and the other methodology is the Load and Resistance Factor Rating (LRFR). The bridge load rating consists in comparing the bending moment and shear force demand that the specific design vehicle produces on various structural components with the available capacity after subtracting the dead load effect.

In order to obtain the live load effects in the supporting members of a bridge, a distribution factor is used by design codes such as AASHTO (2003). Live load distribution is important for the design of new bridges as well as for the evaluation of existing bridges. The distribution factor affects a beam design or rating because it determines the percentage of vehicular load (expressed in terms of moment or shear) that must be carried by the beam. The distribution factor depends upon the relative stiffness characteristics of the deck-slab, the supporting beams, and on the loading pattern and position of the vehicle on the bridge. For this study the distribution factor equations prescribed in the codes were not applicable since the bridge does not meet minimum requirements established by AASHTO such as the numbers of beam, the beam spacing and slab thickness. For that reason, a lever rule procedure (based on static equation of equilibriums) was used to estimate the amount of wheel line load that the exterior and interior beams carry.

1.2 Related Studies

The procedure for a bridge load rating can be found in many publications and studies. The purpose of conducting a bridge load rating analysis is to establish the live load weight limit for those bridges in which structural integrity is compromised or unknown. These live loads are established by using current bridge design codes. The AASHTO "Standard Specifications for Highway Bridges" (2002) contains simplified procedures to be used in the analysis and design of bridges. The analysis of a bridge superstructure is reduced to the analysis of a single member with the introduction of wheel load distribution factors. The majority of the equations and approaches prescribe in the bridge design codes can only be used in structural elements in which the cross-sectional area is uniform along the entire length. The beams that made up the Lahontan bridge have a non-prismatic section (see Figure 1.1.1). Also many design codes were developed based on structural elements with simply supported conditions, even though that is not the case for all types of bridges. For example, the bridge on this study has three beams integrated at the abutments and piers along the five continuous spans.

Zoghi et al. (2008) studied in detail the effect of the haunches on several types of bridges. They pointed out that precast-concrete, skewed bridges with integral abutment walls are typically designed as simplified plane rigid portal frames, neglecting the degrading effects of the skew angle, the influence of haunches between the abutment walls and the deck, and laterally unsymmetrical vertical loading. This practice produces under-designed bridges for certain aspect ratios. To evaluate the limitations of this practice, an experimental and analytical study was carried out for the live load response at the linear service level. Also they observed that for certain bridge configurations, both the positive and negative moment stresses are higher than the stresses given by plane frame analysis.

Marefat et al. (2004) evaluated the remaining strength of a plain concrete arch bridge. They performed a static and dynamic test on the arch bridge. The bridge showed a relatively stiff and strong response, despite the initiation of enormous cracks. It yielded under load levels much greater than the service load. The behavior could be compared to a multi-layered continuous structure rather than an arch form. The study showed that the bridge still had a relatively large strength reserve and proper dynamic performance, despite the presence of deep and wide cracks, the fact that was suffering from carbonation, and being more than 60-years old.

Since the live load structural capacites of open-spandrel arch bridge structures is difficult to quantify, Garrett (2007) performed a study using a nonlinear three-dimensional finite-element (3D) model following AASHTO publications. He tried to capture some effects on the shallow concrete arch bridge in addition to live and dead loads. Parameters such as geometric nonlinear effects, temperature effects, and material behavior were considered on his model. As a result of the study, a refined analysis is recommended for load rating arch bridges based on the contrast of a base-line elastic analysis and the standard specifications method on moment magnification. Garrett's results showed that, as expected, in general the elastic analysis resulted in the highest live load ratings. The elastic analysis would be acceptable for live load rating and similar to the design of arch bridges, the rating of such structures should include some form of second-order analysis.

Boothby and Fanning (2004) developed a procedure for load-rating of masonry arch bridges. The procedure uses the Load Factor Method (LFM) of the 1994 AASHTO Manual for the Condition Evaluation of Bridges (MCEB), performed on analysis using a frame model of a masonry arch spanning from abutment to abutment. The procedure is based on the assumption that the arch barrel has no tensile strength. Their study complements the initial procedure by Boothby (2001) enabling the assessing engineer to exercise discretion in deciding whether or not a small value of tensile strength should be allowed in determining a suitable rating for masonry arch bridges. In addition the initially proposed strength values, which are considered overly conservative, are increased. They revised the recommendations provided by Boothby (2001) for the compressive strength of the modeled arch and adjusted it for tensile capacity. Their contribution to the load rating procedure of stone masonry arch bridges may lead to a more accurate assessment.

Barker (2001) compared analytical rating with field test rating and showed that the structure usually exhibits field test capacities higher than the analytical load capacity rating predictions. Field testing is useful for evaluating existing bridges. It allows the owner to reduce the conservatism of analytical rating methods and safely rate the bridge for higher loads. Many factors such as bearing restraint effects, unaccounted system stiffness, and actual lateral live load distributions not considered in the design contribute to the response of a tested bridge.

1.3 Research Objectives

The main objective of this research is to carry out a live load assessment of a reinforced concrete arch beam bridge. More general objectives of this study include the following:

1. Study the behavior of continuous arch beams.
2. Determine nominal capacities for the exterior and interior arch beams following the AASHTO and the LRFD methodologies.
3. Construct a two-dimensional (2D) finite element model of the five spans arch beam bridge for the determination of the bridge response to dead and live loads.
4. Compare the Load Rating factors of the bridge using the LFR and LRFR method.
5. Establish the limit weight capacity of the bridge to determine whether the bridge can be open to the normal vehicles traffic.
6. Develop recommendations to improve the load rating results of arch bridges.
7. Perform a parametric analysis to examine the possibility of determining the behavior of arch beams using a simplified frame model.

1.4 Methodology

The methodology used in this investigation can be divided into three stages. The first stage consists in the computation of the arch beam structural capacities. The nominal bending moment and shear force on four different locations are determined to identify the effects of the cross-sectional area variation. The second stage involves the development of a detailed Finite Element Model (FEM) to analyze the dead and live load effects along each arch beam. The third stage of the study is the interpretation of the finite element analyses to conduct the load rating of the bridge. Equations from two different methods (LFR and LRFR) are considered to determine the bridge weight limit capacity. The analysis of the bridge is performed considering the elastic range of the materials with the intention of avoiding any further damage on the bridge other than the one that is already present. A summary of each step is presented below.

1.4.1 Capacity of the Arch Beams

Because of the variation on the cross-sectional area due to the arch shape of each beam, it was necessary to evaluate the section at different locations. Another complication of the capacity analysis of the bridge was the different widths of three beams that comprise the structure. For that reason both the exterior and interior beams were analyzed separately to identify the changes on capacities and geometric properties that can affect the behavior of the bridge.

The determination of the beam capacities was based on the construction drawings provided from the U.S. Army Corps of Engineers, Sacramento District (2009). Since the bridge was built in 1914, the reinforcing steel bars have a square cross-section, and therefore the area of steel used was different than that recommended by modern construction building codes.

There was a lack of information regarding the yield stress of the steel reinforcement and the compressive strength of the concrete. Based on the construction year of the bridge, the AASHTO Bridge Manual suggests a value of 33 ksi for the yield stress of the steel and 2.5 ksi for the concrete compressive strength in order to be able to perform a bridge load rating. Appendix B shows in detail examples of the computation of the flexural and shear capacities for the exterior and interior arch beam.

1.4.2 Finite Element Model

An important part of the study is to model the arch concrete beams of the bridge using the finite element method to calculate the flexure and shear effects on the beams due to different vehicles loading types. The finite element analysis appropriately considers the interaction between the load vehicles, the beams and support condition at piers, and thus provides more accurate values of the maximum demands.

The analyses were performed using the bridge module integrated into the nonlinear analysis program SAP2000® version 14. The model includes standard linear shell elements for dynamic analysis of moving loads. The bridge model was based on a combination of quadrilateral and irregular shell elements to idealize the concrete arch beams with the piers supports.

The objective of using the finite element bridge model was to study the effect of the variation of the cross-sectional along the span length, to determine the zones of high stress concentration due to dead and live load, and to compare the results with the existing condition of the bridge. The results from the FEM in combination with the structural capacity of each section were used to determine the load rating factors for several locations on the Lahontan Bridge.

1.4.3 Bridge Load Rating

The load rating analysis of this bridge was performed to determine the live load that the structure can safely carry. The bridge was rated at two different stress levels, referred to as Inventory Rating and Operating Rating. Inventory Rating is the capacity rating for a prescribed vehicle type that will result in a load level which can be safely applied to an existing structure for an indefinite period of time. The Inventory load level approximates the design load level for normal service conditions. The Operating Rating will yield the absolute maximum permissible load level to which the structure may be subjected for the vehicle type used in the rating. This rating determines the capacity of the bridge for occasional use. Allowing to circulate on the bridge an unlimited numbers of vehicles with the characteristics of those used for the operating level evaluation will compromise the bridge life. Typically the operating rating level is used to evaluate overweight permit vehicles. Structural capacities and loadings were used to analyze the arch beams to determine the appropriate load rating. The lower value of the load rating may lead to load restrictions of the bridge. In this study the negative moment near the supports area controlled the load rating factor thus establishing the need to place a weight limit posting on the bridge. The details of the procedure and theory for the load rating calculations are presented in Chapter 3.

1.5 Thesis Organization

This thesis is organized into eight chapters and five appendices. Chapter 1 is focused on the presentation of the problem statement, a brief literature review and the main objectives to be accomplished in this study. A detailed description of the Lahontan Spillway bridge and its structural elements are presented on Chapter 2. The load rating method and formulas used to perform the live load assessment of the arch beam are described in Chapter 3, including the calculation of the distribution factor for the exterior and interior beams. A discussion on the differences in the AASHTO methods to load rate a bridge is also presented. The development of the finite element model of the bridge is presented on Chapter 4. Using the material properties suggested in the AASHTO code the dead and live load effects were determined for each arch beam to study the arch behavior. Chapter 5 describes the nominal capacity of the exterior and interior beams taking into consideration the composite action between the slab and the arch beams. Calculations at different locations along the span length are carried out with the intention of capturing in an accurate way the behavior of the bridge considering the variation in the cross-sectional area. Chapter 6 presents the load rating calculations using the two different stress levels; inventory and operating. A series of examples are presented in more detail in the Appendix C. Chapter 7 is devoted to the investigation of the analytical behavior of haunched beams using a two dimensional (2D) simplified model based on frame elements with prismatic sections. The beams are divided into elements with constant sections but each element has different neutral axis. The conclusions and recommendations of the study are presented on Chapter 8.

2 DESCRIPTION OF THE STRUCTURAL SYSTEM

2.1 Bridge Inspection Report Logistic

Prior to rating an existing bridge, it is necessary to review the results of the most recent inspection. A bridge inspection consists of an evaluation of each component of the bridge and rating these in order to assess their condition. A complete description of the bridge, as-built plans, modifications, and its present condition are captured by the inspection report. By law, all bridges on the National Bridge Inventory (NBI) are required to be inspected at least once every two years. The bridge inspections are done in conformance with AASHTO's "The Manual for Bridge Evaluation" (AASHTO 1994), FHWA's "Recording and Coding Guide for Structure Inventory and Appraisal of the Nation's Bridges" (FHWA, 1995), Delaware Department of Transportation (DelDOT) "Bridge Management Manual" (DelDOT, 2005), and DelDOT's "Element Data Collection Manual" (DOT, 2009).

Sometimes bridges will require more detailed inspections to determine their actual condition and capacity. Bridges in poor structural condition require more frequent inspections. When the bridge shows advanced structural deficiencies such as cracks near high stress zones, lateral movement, severe corrosion, section loss, etc. it is important to perform a structural evaluation of the bridge.

When conditions warrant, reduced sections or reduced allowable stresses should be used to obtain a load rating that indicates the actual condition and capacity of the structure. Areas of deterioration should be given special attention during field inspection, since a primary member with a reduced section may control the capacity of the structure.

2.2 General Description of the Lahontan Dam Bridge

The Lahontan Dam is an earthfill embankment structure on the Carson River located approximately 45 miles northeast of Carson City, Nevada and 16 miles west of Fallon, Nevada. Two bridges span across the spillways located within the Lahontan Dam embankment. The bridges were constructed in 1914 and the available bridge design drawings are shown in Figure 2.2.4 through Figure 2.2.7. There are two spillways, one near each abutment. Each spillway consists of a 250-foot-long uncontrolled concrete overflow crest (see Figure 2.2.1). Each bridge is 260.22 ft long and has five spans with one lane. The exterior spans have a length of 50.012 ft and the other three interior spans are 51.40 ft long. The two bridges have exactly the same geometry, therefore only one bridge was analyzed under this study.

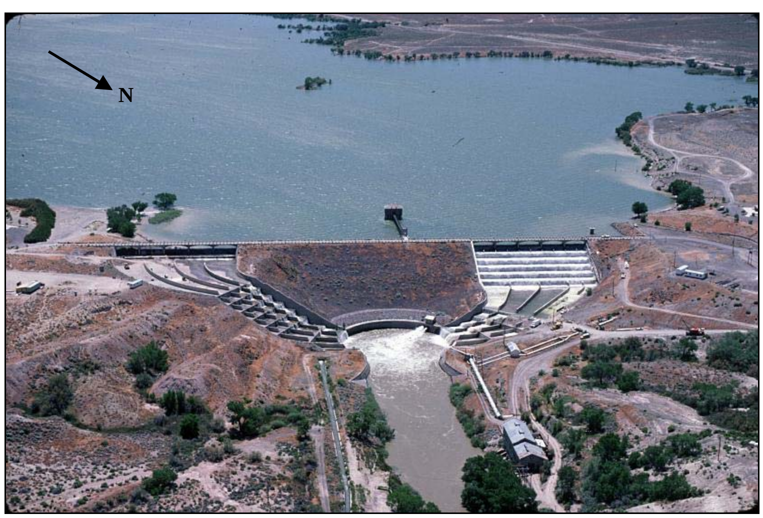

Figure 2.2.1 Aerial view of the Lahontan Bridge

An elevation view of the north bridge is shown in Figure 2.2.2, where the 5 spans of the can be observed and Figure 2.2.3 shows a longitudinal view of the bridge's north approach. For reference purposes of some of the bridge components a schematic sketch of the bridge is shown on Figure 2.2.5.

Figure 2.2.2 Elevation view of the north bridge

Figure 2.2.3 Longitudinal view of the north bridge approach

The superstructure consists of three parallel concrete arch beams (ribs) supported by concrete piers and abutments. The concrete deck is approximately 15 in. thick and is lined on each side by concrete curbs and railings which consist of concrete post as shown on Figure 2.2.3. The roadway is 13 ft wide.

At the time of the development of this study the bridge was closed to all traffic, with the exception of lightweight maintenance vehicles. This was due to the combination of crack propagations in most of the arch beams and the lack of knowledge of the structure capacity.

The last inspection of the bridge was performed on January 2009 by the US Army Corps of Engineers Sacramento District and it was given a NBI rating of 4 ("Poor Condition").

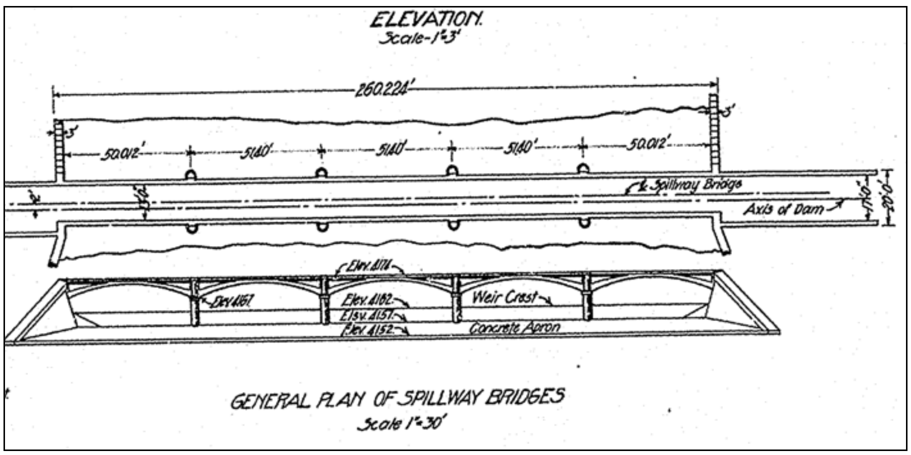

Figure 2.2.4 Elevation view of bridge

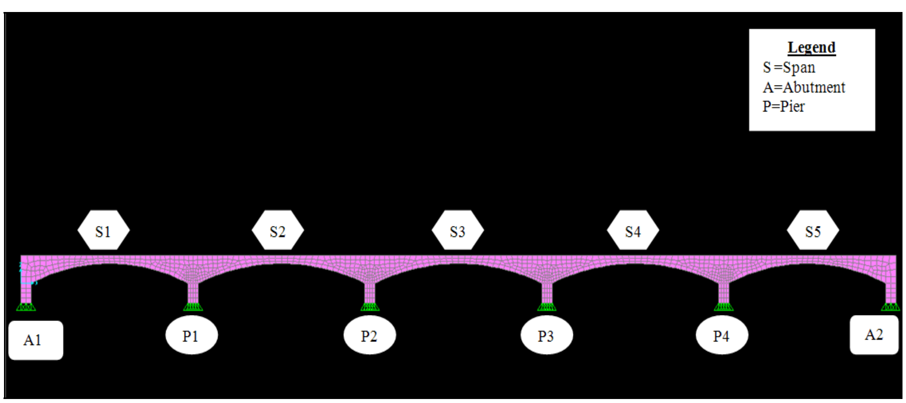

Figure 2.2.5 Schematic sketch of the bridge

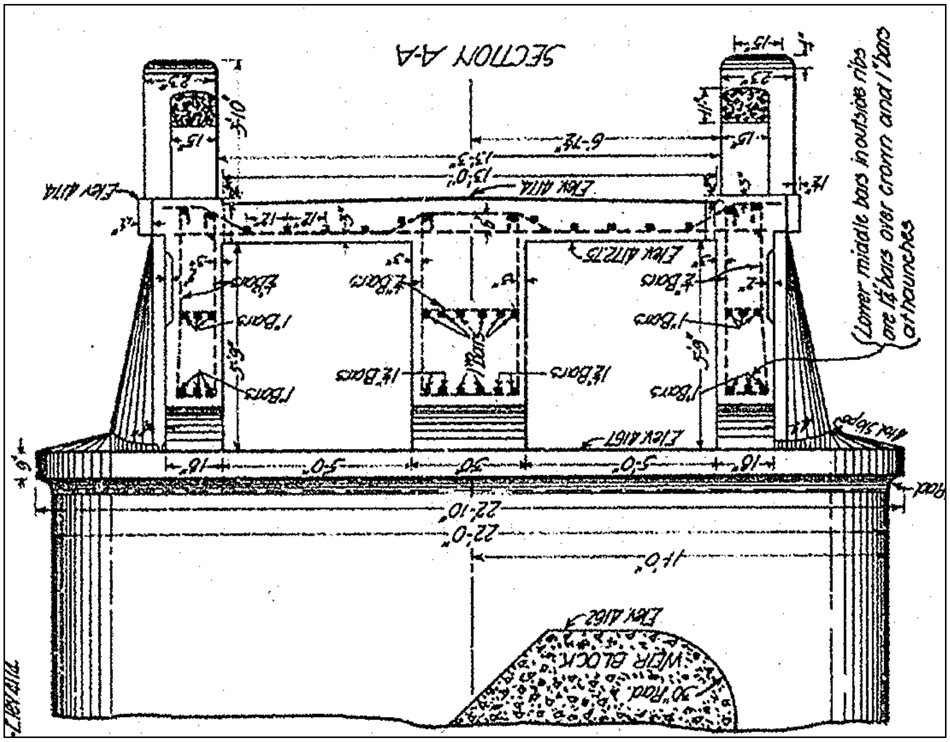

Figure 2.2.6 Typical bridge cross section

Note: Text is upside down on Figure 2.2.6 (the picture was obtained from the original plans of the bridge).

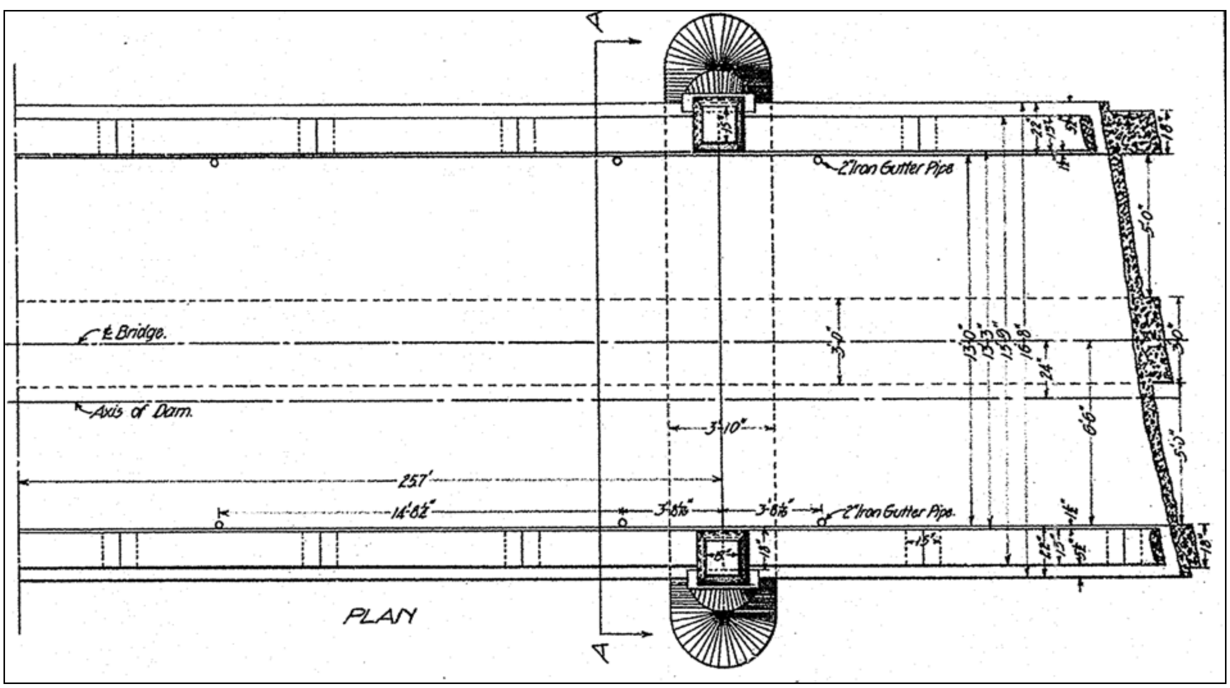

Figure 2.2.7 Bridge plan view

2.3 Bridge Inspection Results

The results from the latest visual bridge inspection following the AASHTO Manual for Condition Evaluation of Bridges (MCEB) standards are presented in this section.

The approach roadways for the bridge were in good condition with minor cracking found in the concrete slab as shown in Figure 2.3.1.

Figure 2.3.1 Longitudinal crack in right approach roadway

The deck was in fair condition with no signs of distress. Minor cracks were noted on the topside of the deck. Concrete spalling is typical at most of the approach deck joints as shown Figure 2.3.2.

Figure 2.3.2 Spalling of deck joint above north approach

Some of the railing posts are in poor condition. Extensive spalling was noted at a railing post above the left abutment, as displayed in Figure 2.3.3. This damage apparently was due to Alkali Silica Reaction (ASR) and potentially aggravated by freeze-thaw exposure. A major crack was found in a railing post (upstream side) near the right approach. The crack appeared to go through the entire thickness of the post. This crack also appeared to be due to ASR as indicated by the darkened surface adjacent to the crack.

Figure 2.3.3 Crack in railing post near right approach (upstream side of deck).

The superstructure was in poor condition with major horizontal cracks found in most of the girders. These cracks occurred at locations where high bending moments and shear forces are expected. The horizontal crack typically started at the location of the girder supported by the bridge pier at approximately mid-height of the section, and extended in the longitudinal direction for about 2 to 3 feet (both ways) from an existing deck joint and an induced vertical crack, Figure 2.3.4 shows the crack in the downstream beam. These major horizontal cracks may have been caused by the bending of the girders on each side of the deck joint in conjunction with the restraint of the girder at the top of the piers. The major horizontal cracks in the beams could potentially affect the structural integrity of the superstructure.

Figure 2.3.4 Horizontal crack in upstream face of downstream beam

In addition, as shown in Figure 2.3.5 spalling was noted at the bottom of the downstream beam at Piers.

Figure 2.3.5 Spalling at bottom of downstream beam

The substructure was in fair condition with no visible signs of distress, differential movements, and misalignments noted on the two abutments and concrete piers. Minor cracking and surface spalling were observed at isolated locations of the two abutments. Erosion of concrete at the bottom 2 to 3 feet of the upstream nose of each pier resulted in some significant loss of paste, as evidenced in Figure 2.3.6. The erosion was indicative of "chemical" erosion rather than fluid or water erosion. A chemical reaction could occur if this area was in the wash or splash zone in which there were significant organics in the water.

Figure 2.3.6 Erosion of concrete at upstream nose of Pier 2

An ASR related horizontal crack (approximately 0.03 inch wide) was found at the top of Pier 4 (see Figure 2.3.7). Another notable crack was found in the concrete footing slab in the vicinity of the upstream end of Pier 4, with signs of delamination and minor spalling. The aforementioned conditions do not appear to affect the structural integrity of the substructure.

Figure 2.3.7 Horizontal crack at top of Pier 4

2.4 Exterior Beam Description

The two exterior arch beams of the bridge have an 18-in. wide by 80-in height cross-section at the supports which vary towards mid-span at a haunch height linear variation of 0.1815-in/in: Over each exterior arch beam lie the concrete post and bridge rail which adds a uniform load of 0.25 kip/ft to each individual beam on the bridge. Each span has 4 main concrete posts and 12 intermediate posts. In Appendix B are presented detailed information and the considerations concerning the concrete rail. The American Association of State Highway and Transportation Officials (AASTHO) Load and Resistance Load and Resistance Factor Design (LRFD) establishes that weights coming from a barrier (i.e. concrete rails, sidewalks, etc.) need to be distributed on each longitudinal element as an equal portion when transverse elements such as diaphragms are present. The geometry and location of the principal steel reinforcement at the intersection of the arch beams and a pier, herein denoted as the edge of each section, is shown in Figure 2.4.1 for the exterior arch beams. Each exterior arch has three layers of longitudinal reinforcement, No.5 on top and No. 8 for the middle and bottom location. The shear reinforcement used was No.4 stirrups spaced at 2ft -5in center to center, with the first stirrup located 2ft-8⅞ -in from the center of each pier. A composite section action between the concrete slab and the arch beams was assumed since part of the shear steel stirrups goes through the top slab.

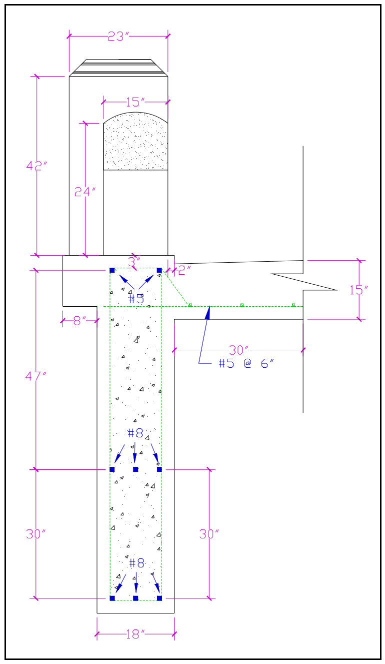

Figure 2.4.1 Exterior beam cross-section at the edge

2.5 Interior Beam Description

The interior arch beams on the bridge have a 36-in wide by 84-in height cross-section at the supports which vary towards mid-span at a 0.1815-in./in rate. The geometry and location of the principal steel reinforcement at the intersection of the interior arch beams and a pier, herein denoted as the edge of each section, is shown on Figure 2.5.1. Same as the exterior arch beams, the interior beam has three layers of longitudinal reinforcement but with a different configuration since the interior beam has a wider web. At the top section, four No.5 rebars are in place and at mid height six No.8, while the bottom section has a combination of four No.12 and two No. 8. Shear reinforcement consists of No.4 stirrups spaced at 2ft -5in centers to center, with the first stirrup located 2ft-8⅞ -in from the center of each pier. A composite section action between the concrete slab and the arch beams was assumed since part of the shear steel stirrups goes through the concrete deck. The slab longitudinal reinforcement pattern, which consists of No.5 bars at 12-in spacing, was considered continuous over the beam's web which suggests the beam behaves as a T-beam.

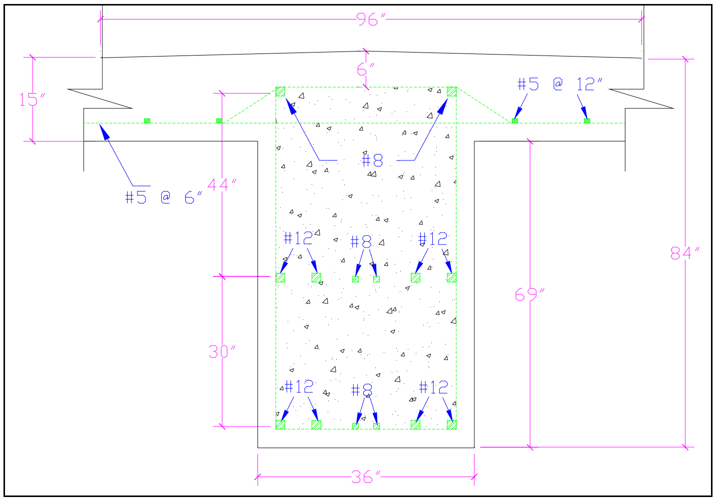

Figure 2.5.1 Interior beam cross-section at the edge

2.6 Abutment and Piers Description

The reinforced concrete abutments have a height of 18-ft height and are 22-ft wide and 3ft thick. The vertical and horizontal steel rebar sizes for the backwall are No.5 spaced 6-in and No.8 spaced 18-in respectively. Some minor spalls and hairline cracks were found at various locations at the backwall. For the footing, No. 12 steel rebar staggered every 12-in center to center were used.

The substructure (i.e. piers and abutments) were assumed to be adequate to resist superstructure loadings. This is a typical assumption, since the substructure is typically designed to be stronger than the superstructure.

3 DESCRIPTION OF LOAD RATING METHODS

3.1 Introduction

There are numerous guidelines and criteria for the load rating of bridges based on the use, materials and type of bridge using AASHTO procedures. Bridge load rating analysis can be performed using any of the two rating methods developed by AASHTO. These methods are: Load Factor Rating (LFR) (AASHTO, 1994) and Load and Resistance Factor Rating (LRFR) (AASHTO, 2003). The LFR provides recognition that types of loads are different and the LRFR provides a probability-based mechanism to select load and resistance factors. The rating systems for both the LFR and LRFR are broken down into a series of levels under which bridges can be evaluated, each level corresponding to a different level of safety. The LFR has a simple two-level system, whereas the LRFR has a more complex three-level system.

The two levels of the LFR system are the Inventory and Operating levels. The Inventory level of rating is the highest level of safety corresponding to a live load, which can safely utilize an existing structure for an indefinite period of time, according to the AASHTO MCE (1994). Rating results under the HS20-44 design truck at this level are used in reporting to the Federal Highway Administration (FHWA) for the National Bridge Inventory, NBI (Lichtenstein 2001). The Operating rating level is a secondary lower level of safety corresponding to the maximum permissible live load to which the structure may be subjected, according to the AASHTO MCE (1994). The results from the Operating level of rating can be used for determinations of load postings, bridge strengthening, and possible closure (AASHTO 1994). Permit vehicles can be recommended only for bridges that are found to be satisfactory at the Operating level of rating under the HS20-44 load model (AASHTO 1994). Operating load rating refers to live loads that could potentially shorten the bridge is life if applied on a routine basis.

The three levels that make up the LRFR rating system are the Design, Legal and Permit load rating levels.

The procedure that the LRFR uses in its rating system is shown in the flow chart in Table 3.1.1 as given in AASHTO MCE LRFR (2003). The process starts with a bridge first being rated at the Design Inventory level under HL- 93 load model. If the bridge is found to be satisfactory at this level of rating, it is not considered to require posting for AASHTO legal loads and state legal loads within the LRFD exclusion limits, and hence the bridge can be evaluated directly for permit load vehicles.

If a rating factor (RF) greater than one is obtained for the Inventory level, the strength limit state of the bridge complies with a desired level of reliability. Thus, no additional checks are needed, except for permit vehicles. If this is not the case, an additional evaluation is performed using an Operating level reliability with the same design loads. If RF ≥ 1, restrictive posting are not required and only permit vehicles may be evaluated. On the other hand, if the bridge is found to be unsatisfactory (RF<1), the second type of loading known as legal loads shall be evaluated. If a RF < 1 results from a legal load evaluation, load posting will be required and no permit vehicles analysis is allowed.

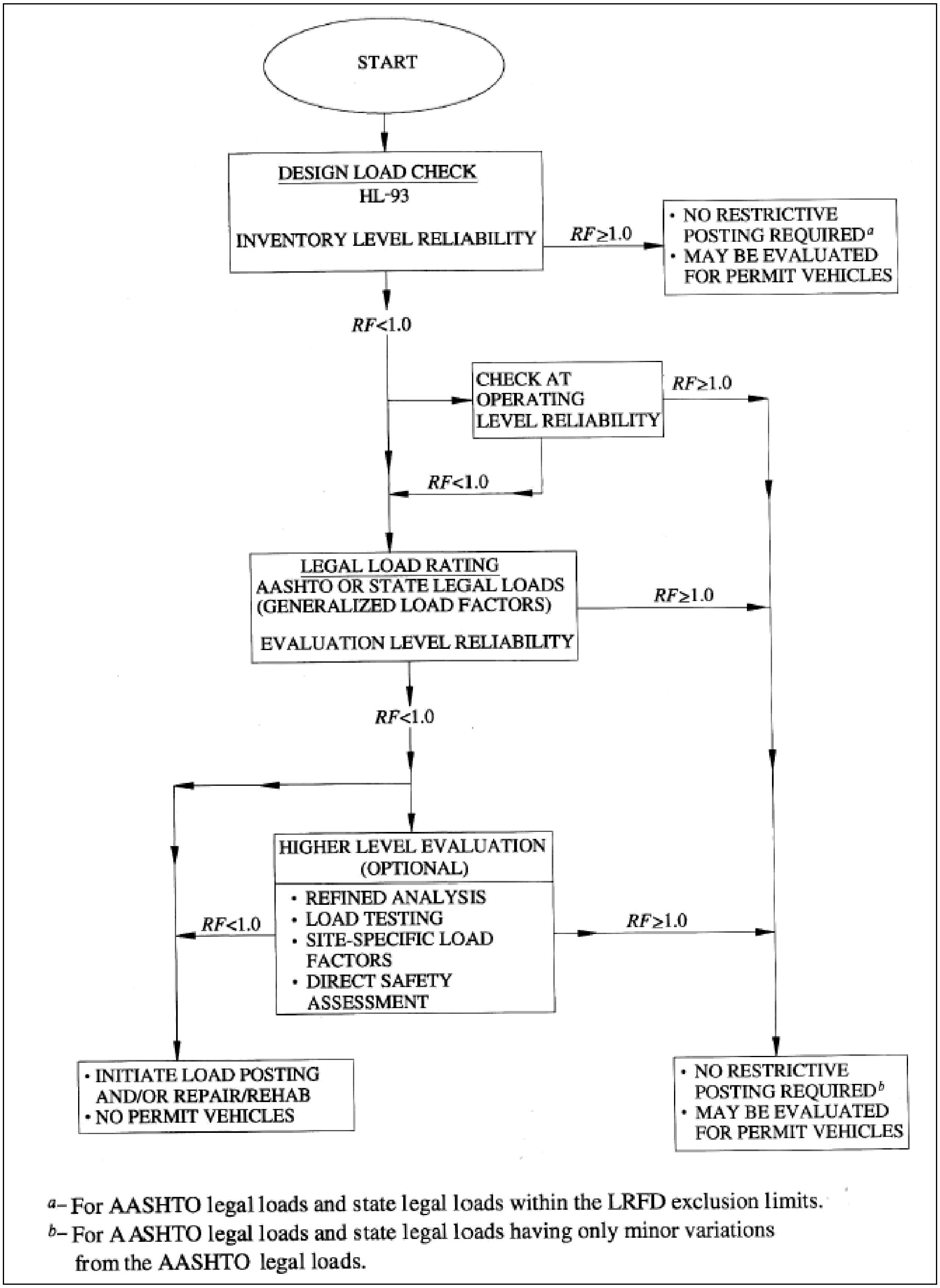

Table 3.1.1 LRFR flow chart from the AASHTO MCE LRFR (AASHTO, 2003)

3.2 Load Factor Rating (LFR)

The first method to be discussed is the LFR. The MCEB Section 6.5 provides the load rating equation and the inventory and operating factors. The MCEB 6.5.1 defines the load rating factor equation for flexural and shear strength, as:

$$RF = \frac{C - A_1 D}{A_2 (LL)(DF)(1+I)} \tag{3.1}$$

where,

C = Capacity of the beam

A_1 = Dead Load Factor (1.3 for Operating and Inventory)

D =Dead Load

A_2 = Live Load Factor (1.3 for Operating; 2.17 for Inventory)

LL = Live Load

DF = Distribution Factor

I = Impact Factor

The LFR method is an alternative method for the rating of simple and continuous structures. This rating method gives emphasis to the ultimate limit state, but the serviceability limit state is typically checked for compliance. The inventory load rating accommodates live loads that a bridge can carry for an indefinite period, while the operating load rating refers to live loads that could potentially shorten the bridge life if applied on a routine basis. The nominal strength calculations should take into consideration the observable effects of deterioration. The resistance factors depend on the type of the load effects (e.g., flexure, shear, torsion, etc.) and on the special characteristics of the loaded member (e.g., reinforced concrete, pre-stressed concrete, pre-cast, cast-in-place, etc.).

The inspection report of the Lahontan Bridge (2009) confirmed that damage was limited to concrete cracking and small to medium spalls that did not expose structural rebar and should not compromise the integrity of the design section. Therefore, design sections were used to calculate section capacities as explained in Chapter 5.

3.3 Load and Resistance Factor Rating (LRFR)

The LRFR methodology is a modified version of the LFR methodology where each component and connection must satisfy the design procedures. LRFR incorporates state-of-the-art analysis and design methodologies with load and resistance factors based on the known variability of applied loads and material properties. These load and resistance factors are calibrated from actual bridge statistics to ensure a uniform level of safety. LRFR focuses on a design objective or limit state, which can lead to a similar probability of failure for each component. Bridges rated with the LRFR specifications should have more uniform safety levels, which should ensure superior serviceability and long-term maintainability. Each component and connection shall satisfy the rating equation for each limit state, unless otherwise specified.

The general LRFR equation to define the rating factor is:

$$RF = \frac{C - \gamma_{DC} DC - \gamma_{DW} DW}{\gamma_L \left(LL + IM \right)} \qquad 3.2$$

Where,

C = capacity of the member

DC = dead load effect (structural members and attachments)

DW = dead load from bridge deck overlays and utilities

$LL+IM$ = live load influence including dynamic impact

γ_{DC} = LRFD load factor for structural components and attachments

γ_{DW} = LRFD load factor for deck overlays and utilities

γ_L = evaluation live load factor

RF is first calculated for a design load rating using the HL93 notional loading. If RF<1, then a legal load rating is performed to determine a bridge rating in tons (LRFR 6.4.4.4):

$$RT = RF \times W \quad \textbf{3.3}$$

Where,

RT = rating of the bridge in tons

RF= rating factor

W= gross vehicle weight

The flexural capacity of the exterior and interior beams C is defined as:

$$C = \varphi_c \varphi_s \varphi R_n \quad \textbf{3.4}$$

Where

R_n = nominal member resistance

φ_c = condition factor (Table 3.3.1)

φ_s = system redundancy factor (Table 3.3.2)

φ = LRFD resistance factor

$\varphi_c\ \varphi_s \geq 0.85$

Table 3.3.1 Condition factor (from AASHTO, 2003)

Structural Condition of Member	φ_c
Good or satisfactory	1.00
Fair	0.95
Poor	0.85

Table 3.3.2 System factor (from AASHTO, 2003)

Superstructure	φ_s
Welded Members in Two-Girder/Truss/Arch Bridge	0.85
Riveted Members in Two-Girder/Truss/Arch Bridge	0.90
Multiple Eyebar Member in Truss Bridge	0.90
Three-Girder Bridges with Girder Spacing ≤ 6 ft	0.85
Four-Girder Bridges with Girder Spacing ≤ 4 ft	0.95
All Other Girder Bridge and Slab Bridge	1.00
Floor-beams with Spacing >12 ft. and Non-continuous Stringers	0.85
Redundant Stringer Subsystems Between Floor-beams	1.00

Table 3.3.3 shows the load factors for the different limit states that shall be considered depending of the bridge construction material. The Strength I is defined as the basic load combination related to the normal vehicular use of the bridge without considering wind and earthquake loads. The Strength II is defined for the same load combinations of Strength I, but is applied to owner-specified special design vehicles. The state limit Service I is used to verify the 0.9 F_y (Yield Stress) stress limit in reinforcing steel during permit loads. However, for the arch bridge under study the only requirement of performance is that for a normal vehicle. Therefore, the applicable limit state on this investigation was Strength I corresponding to the LRFR method.

The Strength I factor for the legal load rating is determined by the Average Daily Truck Traffic (ADTT), which was reported as 0 in the 2009 inspection report due to closure of the bridges. For the purposes of the analysis conducted in this project, the live load factor used was 1.80, which corresponds to an unknown ADTT, (AASHTO, 2004). This factor considers the fact that the bridge could be reopened at some future time.

Table 3.3.3 Limit States and Load Factors for Load Rating (AASHTO, 2004)

Bridge Type	Limit State*	Dead Load γ_{DC}	Dead Load γ_{DW}	Design Load Inventory γ_{LL}	Design Load Operating γ_{LL}	Legal Load γ_{LL}	Permit Load γ_{LL}
Steel	Strength I	1.25	1.50	1.75	1.35	Tables 6A.4.4.2.3a-1 and 6A.4.4.2.3b-1	–
	Strength II	1.25	1.50	–	–	–	Tables 6A.4.5.4.2a-1
	Service II	1.00	1.00	1.30	1.00	1.30	1.00
	Fatigue	0.00	0.00	0.75	–	–	–
Reinforced Concrete	Strength I	1.25	1.50	1.75	1.35	Tables 6A.4.4.2.3a-1 and 6A.4.4.2.3b-1	–
	Strength II	1.25	1.50	–	–	–	Tables 6A.4.5.4.2a-1
	Service I	1.00	1.00	–	–	–	1.00
Prestressed Concrete	Strength I	1.25	1.50	1.75	1.35	Tables 6A.4.4.2.3a-1 and 6A.4.4.2.3b-1	–
	Strength II	1.25	1.50	–	–	–	Tables 6A.4.5.4.2a-1
	Service III	1.00	1.00	0.80	–	1.00	–
	Service I	1.00	1.00	–	–	–	1.00
Wood	Strength I	1.25	1.50	1.75	1.35	Tables 6A.4.4.2.3a-1 and 6A.4.4.2.3b-1	–
	Strength II	1.25	1.50	–	–	–	Tables 6A.4.5.4.2a-1

3.4 Distribution Factors

A distribution factor (DF) is a method of analysis to determine the lateral live load distribution on individual beams for typical highway bridges. Lateral live load distribution factors are dependent on multiple characteristics of each bridge. Live load distribution is important for the design of new bridges as well as for the evaluation of existing bridges. AASHTO's Standard Specifications for Highway Bridges (AASHTO, 2002) and the LRFD Bridge Design Specifications (AASHTO, 2004), contain the most common methods in use for computing live load distribution factors.

AASHTO provide simplified DF equations for moment and shear which depend on the type and bridge configuration. However, these equations have some requirements, such as:

- The span must have more than four transversal beams.
- The deck width must be constant, and between 4.5 in. and 12 in.
- All the transversal beams must have approximately the same stiffness.
- Overhangs must not exceed 3 ft.

- The beam spacing must be between 3.5 ft and 16 ft.

Since the bridge under study has only three concrete arch beams, the equations from the LRFD Tables 4.6.2.2.2 and 4.6.2.2.3 cannot be utilized. Therefore, the lever rule methodology was used to calculate the DF for both the exterior and interior beam. Only one calculation was performed since the same DF is applicable for both moment and shear. The lever rule assumes that the deck in its transverse direction is simply supported by the arch beams and uses statics to determine the live load distribution. The multiple presence factors "m" (lanes loaded simultaneously) is not considered on the DF calculation, since this bridge only has one lane.

A transverse spacing between wheels of the design vehicle HS20-44 of 72 in. was used to calculate the distribution factor for both arch beams. The calculations and the geometry involved are shown in Figure 3.4.1 for the exterior beam and in Figure 3.4.2 for the interior beam. In both figures *P* represents the wheel load.

For the exterior beam DF calculations (see Figure 3.4.1), the first wheel load was positioned at 1 ft from the parapet, according to AASHTO (2002). A distribution factor of 0.69 was obtained for the exterior beam, which indicates than 69% of the wheel line load of the vehicle is carried by the exterior beam.

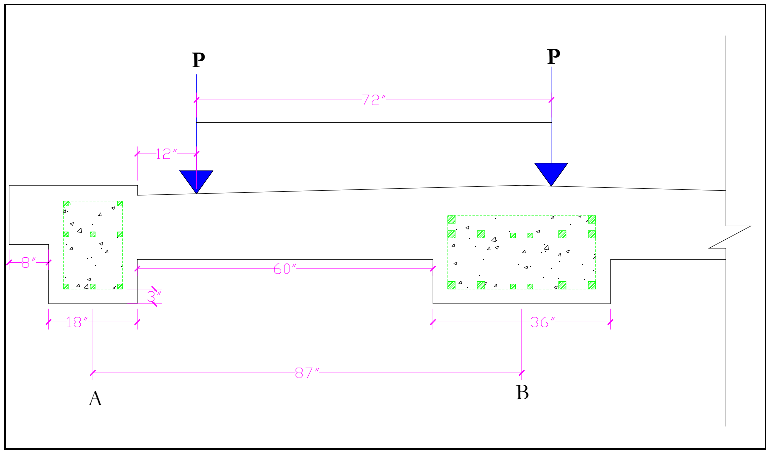

Figure 3.4.1 Distribution factor for the exterior beam

$$\sum M_B = 0$$

$$6P - 66P + 87R_A = 0$$

$$DF_{Ext} = \frac{60}{87} = 0.69 \qquad \textbf{3.5}$$

For the interior beam DF calculations (see Figure 3.4.2), the first wheel load was positioned at the centerline of the interior beam, since this configuration produces the worst case scenario for this case. A distribution factor of 1.17 was obtained for the interior beam, which represents an increase of 17% on the live load.

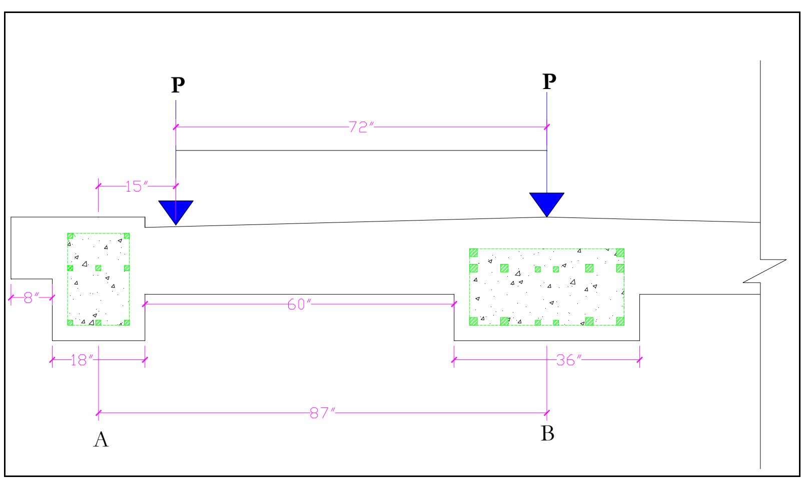

Figure 3.4.2 Distribution factor for the interior beam

$$\sum M_A = 0$$

$$15P + 87P - 87R_B = 0$$

$$DF_{Ext} = \frac{15+87}{87} = 1.17 \qquad \textbf{3.6}$$

3.5 Dynamic Impact Factors

Significant dynamic effects due to moving traffic loads cannot be neglected neither when evaluating existing bridges nor when designing a new bridge. Impact factor (now called dynamic allowance) is commonly used to account for the dynamic effects of wheel loads on bridges. This single factor includes complex physical and mechanical phenomena involving the bridge and vehicle characteristics. Various bridge design specifications are used around the world, which give dramatically different factors (Paultre and Chaalial, 1992).

The impact factor is calculated differently for each of the rating methods. The LFR impact factor is based on a formula where the impact factor increases with a bridge's span length and is determined by the following formula from AASHTO (2004):

$$I = 1 + \frac{50}{L+125} \leq 1.30 \qquad \textbf{3.7}$$

where I is the impact factor, which should not be greater than 0.3; and L is the length in feet of the portion of the span that is loaded to produce the maximum stress in the member. Evaluating Equation 3.7 for a value of L = 51.4 ft which represents the maximum length for the interior span, gives an impact factor (I) equal to 1.28, which means an increase on the order of 28%.

The impact factor for the LRFR method is fixed to 33% for all design and legal loads. However, the code allows for the factor to be lowered based upon riding surface conditions (Lichtenstein 2001).

4 ANALYSIS OF THE ARCH BEAMS

4.1 Introduction

The object of this chapter is to describe in detail the behavior of the exterior and interior arch beams under dead and live load. To be able to represent the cross section complexity of each arch beam, a two-dimensional (2D) a finite element model (FEM) was developed. The structural analysis software SAP2000® was used for this purpose. These models were used to determine the maximum bending moments and shear forces on the bridge due to the dead load (DL), superimposed dead load (SDL) and live load (LL). The FEM included the five spans with the piers and abutments. The objective was to capture in on accurate way the behavior of the bridge. All the analyses were limited to the elastic range of the materials.

4.2 Finite Element Model Considerations

A 2D model of the main structural members was used to represent the five spans of the bridge. Because of the difference in cross sectional area between the exterior and interior arch beams, two different models were formulated to represent the bridge response. The first model was used to evaluate the behavior of the exterior arch beam for the critical span and the second model was used to evaluate the performance of the interior arch beam under the same load conditions as the exterior beam.

The concrete arch beams with piers were modeled using 954 shell elements and a total of 1164 nodes, with six degrees of freedom per node.

4.2.1 Dead Load Effects

To obtain an accurate response of the arch beam due to its self weight or dead load (DL), a 2D model was used. A value of 150 pcf was used as a unit weight for the reinforced concrete (RC). The bending moment and shear force effects were calculated at every one-third section of the mid-span as shown in Figure 4.2.1. The goal was to determine how the design parameters changed with respect to the span length due to the arch shape of the beams. Because of the symmetry, only one side of the beam to the left of the mid-span was analyzed for load rating purposes.

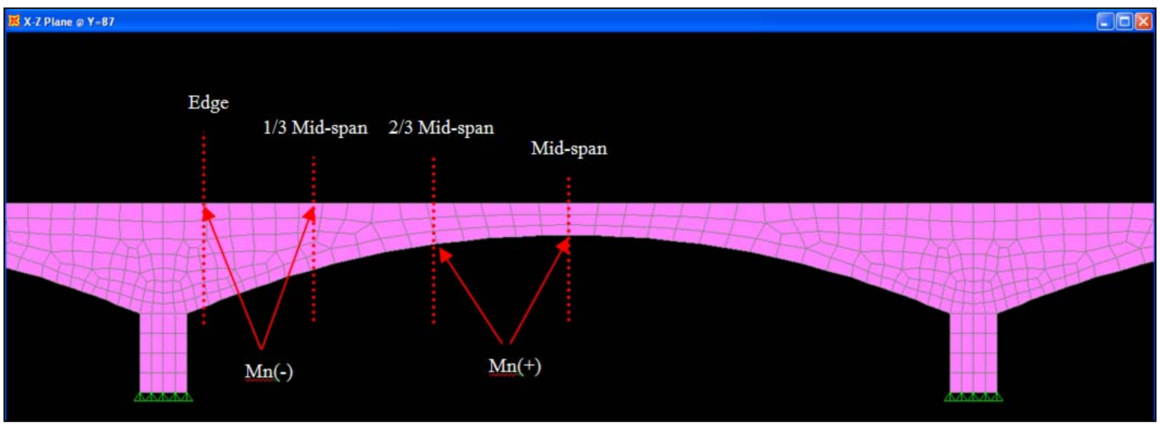

Figure 4.2.1 Locations for calculation of moments, shear and capacity

4.2.2 Superimposed Dead Load (SDL) Effects

The only superimposed dead load (SDL) considered in the 2D model was the bridge concrete railing. No asphalt wearing surface was identified on the deck plans and even in the previous inspection. The weight of the bridge railings equals to 0.25 k/ft and it was assumed to be distributed evenly over the three arch rings cast-in-place units. The calculation of the distributed weight of the rail (w_{SDL}) is provided in Appendix B in detail.

Typical stress distributions were found on the arch beam, such as the tension on top of the supports and the tension at the bottom of the mid-span, due to the combination of dead and live load as shown in Figure 4.2.2. The compression bending stresses at the supports extend for 14.98 ft at both sides, while 21.44 ft of the arch beam experienced tension bending stresses.

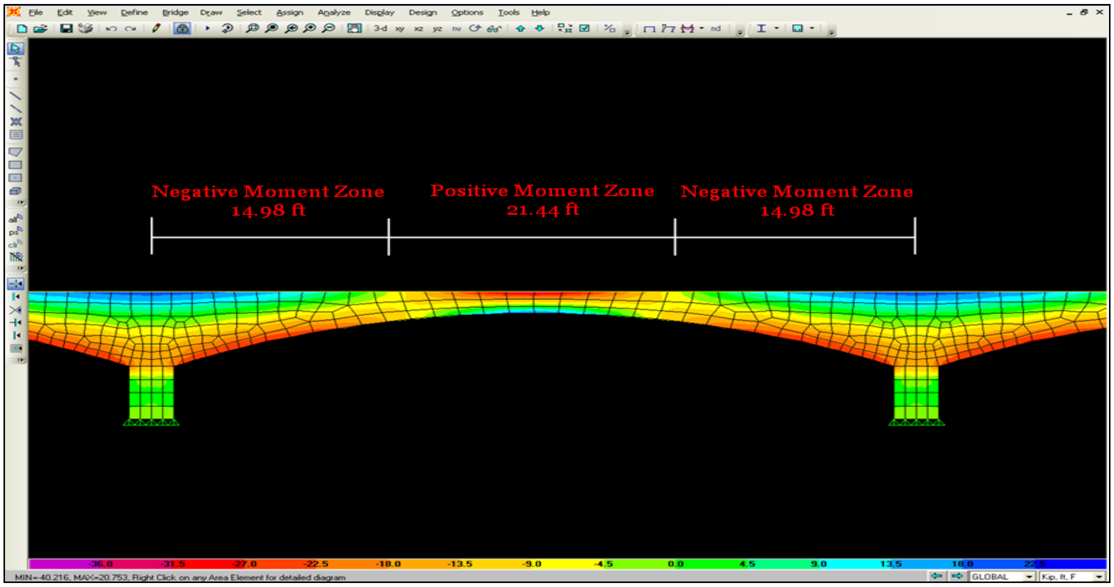

Figure 4.2.2 Stress distribution due to DL and SDL

The bending moment and shear force for both beams (exterior and interior) due to the DL and SDL were obtained from the FEM. To determine the values of moment and shear force from the stress diagram of the FEM, a tool from SAP2000® called "Section Cut" was used. This command calculates the forces at a section cut by summing the element joint forces from the shell elements included in the group that defines the section cut. Figure 4.2.3 shows an example of the implementation of the implementation of the "section cut" too: in this case it permits to determine the maximum negative moment of -354.28 kip-ft for the exterior arch due to self weight plus the superimposed weight.

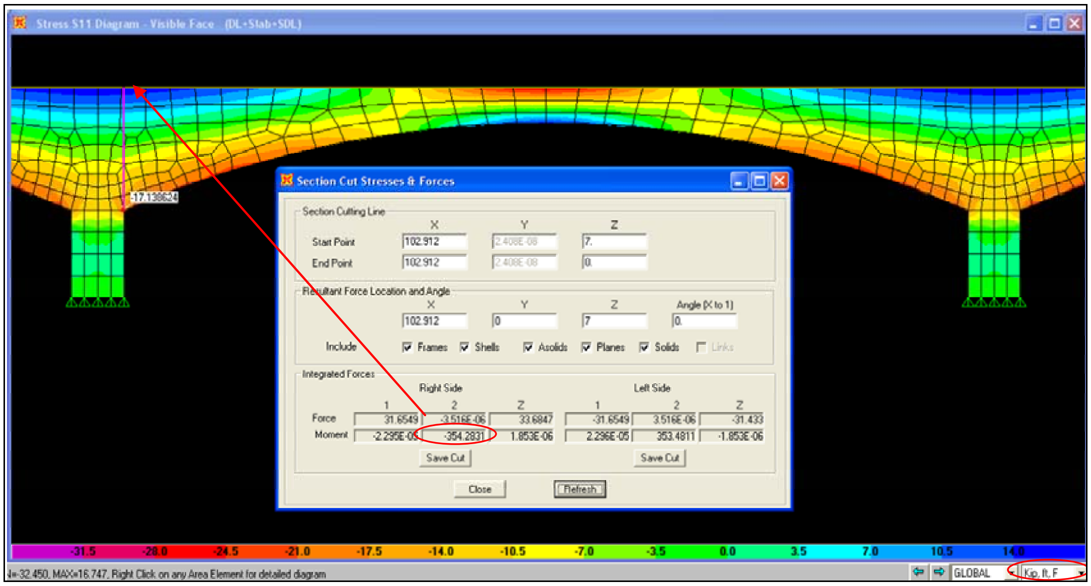

Figure 4.2.3 Maximum negative moment at the edge section of the exterior beam due to DL+SDL

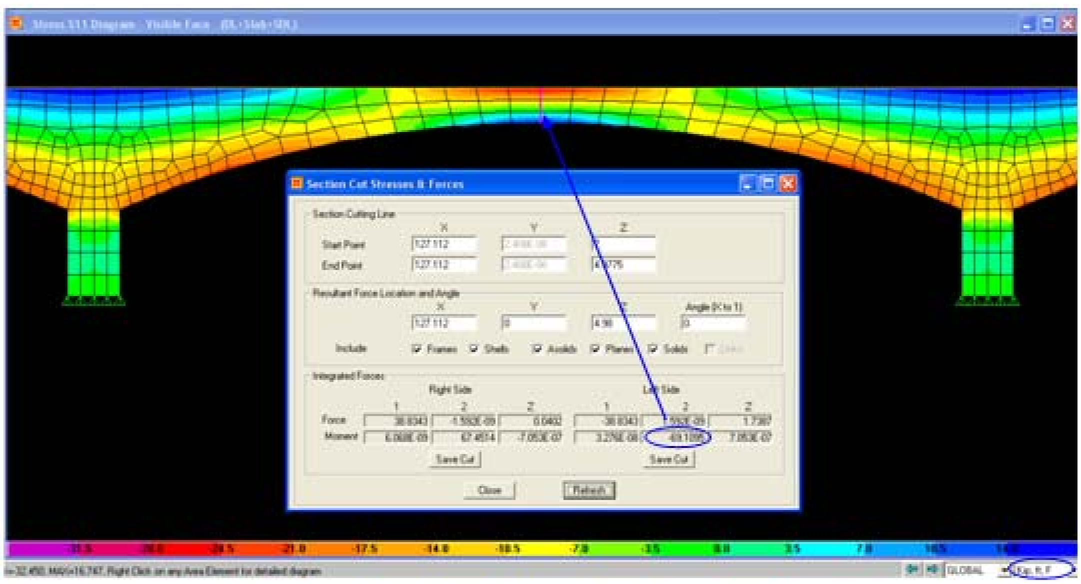

Figure 4.2.4 Maximum positive moment at the mid-span section, exterior beam due to DL+SDL

Figure 4.2.4 shows the maximum positive moment of 69.10 kip-ft for the exterior beam due to the DL and SDL identified by means of the “section cut” command. The gradual reduction in cross sectional area tends to decrease significantly the positive bending moment in approximately 80% compared with the negative moment. For the case of a continuous beam with an uniform cross sectional area, the difference in magnitude between the negative and positive moment is in the range of 42% (LRFD, 2004). This implies that the positive moment in an arch beam with a haunch height ratio between 0.18-in/in to 0.20-in/in tends to be 20% lower than the one in a beam with a prismatic section. Also, the negative moment in the arch beam tends to be approximately 53% smaller than the one produced in a beam with a prismatic section. In summary the variation in cross sectional area in the arch beam produces a decrease in both the negative and positive moment.

On the other hand, the shear force did not show a significant change in comparison with a beam with uniform cross sectional area. Table 4.2.1 and Table 4.2.2 summarize the results from the FEM analysis due to the DL and SDL for the exterior and interior beams, respectively.

Table 4.2.1 Summary of bending moment and shear force of the exterior beam due to dead load and superimposed dead load

Load	Location along the beam			
	Edge	1/3 mid-span	2/3 mid-span	mid-span
Bending Moment, kip-ft	-354.28	-164.88	40.11	69.10
Shear Force, kip	33.68	21.42	11.89	1.73

Table 4.2.2 Summary of bending moment and shear force of the interior beam due to dead load and superimposed dead load

Load	Location along the beam			
	Edge	1/3 mid-span	2/3 mid-span	mid-span
Bending Moment, kip-ft	-618.49	288.44	66.81	114.34
Shear Force, kip	59.26	37.15	20.22	3.31

4.3 Live Loads (LL) Demands

The live load moments and shear forces presented in this section are the maximum values calculated from the FEM analyses result at the four locations in the beam previously shown in Figure 4.2.1. For each analysis, the loading was simulated by moving the axle loads of the rating vehicle along the center of a beam web. Figure 4.3.1 shows an example of the FEM used to analyze the structure for each vehicle. The blue line represents the lane path used (option from SAP2000) which describes how vehicles move on the structure (i.e. strait line, centerline offset, etc). To ensure that each axle of the vehicles in consideration load the first spans the lane path was extended 15ft to each side of the bridge.

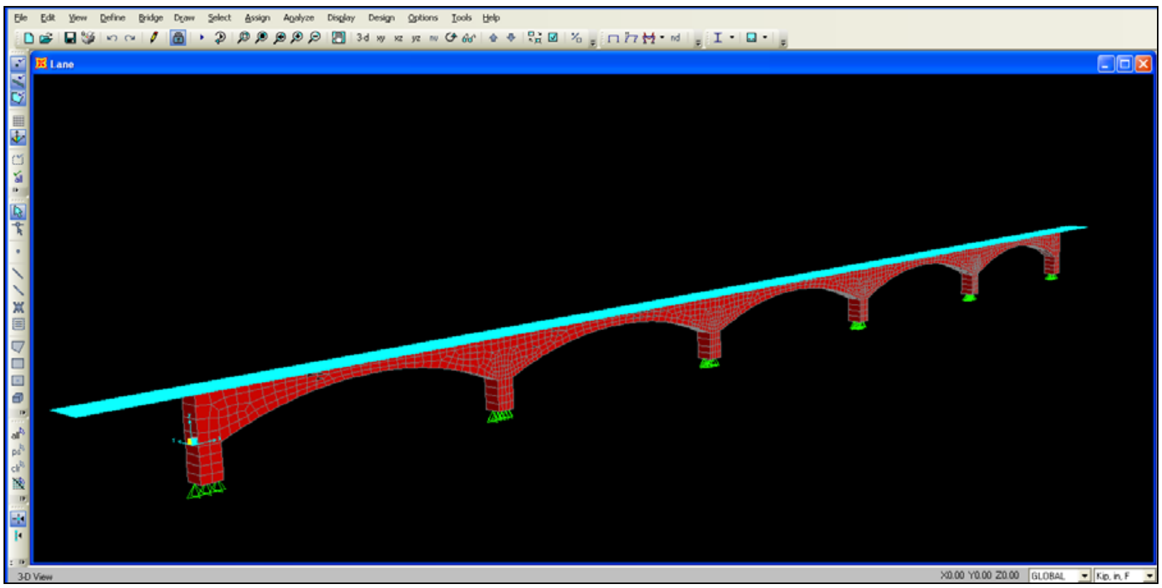

Figure 4.3.1 FEM of the exterior arch beam with the lane path

4.3.1 Live Load LFR and LRFD Analysis

The Load Factor Rating (LFR) analysis at the Design Inventory and Operating rating level uses the maximum load effect from the HS20-44 vehicle shown in Figure 4.3.2. The letters HS are associated to three axles consisting of a tractor truck with semi-trailer. The number "44" identifies the year when that design truck was adopted by AASHTO. The three axles weighs 8 kip, 32 kip and 32 kip and they are spaced 14 ft apart for the tractor portion and between 14 ft to 30 ft for the semi-trailer portion, as shown in Figure 4.3.2.

The variable spacing of the last axle is used to maximize the desired load effect (AASHTO 2002).

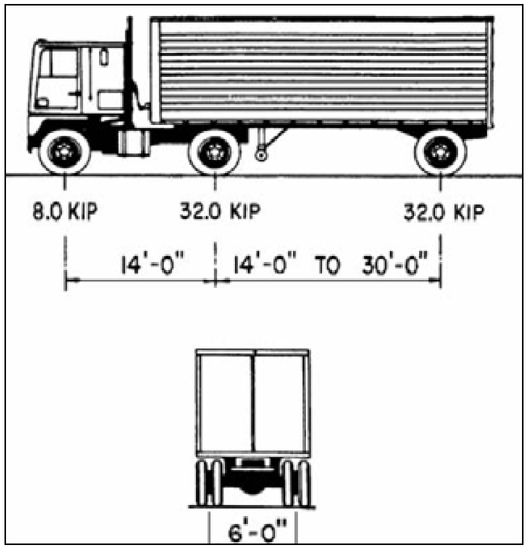

Figure 4.3.2 Design truck HS20-44 (adapted from AASHTO, 2004)

The Load and Resistance Factor Rating (LRFR) methodology at the Design Inventory and Operating rating level uses the HL-93 live load model as defined in the AASHTO LRFD Specification according to the LRFR (2003). The HL-93 load model is composed of three parts: the design truck, the design tandem, and the design lane load. The design truck configuration is defined by AASHTO as the HS20-44 model discussed previously (see Figure 4.3.2). The design tandem is composed of two concentrated loads of 25 kip spaced at 4 ft as shown in Figure 4.3.3. The design lane load is consists of a uniform load of 640 lb-ft. The live load effect used in rating analysis is the combined maximum effect of the design lane load with either the design truck or the design tandem.

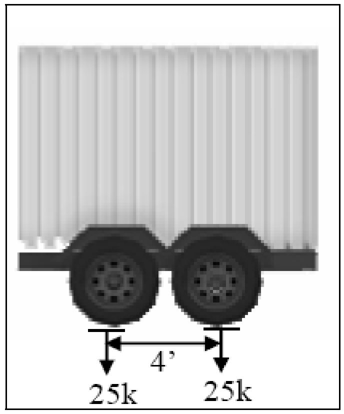

Figure 4.3.3 LRFD tandem loading

4.3.2 Live Load Analysis Using Legal Loads

Bridges that do not have sufficient capacity under the design-load rating shall be load rated for legal loads to establish the need for load posting or strengthening. This second level rating provides the safe load capacity of a bridge for the AASHTO family of legal loads. Three typical legal load models were considered: the Type 3, Type 3S2, and the Type 3-3 as shown in Figure 4.3.4 through Figure 4.3.6.

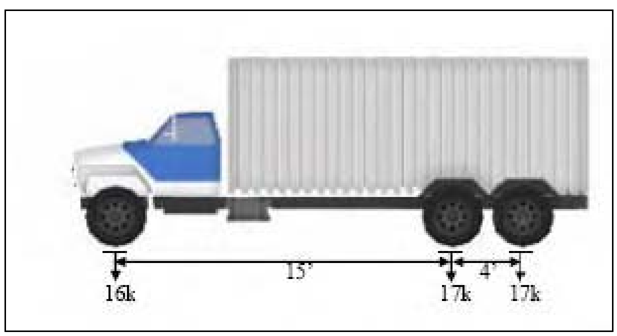

Figure 4.3.4 Legal Load Type 3

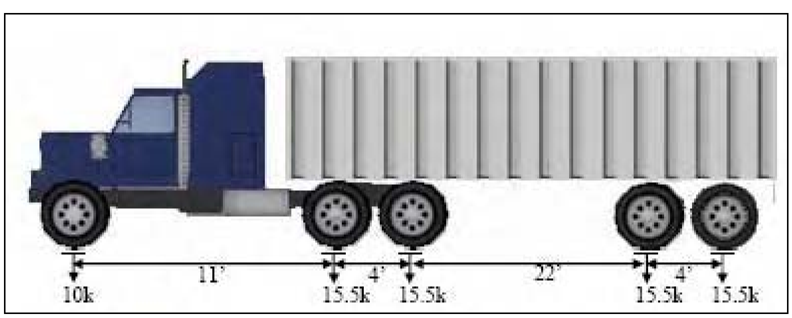

Figure 4.3.5 Legal Load Type 3S2

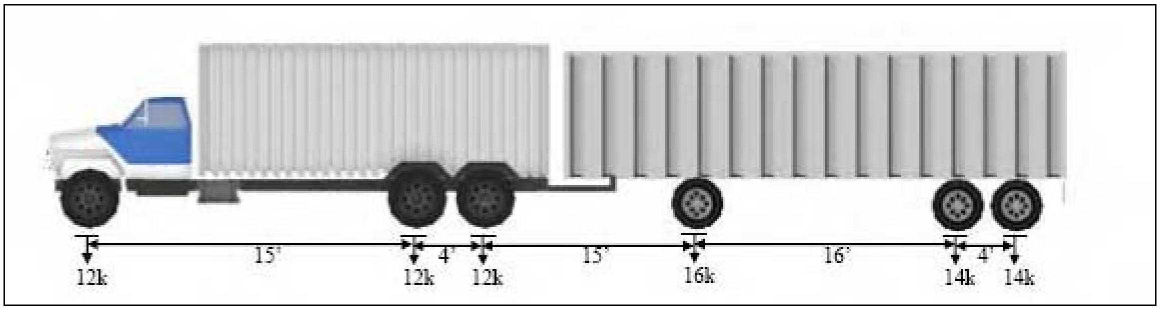

Figure 4.3.6 Legal Load Type 3-3

Each legal load vehicle described before was analyzed using the FEM and the moving load tool from SAP2000® to determine the live load effect. What the moving load analysis does is calculate the most severe response (i.e., bending moment, shear force, axial force, etc) due to vehicle loads moving along lanes on the bridge. The maximum bending positive and negative moments as well as the shear force were identified from the analysis. Figure 4.3.7 shows an example of the deformed shape of the FEM for the HS20-44 loading along the entire bridge. As expected, the maximum downward displacement occurs at mid-span while upward displacements occur near the piers of each span.

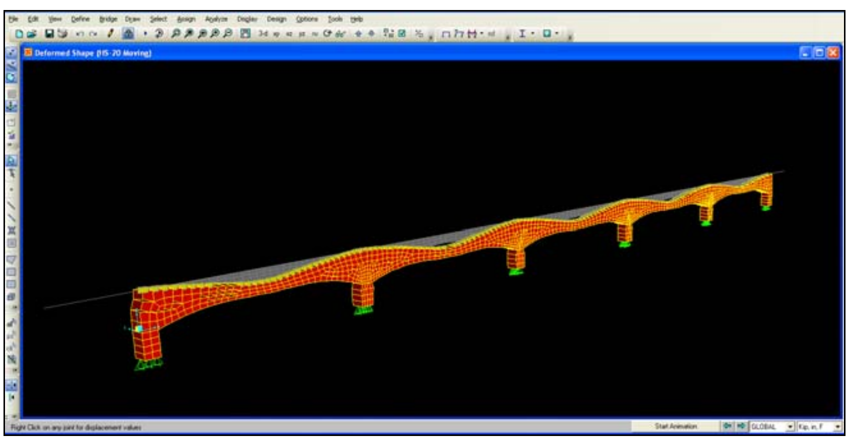

Figure 4.3.7 Deform shape of the arch beam due to HS20-44 loading

Each vehicle was defined on the FEM using the axle weight and spacing configuration. A combination of two point loads defines each axle as shown in the example presented in Figure 4.3.8 for the HS20-44 vehicle.

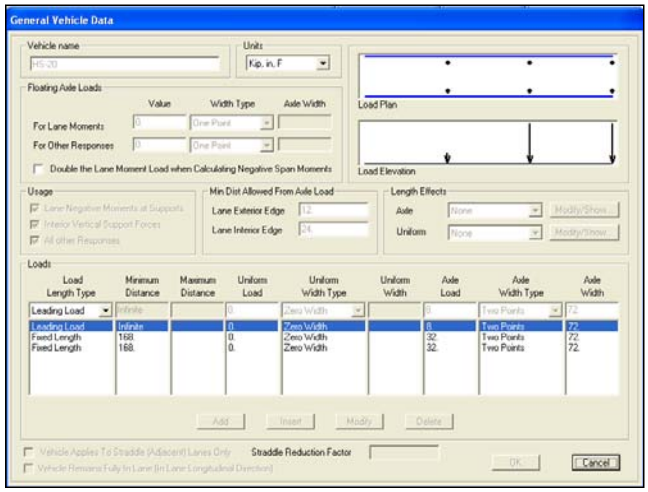

Figure 4.3.8 HS20-44 Configuration used on the FEM of SAP2000®

4.3.3 Live Load Moment and Shear from the SAp2000 ® model

After the analyses using each individual vehicle, a summary of the maximum bending moment and shear forces was generated to identify the live load demand. Figure 4.3.9 shows the maximum negative moment and shear force at the edge location for the HS20-44 loading. The moment called $M_{LL(HS20-44)}$ is equal to -591.77 k-ft and the shear force $V_{LL(HS20-44)}$, is equal to 59.55 kip. Figure 4.3.10 shows the maximum positive value of $M_{LL(HS20-44)}$, which is equal to 209.01 k-ft, and the maximum shear at mid-span, $V_{LL(HS20-44)}$, which is equal to 23.72 kip. These values are in terms of the axle load. To obtain the values for a wheel line the axle load is divided by two.

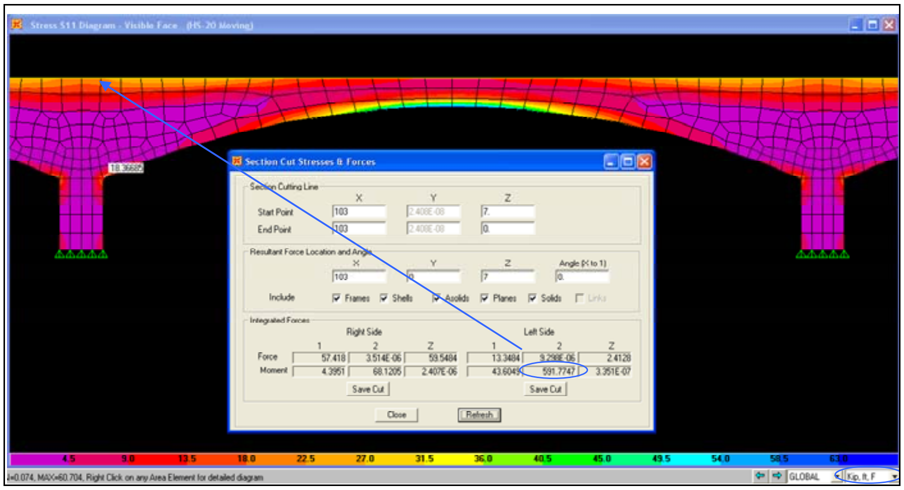

Figure 4.3.9. Maximum bending moment at the edge section of exterior beam for HS20-44 loading

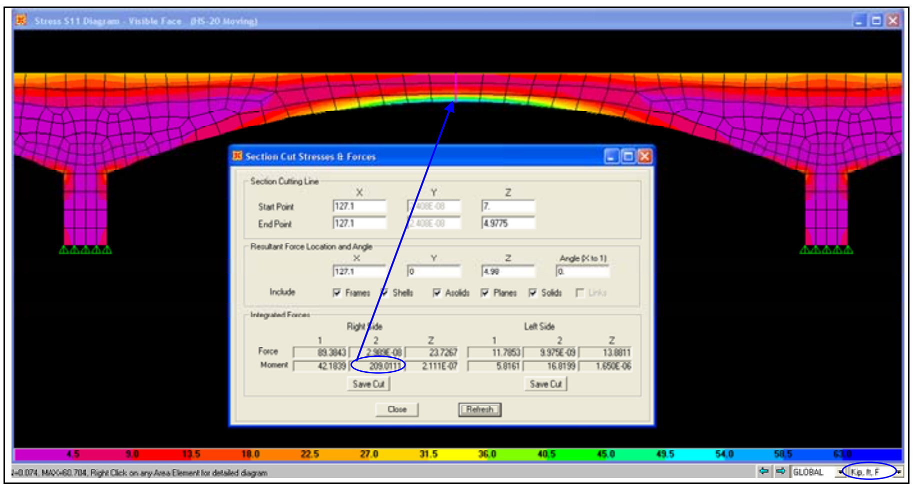

Figure 4.3.10 Maximum bending moment at the mid-span of exterior beam from HS20-44 loading

The demand loads for load rating purposes are obtained by multiplying the vehicle live load effect from the FEM by the distribution factor (DF) and the impact factor (I) for the LFR and (IM) for the LRFR, (see Equation 4.1).

$$\mathbf{LL = DF * LL_{FEM} * (I\ or\ IM)} \qquad \mathbf{4.1}$$

Since as discussed in Chapter 3 the LFR and LRFR provide different values for impact factors, separate calculations were performed to calculate the appropriate demand loads for the two methods. Both calculations LFR and LRFR were based on wheel line loads.

For purposes of rating, both bending moment and shear force have the same values of the distribution factor. The only exception is that the DF for the exterior arch beam is 0.69 which is lower than the value 1.17 used for the interior beam as explained in Chapter 3. Therefore, the only major difference in the calculation of live load demands by each method is the value of the impact factor which is 28% for the LRF and 33% for the LRFR (see section 3.5).

Results of vehicle demand loads for bending moment and shear force are summarized in Figure 4.3.12 through Figure 4.3.14 for the LFR method. Figure 4.3.15 through Figure 4.3.18 present similar results for the LRFR method.

Analyzing the results of demand load for the LFR method, the highest negative and positive moment for both beams (see Figure 4.3.11and Figure 4.3.12) are generated by the design vehicle HS20-44. The values of the moments found are -261.33 k-ft (exterior beam), -443.12 k-ft (interior beam) for the negative zone and 92.30 k-ft (exterior), 156.51 k-ft (interior) for the positive region. The shear is also controlled by the HS20-44 with values of 26.29 kip for the exterior and 44.58 kip for the interior arch.

For the LRFR method, the controlling vehicle based on the live load demand for bending moment and shear force is the design vehicle HL 93. The maximum negative moments were -399.22 k-ft for the exterior arch beam and -676.93 k-ft for the interior beam. Regarding the positive moment at mid-span, the HL 93 generated a moment of 127.66 k-ft at the exterior arch and 216.46 k-ft at the interior. The tandem load effect in combination with the lane load produced the worst effect on the beams, as shown in Figure 4.3.15 through Figure 4.3.18. The differences in distribution factors between the beams leads to a 41% higher demand loads for the interior arch beam.

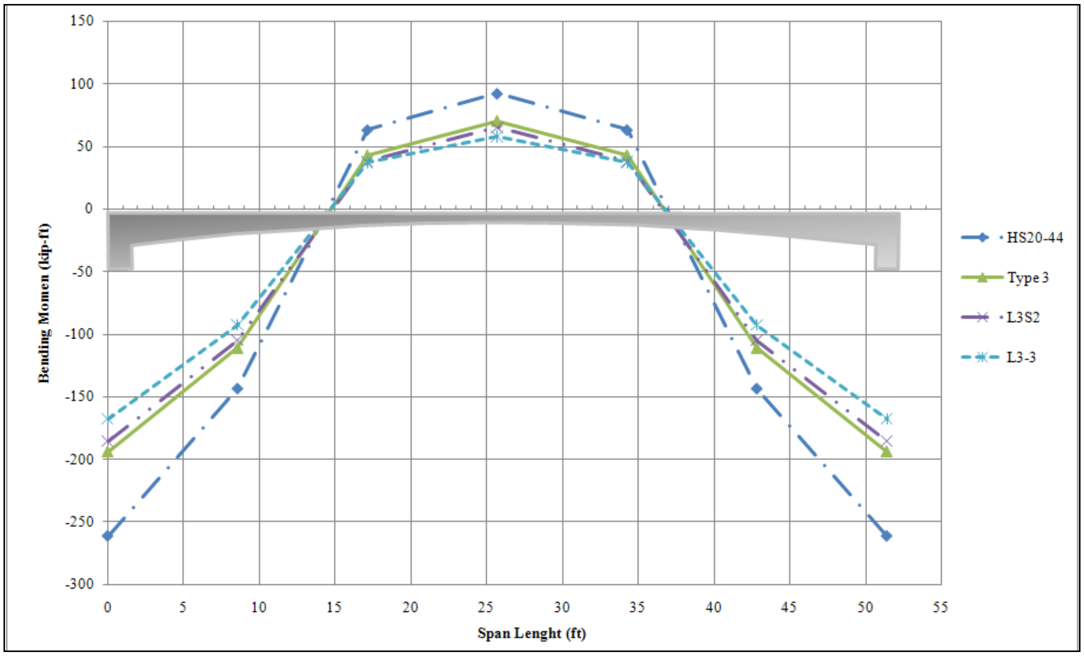

Figure 4.3.11 Vehicles bending moment demand in the exterior arch beam, LFR

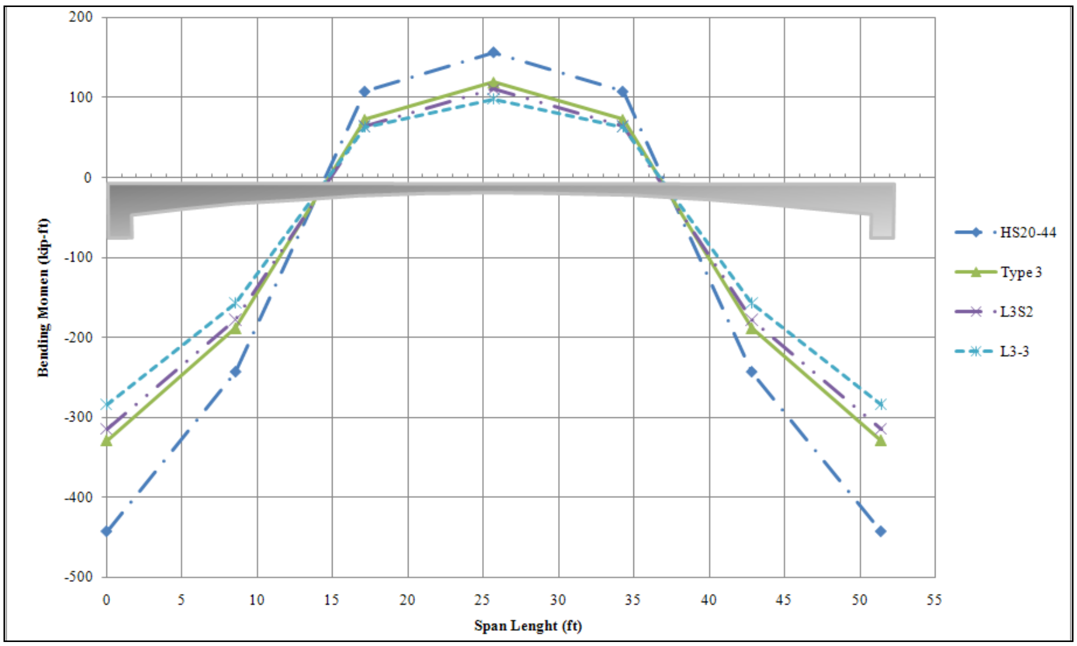

Figure 4.3.12 Vehicles bending moment demand in the interior arch beam, LFR

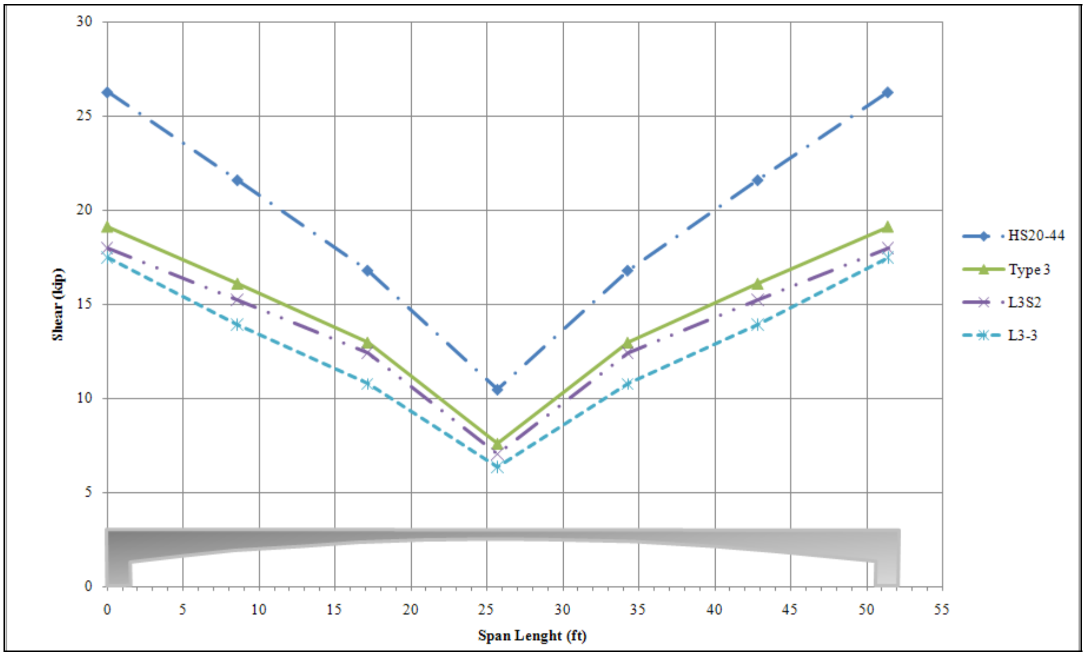

Figure 4.3.13 Vehicles shear force demand in the exterior arch beam, LFR

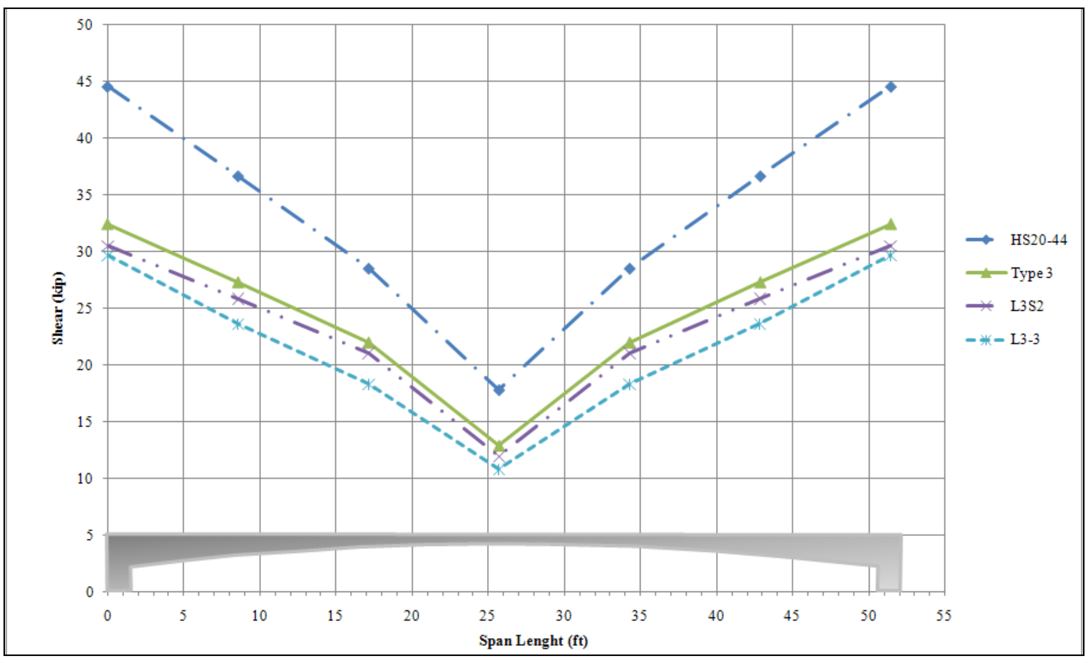

Figure 4.3.14 Vehicles shear force demand in the interior arch beam, LFR

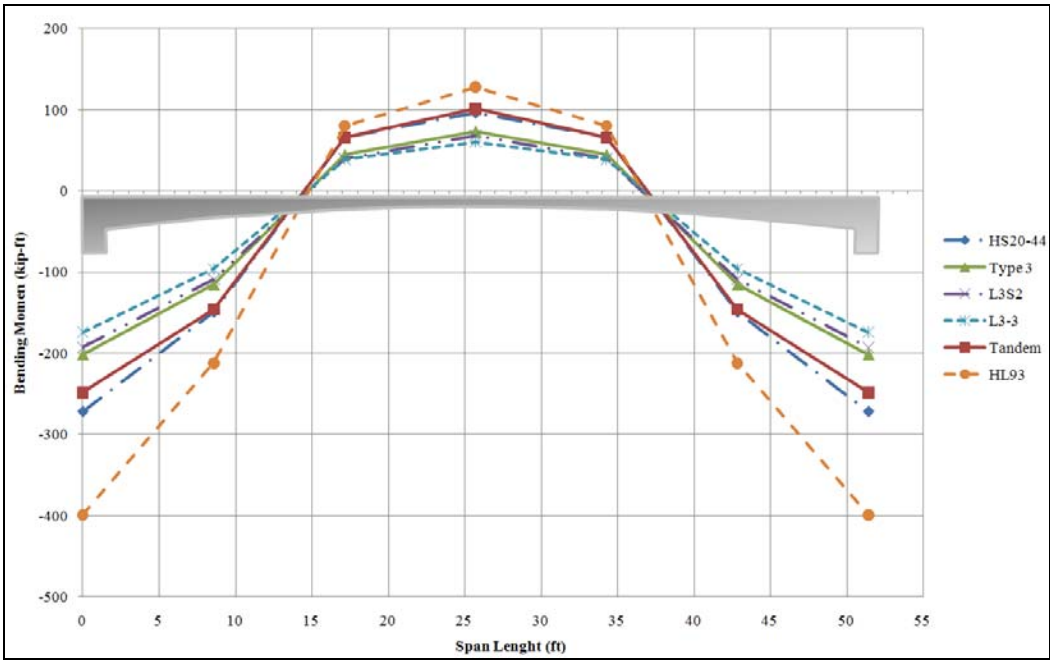

Figure 4.3.15 Vehicles bending moment demand in the exterior arch beam, LRFR

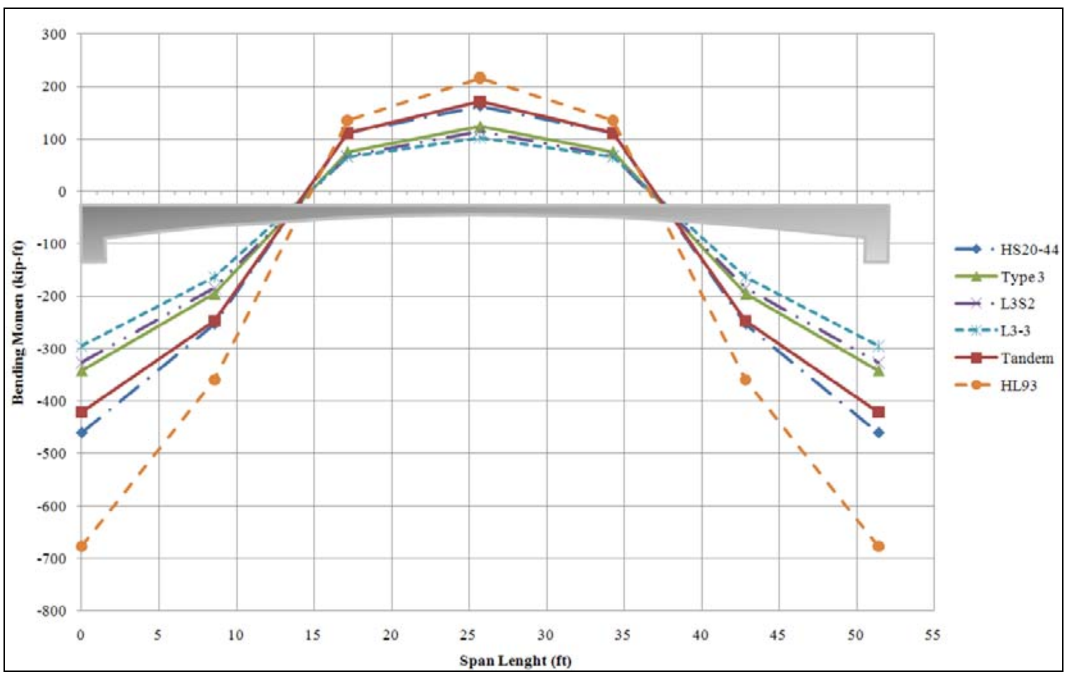

Figure 4.3.16 Vehicles bending moment demand in the interior arch beam, LRFR

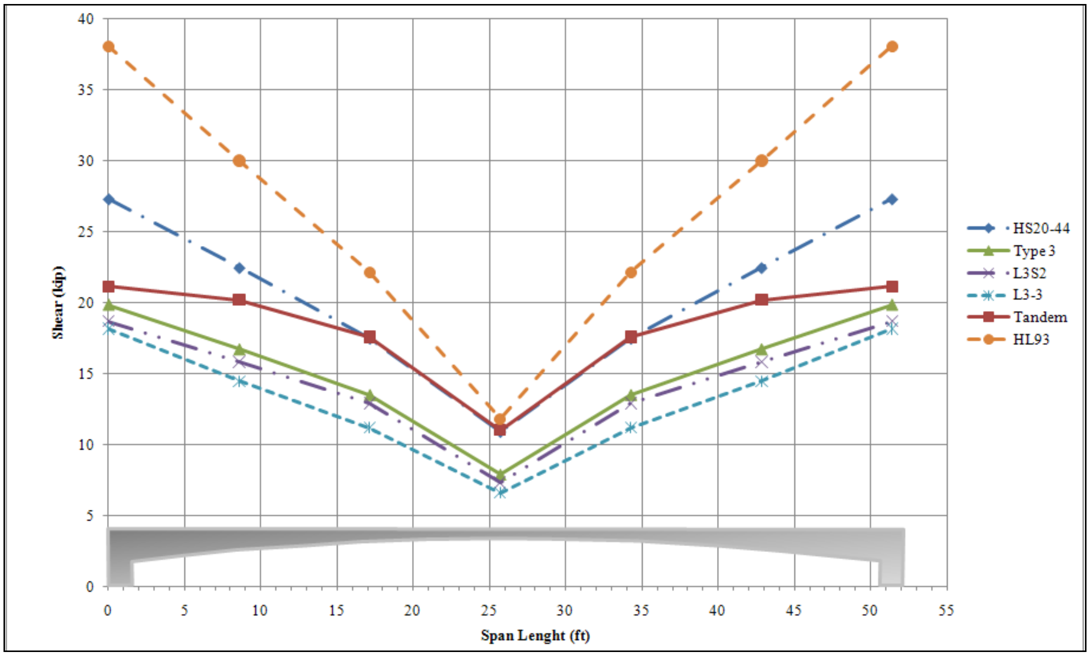

Figure 4.3.17 Vehicles shear force demand in the exterior arch beam, LRFR

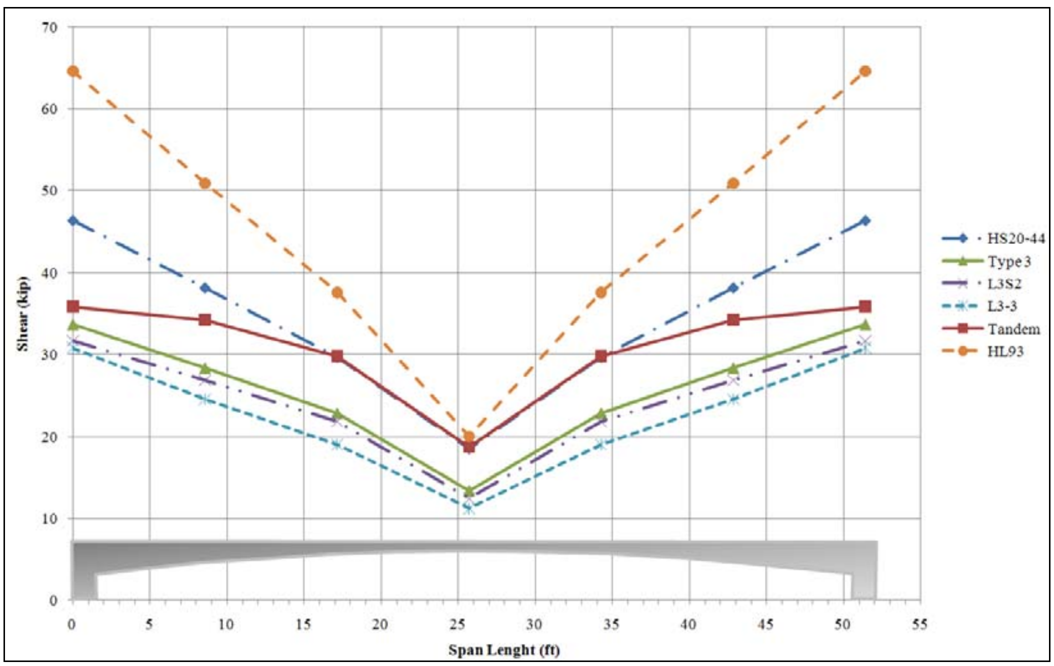

Figure 4.3.18 Vehicles shear force demand in the interior arch beam, LRFR

5 NOMINAL RESISTANCE OF THE ARCH BEAM SECTIONS

5.1 Introduction

Since arch beam bridges are more complicated to model and analyze than prismatic beam bridges, the methods used by structural engineers to study this type of structures usually have higher factors of safety. This can cause the bridges to have overly conservative load ratings. In some cases, overly conservative ratings can cause a bridge that does not need a load posting to be posted (Chajes, 2002).

The strength of some arch bridges has been assessed on the premise that they are safe if they do not show signs of deterioration or distress. This assumption can be made only if one assumes that the present loading of the bridge will be the same as the projected future loading. One cannot use this assumption if the bridge is to carry heavier vehicles than it has in the past (Halden, 1995).

The bridge under study exhibit a non standard design since the exterior and interior arch beams have different geometric properties as described in Chapter 2. Therefore, it was necessary to calculate the nominal capacity for flexion and shear for both arch beams to completely understand the behavior and performance of the entire structure.

5.2 Flexural Resistance of a Concrete Arch Beam

The arch beams and the concrete slab were constructed cast-in-place at the same time forming a monolithic section. Since the slab is connected positively to the beams with shear stirrups, a portion of the slab can be assumed to act in composite action with the beams, Figure 5.2.1 and Figure 5.2.2. Therefore, the flexural resistance of the arch beams section was obtained using the rectangular stress distribution theory for a T-section. This composite action has the effect of producing an equivalent larger and stronger beam than would be provided by one beam alone.

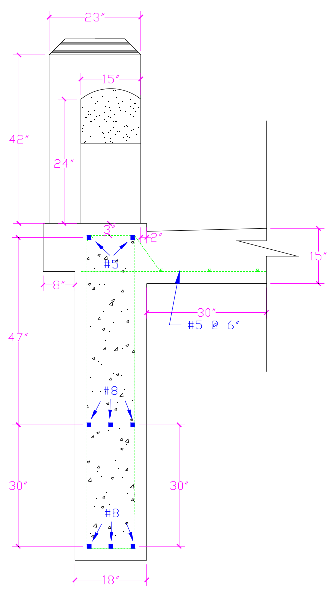

Figure 5.2.1 Exterior beam

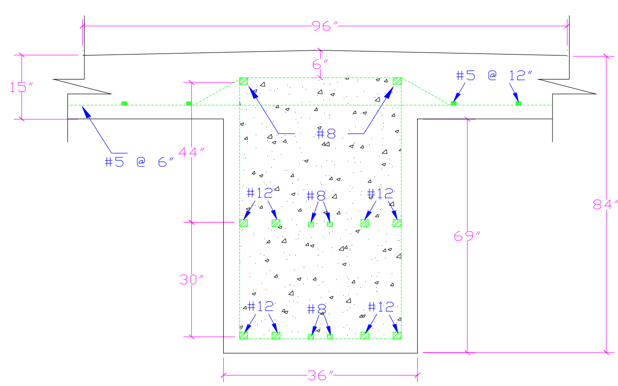

Figure 5.2.2 Interior beam

The T-section geometry of reinforced concrete structures is defined by the following parameters, and is shown in Figure 5.2.3:

- Lower steel area in the tensile zone, A_s

- Upper steel area near the compression zone, A'_s
- Flange depth, h_f
- Effective flange width, b
- Web width, b_w
- Distance from the centroid of the reinforcement to opposite face of the section, d
- Concrete cover, x

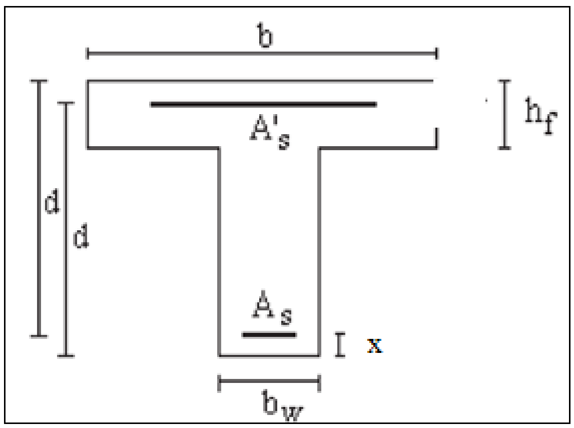

Figure 5.2.3 Geometry of the doubly reinforced T-section

For the bridge under study, the flange at the support location is in tension because of the continuation between spans. Therefore, that part would behave as an inverted doubly reinforced section having the compressive steel (A'_s) at the bottom fibers and tensile steel (A_s) at top fibers. Depending on the depth of the neutral axis on the T-section the following cases can be identified:

- Case I: Depth of neutral axis c less than flange thickness h_f
- Case II: Depth of neutral axis c larger than flange thickness, h_f

Each of the cases mentioned before requires different approaches to calculate the flexural capacity. For Case I, the beam can be treated as a standard rectangular section, provided that the depth (a) of the equivalent rectangular block is less than the flange thickness (h_f).

The flange width (b) of the compression side should be used as the beam width in the analysis.

For Case II, when $c > hf,$ the depth of the equivalent rectangular stress block a could be smaller or larger than the flange thickness (h_f). If the depth of the neutral axis c is greater than h_f and a is less than h_f, the beam could still be considered as a rectangular beam for design and analysis purposes.

If both c and a are greater than h_f, the section has to be considered as a T-section. This type of T-beam (a > hf) can be treated in a manner similar to a doubly reinforced rectangular cross section. The contribution of the flange overhang compressive force is considered analogous to the contribution of an imaginary compressive reinforcement (Nawy, 2003).

Figure 5.2.4 shows the stress distribution in the composite T-beam section, taking into consideration the compression force (C) concentrated at the top concrete block measured from the extreme top fiber of the slab. The variable a represents the height of the Whitney rectangular stress block in inches calculated as the product of the stress block factor (β_1) times the compressive stress region (c) (Whitney, 1942). For a concrete with a compressive strength ($f'c$) less than 4 ksi the value of β_1 should be 0.85. The tension (T) is estimated as the product of f_y A_s, where f_y accounts for the yield stress of steel taken equal to 33 ksi (AASHTO, 1994) and A_s is the total steel area carrying tension.

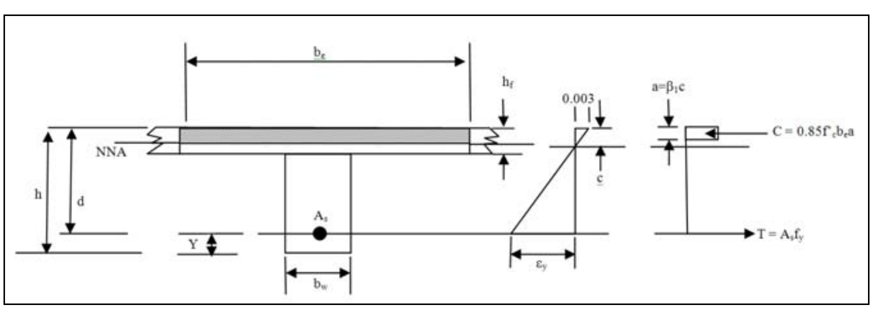

Figure 5.2.4 Stress and strain distribution on T beam

In the current study, the nominal flexural strength (M_n) is determined by static equilibrium in the composite section, assuming that the plastic limit (ε_y) of the steel section is reached when at the balance strain conditions the top extreme compression fiber reaches a maximum strain value of 0.003.

In order to estimate the M_n values it was necessary to establish the area of compression (provided by the concrete) required to balance the area in tension (provided by the steel). The following equation shows how the section behaves, i.e. whether it behaves as a T-section or as a rectangular beam:

$$A_s \leq \frac{0.85 \times f'_c \times b_e \times t}{f_y} \tag{5.1}$$

The value of f'_c used on the calculation on this study was 2.5 ksi, based on AASTHO recommendation for a bridge constructed prior to 1954, (AASHTO, 1994). In this investigation, Equation 5.1 always was satisfied for each section analyzed. Therefore, rectangular beam formulas were valid. Consequently, the tension (T) in the steel and the compression (C) of the concrete can be calculated as described in Figure 5.2.4. The depth of the compression block is calculated by AASTHO 8-17 and LRFR 5.7.3.1.3 as follows:

$$a = \frac{T}{0.85 \times f'_c \times b_e} \tag{5.2}$$

The flexural nominal capacity (M_n) of the beam is defined by AASHTO 8-16 and LRFD 5.7.3.2.2 as:

$$M_n^- = A_s \times f_y \times \left[d - \left(\frac{a}{2} \right) \right] \tag{5.3}$$

Both LFR and LRFR rating methods use the same approach to calculate the nominal section strength. Therefore, only a single calculation is performed for each of the four sections of the beam to determine the flexural capacity for use in the load ratings. The original construction drawings dating from 1914 show that bars with square cross sections were used for reinforcement. Due to the age of the structure, this is probably a correct representation of the reinforcing steel.

The change in cross sectional area in the arch beam leads to different values of strength along the span length. For example, due to the change of height, Figure 5.2.5 shows the variation of the position of the tensile steel centroid (*Y*) respect the span length for both beams. The values are measured from the top extreme surface. As *Y* decreases, the section loses strength, and this is why the higher flexural and shear capacity are obtained at supports. From Figure 5.2.5 it can be noticed that the interior arch has a larger amount of steel near the top surface in than does the exterior arch.

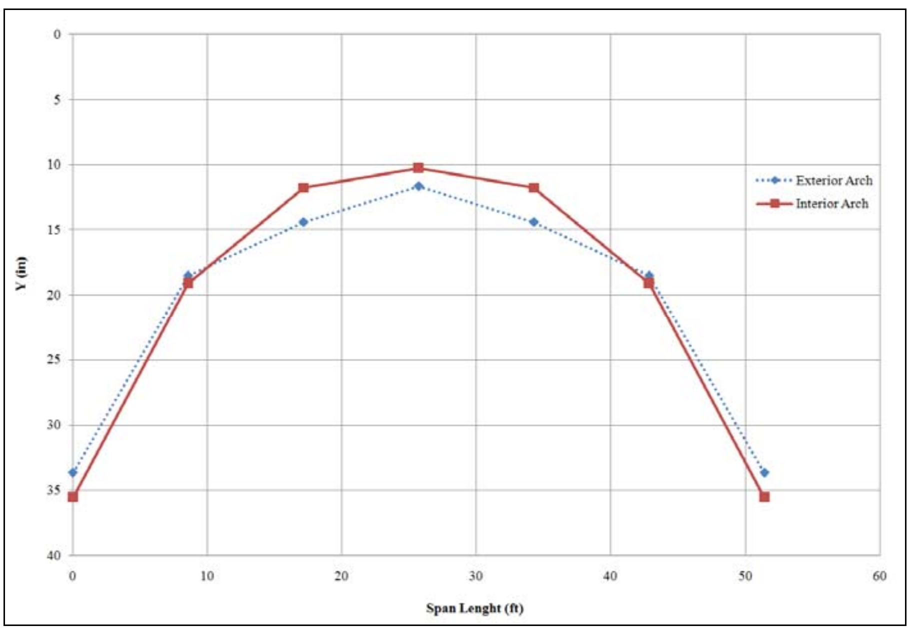

Figure 5.2.5 Tensile steel centroid location (Y)

Appendix C shows in detail the flexural strength calculations for the exterior and interior beams. Figure 5.2.6 illustrates the results of the nominal flexural strength for each arch beam. As expected, the interior arch shows a higher nominal flexural capacity than the exterior one. The interior arch has 43% higher capacity for the negative zone and 60% for the positive in comparison with the exterior one. This is attributed to the differences web width and amounts of tension steel.

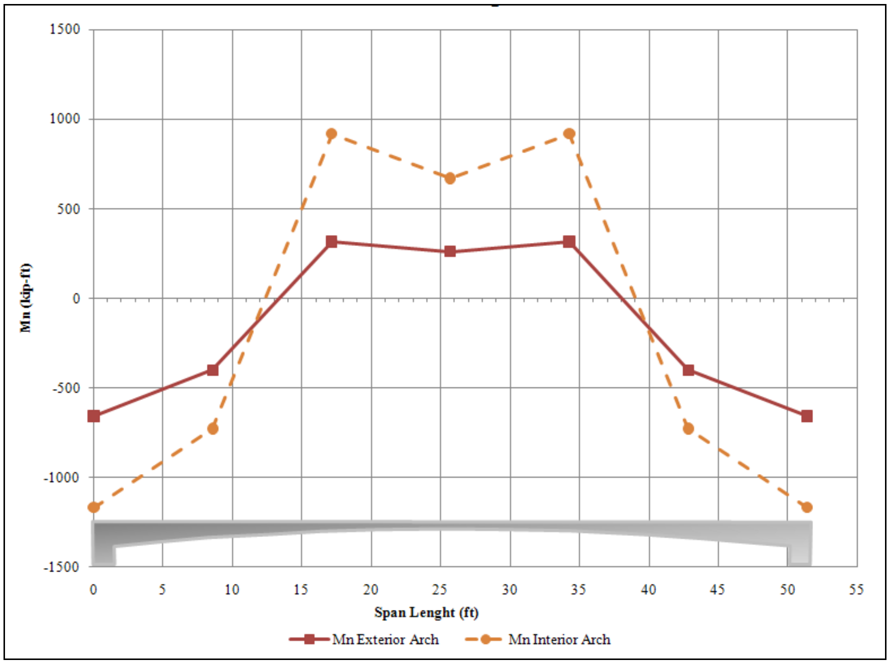

Figure 5.2.6 Nominal Flexural Strength for interior and exterior arch beam

5.3 Shear Resistance of the Concrete Arch Beam

Since the strength of concrete in tension is considerably lower than its strength in compression, design for shear is of major importance in concrete structures. The behavior of reinforced concrete beams at failure in shear is distinctly different from their behavior in flexure. They fail abruptly without advanced warning, and the diagonal cracks that develop are considerably wider than the flexural cracks, (Nawy, 2002).

Calculations for continuous deep beams, unlike those for simply supported ones, are not based on the design shear force at the critical section as defined in ACI 318-08, Chapter 11. Instead, the shear reinforcement at any section is calculated from the design shear force V_u at that location (Kong, 1935).

For purposes of this investigation, the shear strength of the arch beams was studied at the four locations of interest described in detail in Chapter 4.

5.3.1 LRF Shear Capacity

The nominal shear strength of concrete members (V_n) is composed of the contribution of the shear strength provided by the transverse reinforcement (V_s) and the shear strength provided by the concrete (V_c) as shown in Equation 5.4. The reduction factor (ϕ) for shear is equal to 0.85 as defined in AASHTO 8.16.1.2.2.

$$\phi V_n = \left(V_c + V_s\right) \qquad \textbf{5.4}$$

Equation 5.5 is used to estimate the concrete shear strength for the LFR method.

$$V_c = 2 \times \sqrt{f'_c} \times b_w \times d \qquad \textbf{5.5}$$

where V_c is the shear resistance of concrete; f'_c is the ultimate strength of the concrete (2.5 ksi); b_w is the width of the concrete web; d is the effective depth from the extreme compression fiber to the centroid of the tensile reinforcement. Equation 5.6 defines the distance d as:

$$d = h - \overline{y} \qquad \textbf{5.6}$$

where $\bar{y}$ is the position of the centroid of the tensile steel reinforcement measured from the top of the concrete slab, and h is the total height of the beam. For the arch beam, the distance d was calculated four times, one for each location of interest.

The shear strength provided by the stirrups is defined by Equation 5.7 as:

$$V_s = \frac{A_v \times f_y \times d}{s} \qquad \textbf{5.7}$$

where A_v is the area of transverse steel, f_y is the yield stress of the reinforcing bars, and s is the spacing of the vertical web reinforcement.

Figure 5.3.1 shows graphically the results of the shear strength calculation for arch beams. The higher shear strength occurred near the support location with a gradual parabolic decrease as one moves away from the support. For each 10 ft a drop of approximately 30% to 40% of shear strength occurs due to the loss of concrete area. The maximum shear strength was 101.38 kip and 171.72 for the exterior and interior beams, respectively.

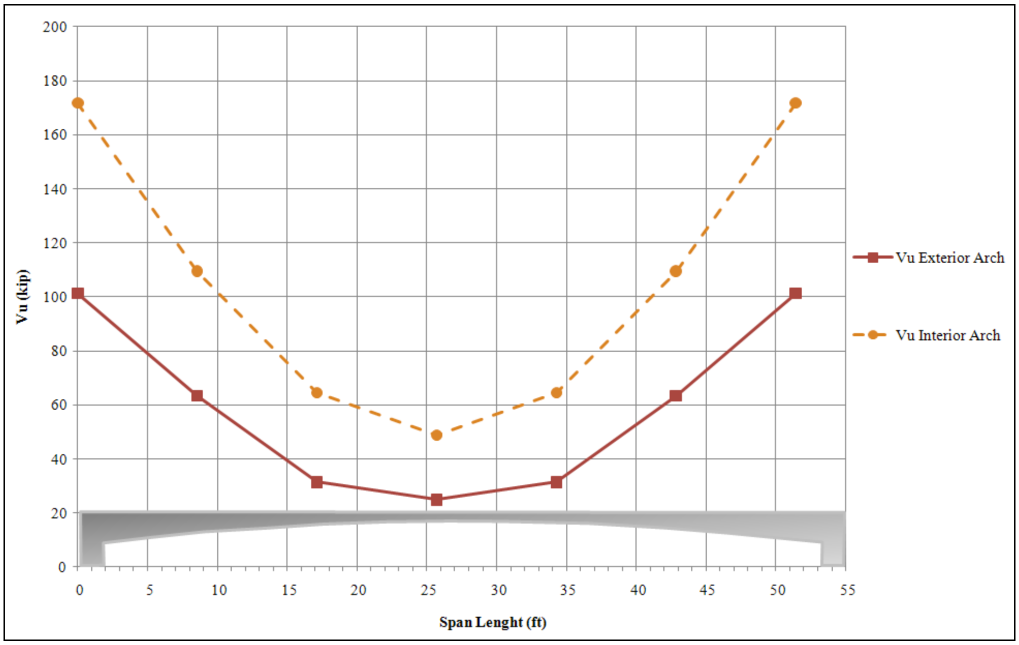

Figure 5.3.1 Shear strength for exterior and interior arch beam using the LFR

5.3.2 LRFR Shear Capacity

The nominal shear resistance for the LRFR is given by the following equation:

$$V_n = (V_c + V_s) \qquad \textbf{5.8}$$

In comparison with the previous equation for the LFR method, Equation 5.8 does not require a reduction factor (ϕ). The nominal resistance of the plain concrete web (V_c) is defined as:

$$V_c = 0.0316 \times \beta \times \sqrt{f'_c} \times b_v \times d_v \qquad \textbf{5.9}$$

where β is the factor indicates the capability of diagonally cracked concrete to transmit tension and shear, b_v is the width of the concrete web and d_v is the effective shear depth of the section.

The shear strength provided by the stirrups is defined by Equation 5.10 as:

$$V_s = \frac{A_v \times f_y \times d_v \times \cot\theta}{s} \quad \textbf{5.10}$$

The θ angle indicates the inclination of diagonal compressive stresses (AASHTO, 2004). These equations are based on the Modified Compression Field Theory (MCFT) and require the determination of β and θ, which requires a depth analysis. A simplified analysis (AASHTO, 2003) suggests the use of β = 45 and θ = 2° and those were the values used for this investigation.

Figure 5.3.2 shows the shear strength calculated for the exterior and interior beams using the LRFR methodology. The maximum shear strength for the exterior beam was 119.21 kip and for the interior beam was 201.90 kip.

Both methods, the LFR and the LRFR, produced similar shear behaviors for the arch beams. A 40% difference between the interior and exterior beams was obtained with both methods due to the differences in the width of the web.

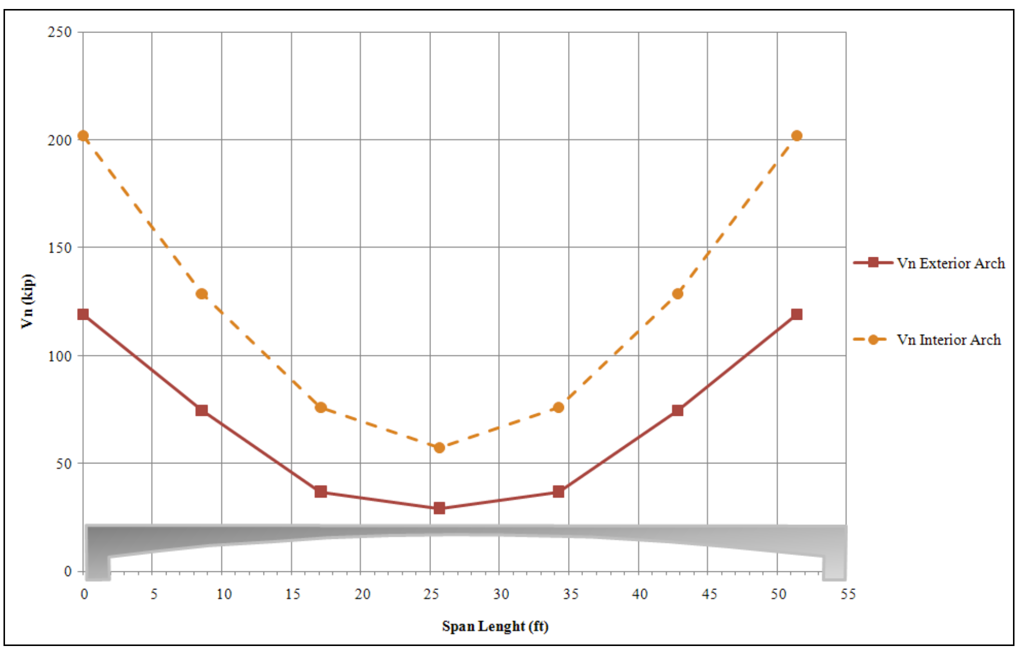

Figure 5.3.2 Shear strength for exterior and interior arch beam using the LRFR method

6 LOAD RATING RESULTS

6.1 Introduction

A load rating analysis was performed for the Lahontan Bridge following the AASHTO procedures for the two rating methods discussed in Chapter 3. Detailed calculations for the load rating analysis are presented in Appendix A. To facilitate the presentation of the results, the discussion of the load rating comparative study has been divided into short sections based on the rating level considered. The data from the LFR rating level is presented in its own separate section as well as the LRFR. Each section will present results of the structural behavior of the beams with regards to flexure and shear rating factors. Both cases exterior and interior beam, were analyzed and combined comparisons for both cases are given. Additionally, the controlling rating factors for the exterior and interior beams are identified for each method of evaluation. It is important to note that the lowest factor controls the overall rating for a given vehicle type on the bridge.

6.2 Design Level Rating Results

Comparisons at the design scale of rating were made between the LFR and LRFR at the Inventory and Operating level for both exterior and interior beams. The live loads used were the HS20-44 design truck for the LFR and the HL-93 truck for the LRFR method.

The flexural and shear rating factor results due to the HS20-44 loading are described in Sections 6.2.1 and 6.2.2, respectively. Similar results but for the case of the HL-93 loading are described in Section 6.2.3 for the flexural moment and in Section 6.2.4 for the shear force.

6.2.1 LFR Moment Rating Factor

Figure 6.2.1 shows a summary of the moment rating factors calculated for the HS20-44 vehicle using the LFR method. Each level of rating (inventory and operating) is plotted for both arch beams. The values below the line of unity (RF=1.0) confirm that the arch beam cannot hold a HS20-44 loading. The negative moment at the supports controls the RF for the exterior and interior beam. The controlling RF value for the exterior arch was 0.23 for inventory and 0.38 for the operating level. For the interior arch the smaller RF values were 0.26 and 0.43 for the inventory and operating level, respectively. Analyzing the results of RF from Figure 6.2.1 it can be seen that the bridge was not designed considering a HS20-44 loading. It is noticeable that the exterior arch beam controls the RF in flexion for the LFR method. All values of RF calculated for the negative moment region were lower than 1 by approximately 70%. With the exception of the inventory RF at mid-span for the exterior beam, all other RF were higher than 1 for the positive bending moment region.

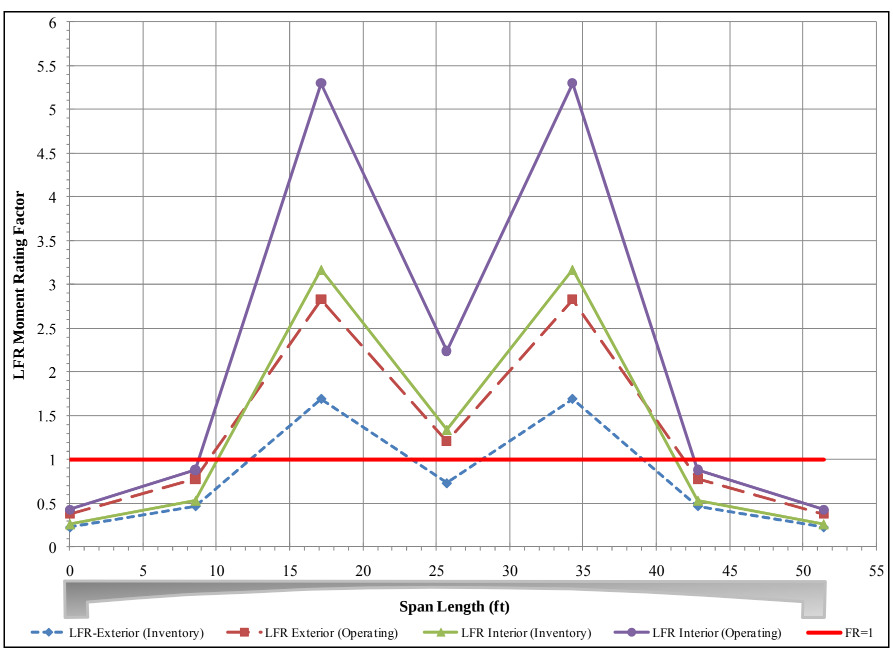

Figure 6.2.1 Flexural RF summary due to the HS20-44 loading

6.2.2 LFR Shear Rating Factor

The shear RF results for both arch beams are presented graphically in Figure 6.2.2 for the LFR method. It can be observed from the figure that neither arch beam meets the required live load demand of the HS20-44 under the shear force category. The only case that met the HS20-44 shear demand (RF > 1.0) was the interior arch under the operating level. For all the other cases evaluated, RF values lower than 1.0 were obtained. The controlling RF at the inventory level for shear was 0.44 and 0.73 at the operating level. These controlling RF values are for the exterior arch, which controlled the bridge weight limit capacity.

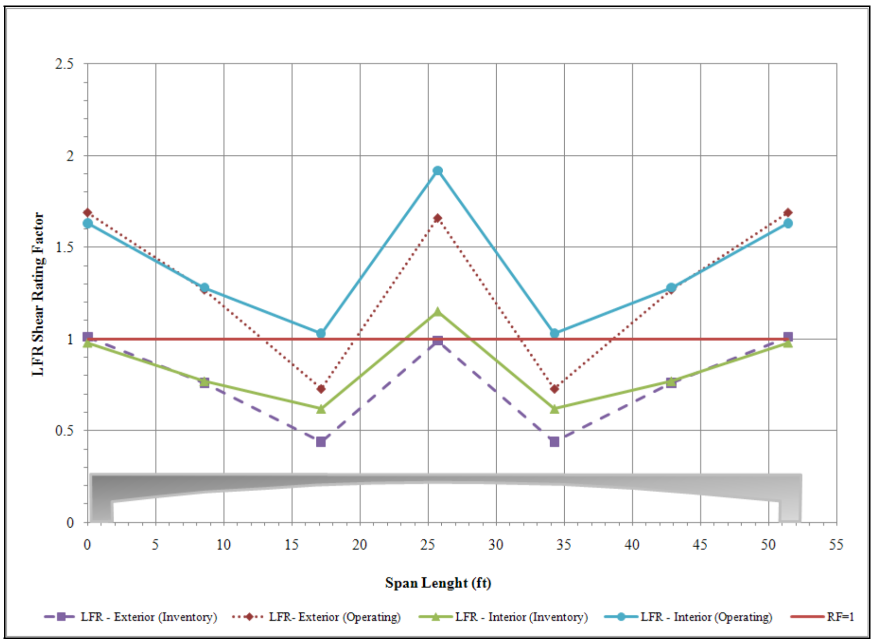

Figure 6.2.2 Shear RF summary due to the HS20-44 loading

6.2.3 LRFR Moment Rating Factor

Only one limit state, Strength I, was evaluated with the LRFR methodology. The Strength I limit state is the basic load combination for normal vehicular bridge used and is the limit state to be used for a legal load rating. The factors for the load case for this limit state are summarized in Table 6.2.1.

Table 6.2.1 LRFR Load Factors for Strength I (from AASHTO, 2003)

Limit State	Dead Load DC	Dead Load DW	Design Rating		Legal Load
			Inventory LL	Operating LL	LL
Strength I	1.25	1.25[a]	1.75	1.35	1.80[b]

DC – Dead load of structural components and nonstructural attachments
DW – Dead load of wearing surfaces and utilities
a Thickness is field verified
b using Unknown ADTT since the bridge is currently closed to traffic but may be opened for unknown public use in the future

Figure 6.2.3 shows a summary of the flexural RF results using the LRFR method and the HL-93 design loading. It can be observed from the figure that all the RF values for the negative zone were less than 1.0 for both arches (interior and exterior). The lower flexural RF obtained from the HL-93 analysis was 0.09 at inventory and 0.11 at the operating level. These controlling RF values are from the exterior arch at the negative flexural region. For the interior arch the controlling RF was 0.1 at inventory and 0.13 at operating level. In both cases, the rating factors are controlled by the negative bending moment, as it was observed for the LFR method discussed previously. The flexural capacity of the bridge under the LRFR is approximately 91% below the capacity required by the HL-93loading.

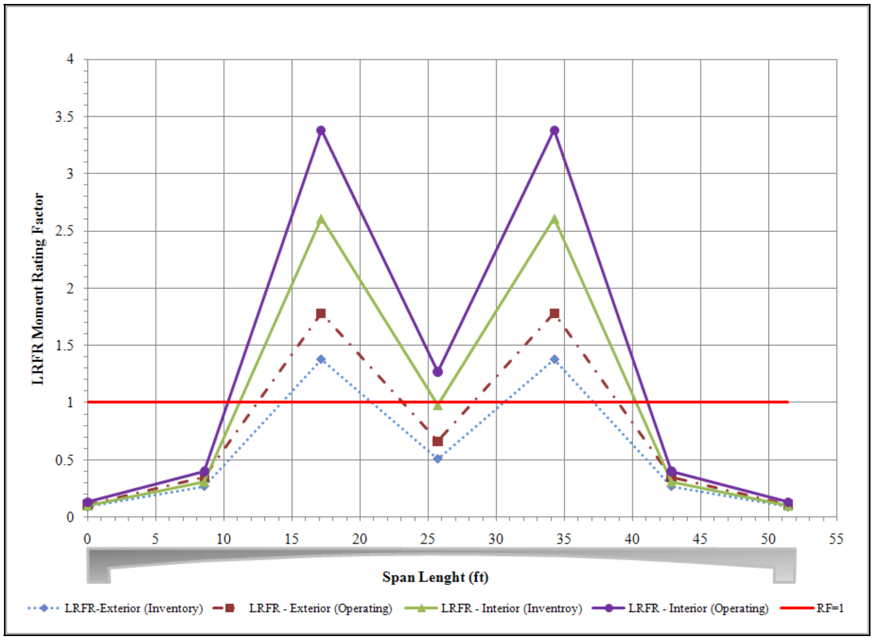

Figure 6.2.3 Flexural RF summary due to the HL-93 loading

The demand load required by the HL-93 truck in comparison with the HS20-44 (described in Section 6.2.1) is approximately 40% and 30% higher at the maximum negative moment zone for the inventory and operating levels, respectively. These results showed that the LRFR demands more available live load capacity on the structural elements to maintain a higher degree of reliability on the structure.

6.2.4 LRFR Shear Rating Factor

The shear RF results using the LRFR method and the HL-93 loading are summarized graphically in Figure 6.2.4 for both arch beams (interior and exterior). It can be observed from the figure that for almost all the locations analyzed the shear RF values were less than 1.0. Only values at mid-span the bride met the RF condition for shear. The exterior arch was responsible for the controlling shear RF, with a value of 0.35 for the inventory and 0.45 for the operating level. From the RF results it can be established that the shear capacity of the bridge is 65% and 55% lower than the required by the HL-93 loading for the inventory and operating levels, respectively.

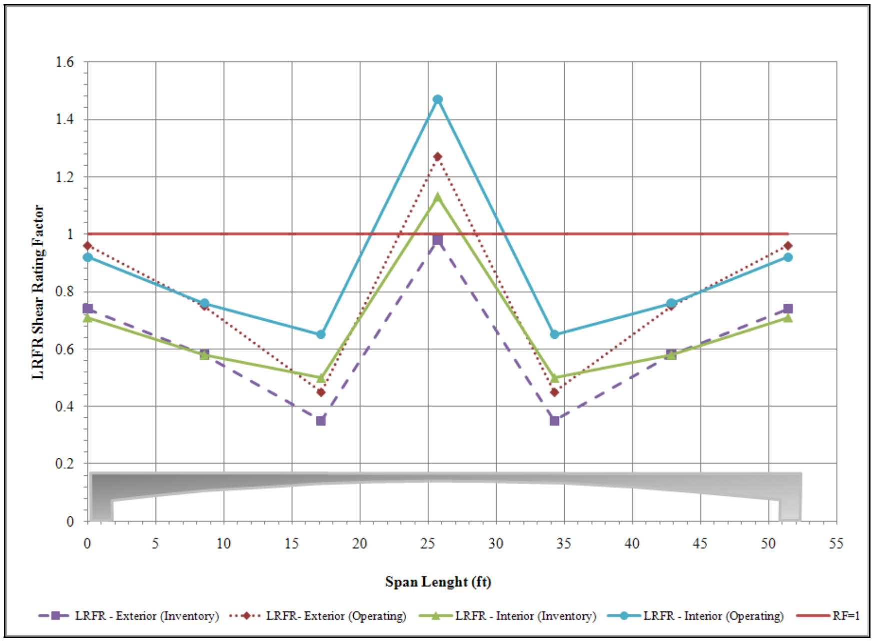

Figure 6.2.4 Shear RF summary due to the HL-93 loading

6.2.5 Discussion of the Results

From the previous sections, it can be established that the bridge does not meet the minimum requirements for the HS20-44 and HL-93 design vehicle. The RF results were always less than 1.0 for the negative moment region for both arches (interior and exterior) at both the inventory and operating levels. The exterior arch controlled the capacity of the bridge since it is there where the lowest overall values of RF were obtained. In terms of the shear RF, it can be established that shear does not govern over the flexural moment. The RF values for the negative flexural moment were always smaller for both beams in consideration under the design vehicles analysis in comparison with the RF values obtained for the shear force.

Due to the poor concrete condition observed in the bridge during the inspection, the load rating results are approximately 40% lower when using the LRFR method versus the LFR. This reduction corresponds to a condition factor (φ_c) equal to 0.85 used on the RF equation.

6.3 Legal Loads Rating Results

Since the two design vehicles evaluated produced rating factors lower than one it was necessary to consider the, load rating using the Legal Loads vehicles described in Chapter 4 (LRFD, 2003). Three legal load vehicles were considered in the analysis: Type 3, Type 3S2 and Type 3-3. The intention of using the Legal Load vehicles is to identify the limit weight capacity of the bridge and to determine the bridge posting requirements. Both methods, LFR and LRFR, were considered for the study of the Legal Loads vehicles. However, the rating factors discussed in Section 6.2 using the design vehicles are still unacceptable under the current standards established by AASTHO. The current evaluation code requires RF values higher than 0.3 in many bridges to keep them open to the traffic. Since the bridge under study was built approximately 97 years ago, the results of RF presented in Section 6.2 confirmed that a lightweight vehicle was used for the design of the bridge.

The inventory and operating levels were considered in the analysis performed with the LFR method. For the LRFR method, only a single level of rating was considered. According to the LRFR, the Strength I factor for the legal load rating is determined by the Average Daily Truck Traffic (ADTT), which was reported as 0 in the 2009 inspection report due to closure of the bridge. However, once the bridge is load rated, it might be opened for public access, and the expected ADTT is considered unknown.

Results from Section 6.2 based on the design loading vehicle showed that the controlling rating factor for the interior and exterior beams is the negative moment near the support. Therefore, since the legal load vehicles are lighter and less demanding than the design load vehicles, the shear RF is not considered for this part of the investigation. This section will only present the results of RF due to flexural moment generated by the legal load vehicles.

6.3.1 LFR Moment Rating Factors

Both arches (interior and exterior) were evaluated considering the three legal load vehicles. Figure 6.3.1 and Figure 6.3.2 show the flexural moment RF values for each vehicle. Inventory and operating levels were analyzed. It can be observed from the figures that rating factors lower than 1.0 are generated by the legal vehicles on both arches (interior and exterior). The negative flexural moment controls the RF at the exterior arch. The controlling vehicle for both arches is the Type 3. For the exterior arch the Type 3 vehicle produced a RF of 0.31 at the inventory and 0.52 at the operating level. For the interior arch the RF was 0.34 and 0.58 at the inventory and operating levels, respectively. The results from the RF shows that the Type 3 loading requires between 70% (inventory) and 48% (operating) more capacity than the actual capacity of the bridge. The Type 3 vehicle has the higher axle weight in comparison with the other two legal loads described in Chapter 4. With 17 kip coming from the rear axle of the trailer, the Type 3 vehicle causes the most damage to the bridge, in terms of the bending and shear effects.

From the figures it can also be observed that the Type 3-3 vehicle is the less demanding. The controlling RF for the Type 3-3 was 0.36 for inventory and 0.6 for operating at the exterior arch.

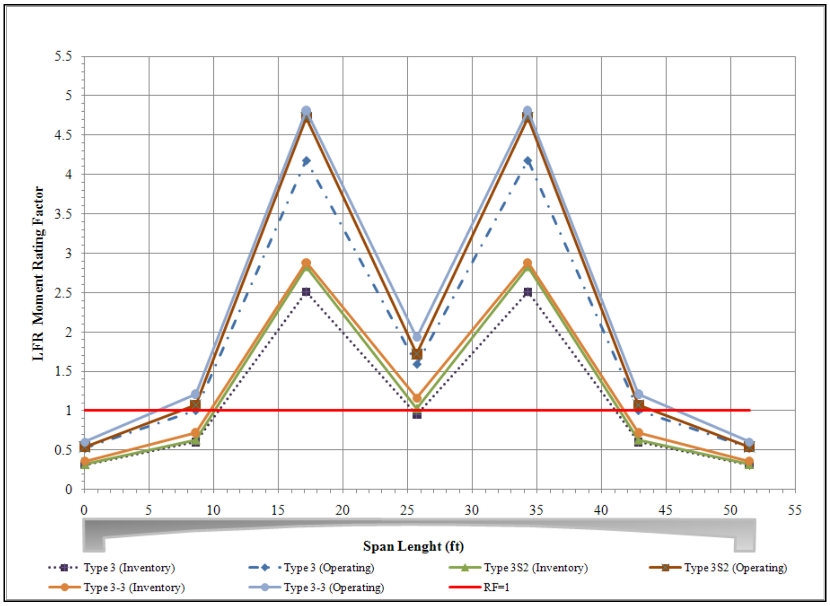

Figure 6.3.1 Flexural RF summary for the exterior beam due to the Legal Load loading for the LFR method

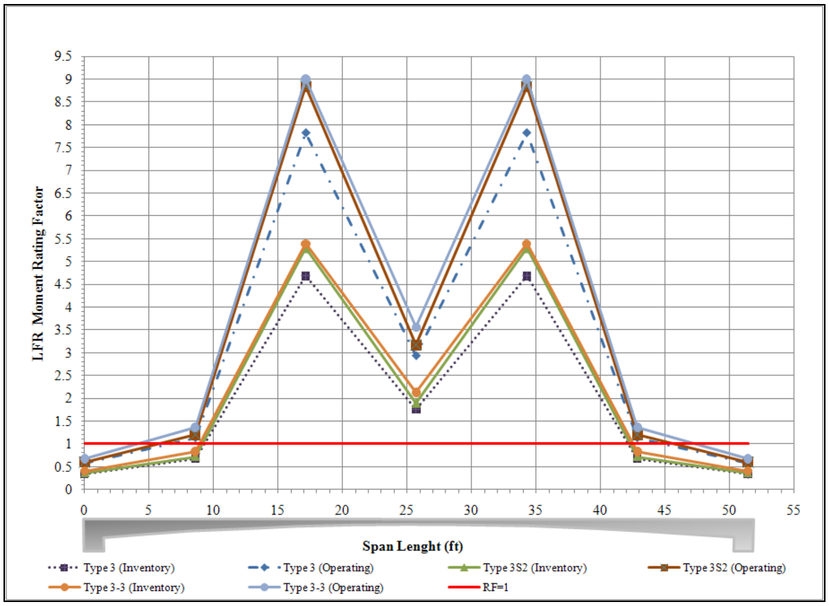

Figure 6.3.2 Flexural RF summary for the interior beam due to the Legal Load loading for the LFR method

The arch bridge did not satisfied the rating factor equation for any of the considered legal load vehicles at the negative moment location, even at the operating level in which the bridge is allowed to carry a 40% additional capacity.

6.3.2 LRFR Moment Rating Factors

Figure 6.3.3 and Figure 6.3.4 show the results of the moment RF values obtained for the exterior and interior arch beam. Analogous to the LFR results presented in Section 6.3.1, the Type 3 legal load vehicle controls the RF on both arches. A value of 0.16 for the exterior and 0.19 for the interior was obtained as a controlling RF due to the flexural negative moment. Results show that in order to the arch bridge be able to carry the Type 3 loading, it needs approximately 84% (inventory) and 81% (operating) more capacity than the existing capacity. Note that for the LRFR the difference between the inventory and operating is approximately 15% versus approximately 40% for the LRF.

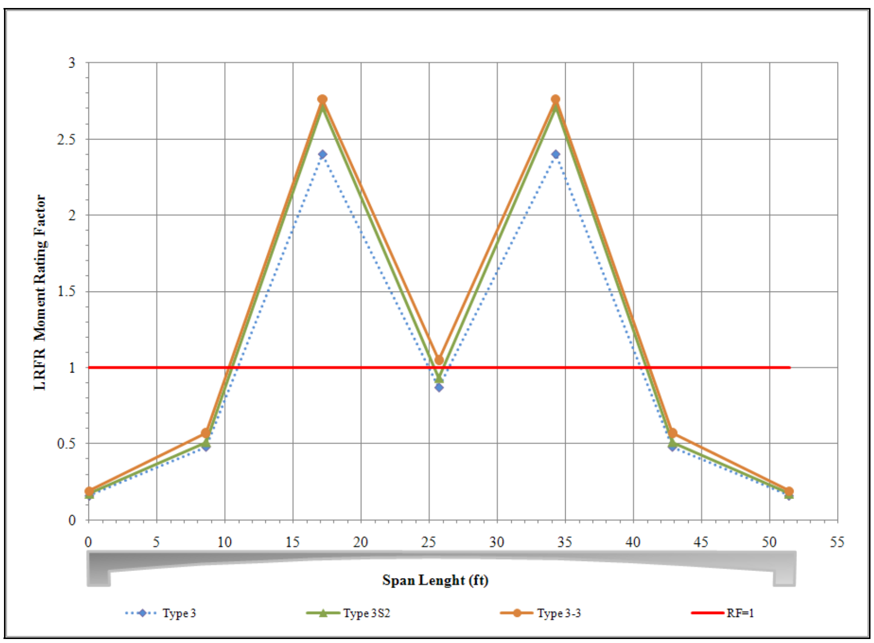

Figure 6.3.3 Flexural RF summary for the exterior beam due to the Legal Load loading, LRFR

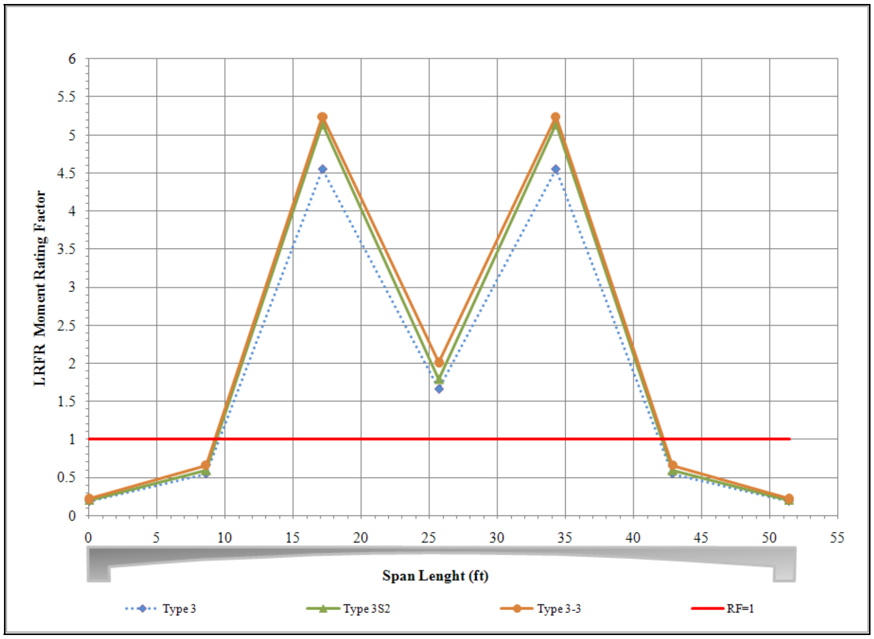

Figure 6.3.4 Flexural RF summary for the interior beam due to the Legal Load loading, LRFR

Due to the continuity between spans, the negative bending moment in the exterior arch beam controls the rating factor of the bridge under the LRFR method. It can be seen from Figure 6.3.3 and Figure 6.3.4 that the positive bending moment rating factor values are in the acceptable range. The load rating results for the positive zone tends to be 80% for the exterior and 90% for the interior higher than the ones obtained for the negative region, which confirms the poor design of the arch beam near the supports.

6.3.3 Discussion of the results

From the previous sections it can be clearly established that the bridge did not meet the minimum requirements for any of the legal load vehicles. The RF results were always less than 1.0 for the negative moment region for both arches (interior and exterior) at both the inventory and operating levels. The Type 3 legal load vehicle controlled the RF results. The exterior arch controls the capacity of the bridge since it generated the lowest values of RF overall.

6.4 Limit weight of the bridge

The purpose of the bridge rating is to provide a measure of a bridge's ability to carry a given live load in terms of a simple factor, referred to as the rating factor. These bridge rating factors can be used by bridge owners to aid in decisions about the need for load posting, bridge strengthening, overweight load allowances, and bridge closures (AASHTO, 2002).

The bridge under study was rated at the design inventory and operating level under HS20-44 and HL- 93 loads, respectively. Both design vehicles generated rating factors for bending moment and shear force less than 1.0, which means that the bridge must be evaluated under the Legal load level. After the evaluation of the legal load vehicles, the bridge rating factors remained less than 1.0. The relatively low amount of reinforcement near the support of each beam resulted in a low rating factor for negative moment on each beam. A summary of the controlling rating factors produced by the design and legal load vehicles in the exterior arch beam is shown on Table 6.4.1, for both the LFR and LRFR method.

Table 6.4.1 Summary of LFR and LRFR load rating results for the exterior beam

Vehicle Load	Load Type	Specification	RF		
			Inventory	Operating	Legal Load
Design Load	HS20-44	LFR	0.23	0.38	---
	HL93	LRFR	0.09	0.11	---
Legal Load	Type 3	LFR	0.31	0.52	---
		LRFR	---	---	0.16
	Type 3S2	LFR	0.32	0.54	---
		LRFR	---	---	0.17
	Type 3-3	LFR	0.36	0.6	---
		LRFR	---	---	0.19

Based on the results shown in the previous table, it was concluded that the bridge design does not follow current standards; thus, a limit weight sign is required to be posted in the bridge for legal loads and no permit analysis is allowed.

To establish the limit weight capacity of the bridge, each rating factor obtained from Table 6.4.1 is multiplied by the corresponding gross weight of each legal load vehicle. Table 6.4.2 shows a summary of the final recommended limit weight based on the inventory level of rating. The reason to use the inventory level of rating is to prevent future damage due to overloading. The last inspection report (discussed in Chapter 2) showed some deterioration issues in many locations in the arch beams as well as in the deck.

Table 6.4.2 Legal Load limit weight (Inventory)

Vehicle Load	Load Type	Specification	Load (Tons)
Legal Load	Type 3	LF	7
		LRFR	4
	Type 3S2	LFR	11
		LRFR	6
	Type 3-3	LFR	14
		LRFR	7

The results presented in Table 6.4.2 are not unexpected since the bridge was built in 1914 and AASHTO standards for truck loads were not published until 1935. The results show that the bridge was designed for a loading lighter than a standard H-15 vehicle, which has a gross weight of 15 tons distributed in two axles spaced at 14 ft. The H-15 corresponds to a single-unit truck, which used to be common on rural highways during the past.

The LRFR methodology provides a more structured format for load posting than the LFR, however it also allows Bridge Owners to use their own posting policies. The LRFR makes an important distinction between bridge inspections and rating, which are considered "engineering-related activities" and bridge posting, which is a "policy decision made by the Bridge Owner" (AASHTO, 2003). The recommended posting procedure outlined in the LRFR calls for bridges to be rated at the legal load level under the legal load truck in question. If the rating factor from the analysis is greater than 1.0, the bridge does not need to be posted for the given truck. If the rating factor is between 0.3 and 1.0, the AASHTO (2003) recommends the following safe posting load based on the rating factor:

$$\text{Sage Posting Load} = W/0.7*[(RF)-0.3] \qquad \textbf{6.1}$$

where,

W = Weight of rating vehicle

RF = Legal load rating factor

If the rating factor from the legal load analysis is below 0.3, AASHTO (2003) recommends restricting the legal truck used in the analysis to cross the bridge. When the rating factors for all three of the AASHTO standard legal loads is below 0.3, the bridge should be considered for closure (AASHTO 2003).

For purposes of this research, the LRFR posting recommendations were not considered since the RF values for all three legal loads were less than 0.3. The results proved that the current minimum requirements established by AASTHO exceed the capacity for which the bridge was designed about 97 years ago.

There is the option for better ways of evaluation. An accurate assessment of ADTT based on historical usage could provide a more conservative value for the LRFR legal load factor. Non-destructive and destructive tests could provide accurate material properties and confirm rebar locations. Concrete coring is one method that could be used to provide actual rather than assumed properties for the concrete and steel rebars. Ground penetration radar (GPR) could be used to identify the exact position of the principal reinforcement and eliminate uncertainties in the sections used to calculate capacities. A diagnostic load test could be performed on the bridge using a vehicle weight lower than the suggested postings to provide a better understanding of the real behavior of the bridge and a more precise load rating.

For all ratings the bridge was modeled as a composite section. Ratings are for the superstructure only. The substructure (piers and abutments) was assumed to be adequate to resist superstructure loadings. This is a typical assumption, since the substructure is normally designed to be stronger than the superstructure.

7 PARAMETRIC STUDY: FRAME ELEMENT vs. FINITE ELEMENT

7.1 Introduction

Nowadays the finite element method is the most powerful numerical technique for solving differential and integral equations associated to initial and boundary-value problems in geometrically complicated regions (Reddy, 1988).

In this study, a two-dimensional finite element model (FEM) was developed to determine the structural behavior of the Lahontan Bridge. The difficult geometry of the arch beams made the shell FEM option the most suitable to model the behavior of the bridge under different load conditions. However, a frame element formulation could be a much simpler methodology to analyze the behavior of the bridge since this kind of element only has six degrees of freedom (three translations and rotations) at each of its joints (nodes). The size of the model is further reduced when plane frames can be used. Never the less, it is necessary to verify that this simple model can be accurately predict the response for the special case of the arch beams of interest in this study.

This chapter presents a numerical parametric analysis that was carried out with the program SAP2000® to study the behavior of arch beams using frame elements. To validate the results of the analysis, a direct comparison with the full FEM was carried out to establish similarities or differences in the arch beam behavior predicted by from each model. Structural parameters such as bending moment, shear force, deflexion and the fundamental natural period were considered as validation parameters. Two different cases were analyzed:

- Case I: A statically determinate beam
- Case II: A statically indeterminate beam

These two cases were considered to determine how is the accuracy of the results, affected by the type of restraints. The results from these analyses are presented in the following sections.

7.2 Frame Section Properties

The span length of the beam was taken equal to 25 ft long for the two cases considered. To accommodate the effect of the variation of the cross sectional area, each beam was divided into five elements of equal length, as shown in Figure 7.2.1. This figure shows the model created in the program SAP2000® for the case I. By dividing the beam into five elements, it was possible to assign different cross sectional properties at different locations along the beam to simulate the shape of an arch. The height of the section was the only parameter that varied from section to section.

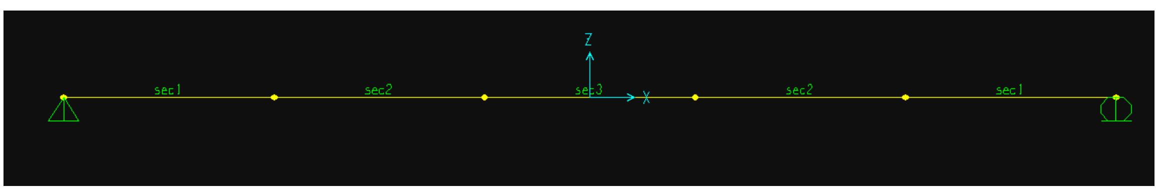

Figure 7.2.1 Model of the simple supported beam

Table 7.2.1 shows the cross sectional properties of the frame element sections used in the parametric study. The only property that varied was the height of each frame element.

Table 7.2.1 Frame Section Properties

Frame	Height (ft)	Width (ft)	Length (ft)	Area (in^2)
Section-1	5.0	0.83	5.0	600
Section-2	4.0	0.83	5.0	480
Section-3	3.0	0.83	5.0	360

The beam's self weight or dead load (DL) was the load condition used to study the beam behavior in flexion and shear. The following reinforced concrete mechanical properties were used in the frame model:

- Compressive strength, f'_c = 4000 psi
- Unit weight, γ_c = 150 pcf
- Modulus of elasticity, E_c = 3,600 ksi

7.3 Case I: Statically determinate beam

A simple supported beam was used to consider a statically determinate case. In this case one end is pinned and the other is restrained using a roller. Two cases were investigated under this condition: the first case represents a beam with a variable section but with the centroid lying on a same straight line. For simplicity, this case will be referred to as the uniform centroid case. The second case represents a beam with a variable section but the vertical position of the centroid change from element to element. Of course, for each individual element the centroid are aligned. From now on, this case will be called the non-uniform centroid case.

A tool available in SAP2000® called "insertion point" (IP) was employed to account for the change in cross sectional area and to replicate the arch shape of the original beam. This tool locates the center of gravity (i.e., the neutral axis) of the frame section at different positions to thus allowing the user approximately represent the characteristics of an arch beam. The insertion point was assigned to the frame sections Sec2 and Sec3, as it is discussed later on in this chapter.

7.3.1 *Beam with varying depth and uniform centroid*

The cross sectional area of the beam was manually altered along the span length. According to the traditional matrix stiffness method (implemented in SAP2000®), the neutral axis of the section remains the same in the entire span, always at H/2*,* where H is the total height of the element. Figure 7.3.1 displays the SAP2000® model with uniform centroid. The dotted line represents the location of the centroid of each element.

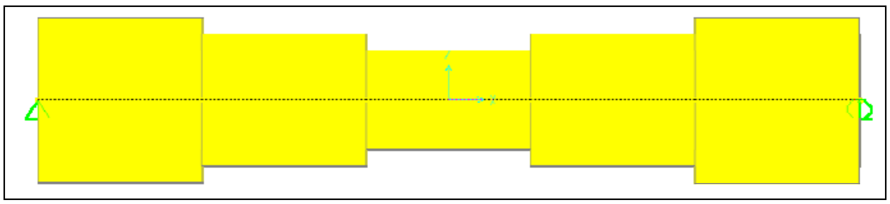

Figure 7.3.1 Extruded view of the beam with uniform centroid

The model was analyzed as a 2D structure, in which only vertical displacements rotations around the *Y* axis were allowed. The horizontal displacements were not restrained but they are null because of the type of loading used. Figure 7.3.2 shows an example of the deformed shape of the beam due to the dead load (DL).

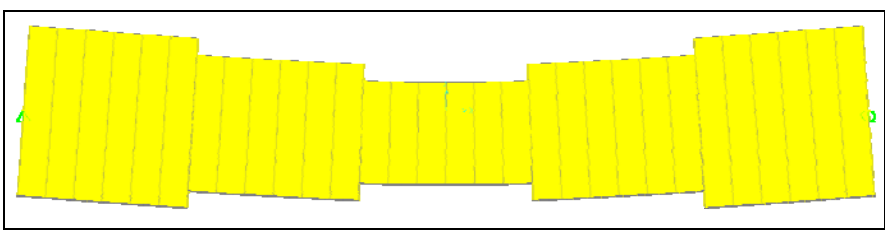

Figure 7.3.2 Deformed shape due to DL for a beam with uniform centroid

It can be observed from the results of the analysis shown in Figure 7.3.3 and Figure 7.3.4 that the maximum value of the bending moment was 36.94 k-ft and 6.56 kip for the shear force. Using these results from the analysis and the formula for the maximum bending moment ($M = wL^2/8$) for a simple support beam, and solving the equation for the uniformly distributed weight (w) a value of 0.47 k/ft was obtained. Using the maximum shear from the diagram and considering the formula for the maximum shear force (V =

wL/2), a value of 0.52 k/ft was obtained. Comparing these two results there is a 9.6% difference, which is attributed to the non-uniformity of the load distribution of the beam's self weight. In this case the deflection at mid-span was 0.018 in. and the fundamental natural period was 0.03917 sec.

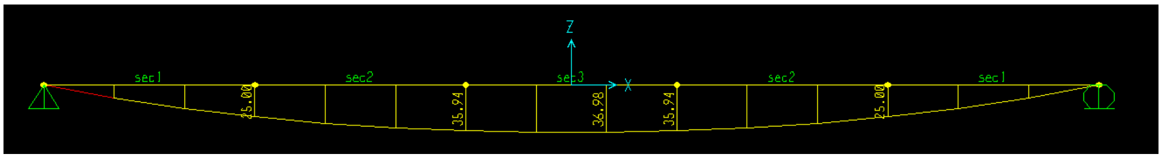

Figure 7.3.3 Moment diagram (k-ft) due to self weight for beam with uniform centroid

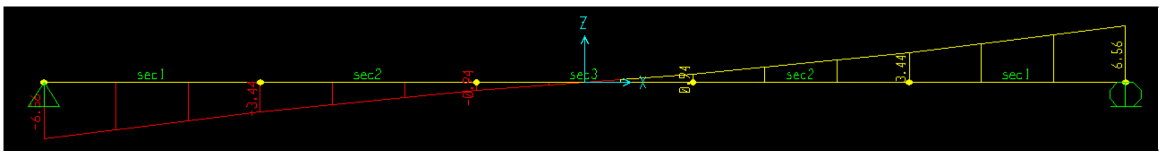

Figure 7.3.4 Shear diagram (kip) due to self weight for beam with uniform centroid

7.3.2 Beam with varying depth and non -uniform centroid

The cross sectional area of the beam was manually altered along the span length, as it was done for the previous case of uniform centroid. The "insertion point" feature of SAP2000® was used to move 0.5 ft upwards the centroid of Section-2 and 1 ft upward that of Section-3 from their original positions. It can be observed from Figure 7.3.5 that all the beam elements are even at the top. Note that, as expected, the dotted line, which represents the location of the centroid, varies with respect to the span height along the beam. The model was analyzed as a 2D structural system and thus only displacements along the X and Z axes and rotation around the Y axis were allowed.

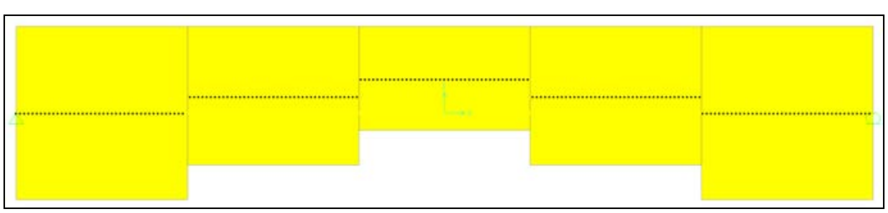

Figure 7.3.5 Extruded view of the beam with non-uniform centroid

Figure 7.3.6 shows the deformed shape of the beam due to the dead load, which produces a maximum deflection of 0.018 in. From the moment and shear diagrams shown in Figure 7.3.7 and Figure 7.3.8, it can be observed that the maximum value of the flexural moment was 36.94 k-ft and 6.56 kip was the maximum shear force. Based on the modal analysis of the beam, the fundamental natural period was 0.03917 sec.

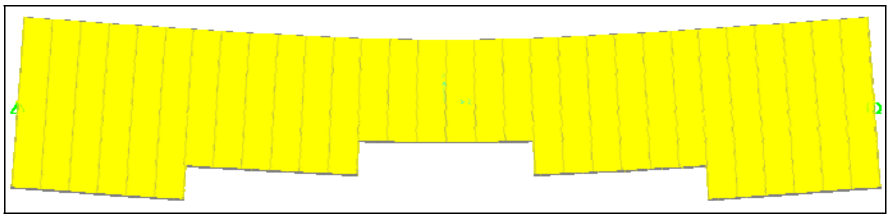

Figure 7.3.6 Deformed shape due to DL for a section with non-uniform centroid

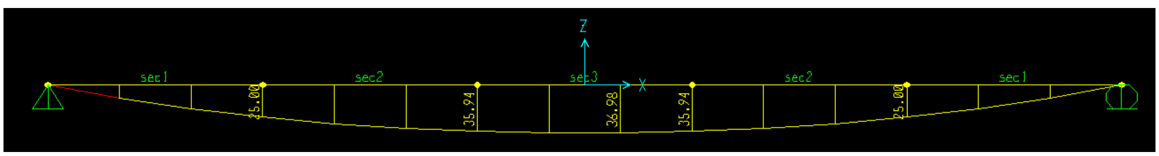

Figure 7.3.7 Moment diagram (k-ft) due to self weight for beam with non-uniform centroid

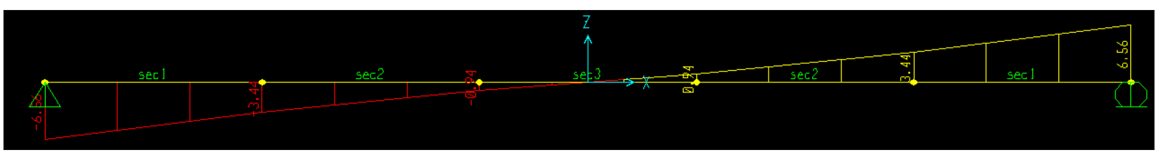

Figure 7.3.8 Shear diagram (kip) due to self weight for beam with non-uniform centroid

7.3.3 Discussion of results of the statically determinate beam model

No significant difference was observed between the model with a uniform centroid and the model with a non-uniform centroid. Table 7.3.1 summarizes the maximum responses and the period obtained for both cases. Note that the only appreciable difference between the models was the natural period of the beam corresponding to the first mode of vibration. The beam with the non-uniform centroid has a 1.38% higher fundamental period than that for the beam with uniform centroid.

Table 7.3.1 Summary of the response - Statically determinate beam models

Case	Moment (k-ft)	Shear (kip)	Displacement (in)	Period (sec)
Uniform centroid	36.97	0.93	-0.018	0.03917
Non-uniform centroid	36.97	0.93	-0.018	0.03972

This behavior was expected because as established by basic Statics principles the position of the centroid does not have any influence on the structural behavior of statically determinate structures (i.e., the bending moments and shears only depend on the global geometry and the loads).

7.4 Case II: Statically indeterminate beam

In order to consider a simple statically indeterminate structure, a clamped-clamped beam model was used. Only displacements in the X-Z plane and rotation around the Y axis are allowed. Two cases were considered, the first case is a beam with a variable section and uniform centroid, and the second case represents a beam with a variable section but non-uniform centroid. To represent the variation of the location of the centroid for the second case in the frame model, an insertion point (a SAP2000® tool) was assigned to the frame section-2 and 3.

7.4.1 Beam with varying depth and uniform centroid

Beam sections with different cross sectional areas were assigned to the different elements of the beam model created in SAP2000®. By default, the program SAP2000® arrange the elements such that the neutral axis of the different sections remains horizontal along the entire span (always at *H/2,* where *H* is the total height of the element). The resulting model is shown in Figure 7.4.1. Note that the middle element of the beam (Section-3) was divided into four smaller sub elements. This was done to obtain more precise results for the bending moments and displacements at mid-span.

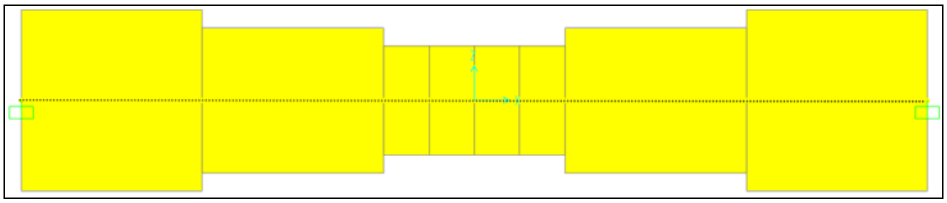

Figure 7.4.1 Fixed-ends beam with a uniform centroid

The beam deflection due to the dead load (DL) is shown in Figure 7.4.2. For this case the maximum displacement was -0.00275 in. Figure 7.4.3 shows the bending moment diagram. It can be observed that the maximum moment (which occurs at the support) was -30.44 k-ft, whereas it is 6.67 k-ft at mid-span. The maximum shear force value was 6.56 kip, as shown in the shear force diagram displayed in Figure 7.4.4.

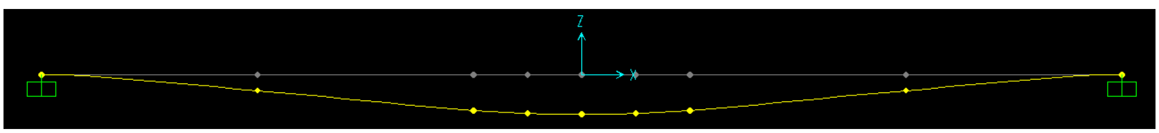

Figure 7.4.2 Deflection due to DL for the fixed-ends beam with uniform centroid

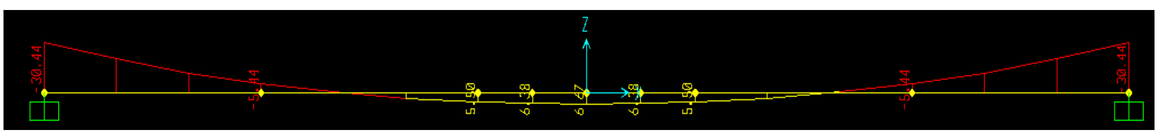

Figure 7.4.3 Moment diagram (k-ft) due to DL for the fixed-ends beam with uniform centroid

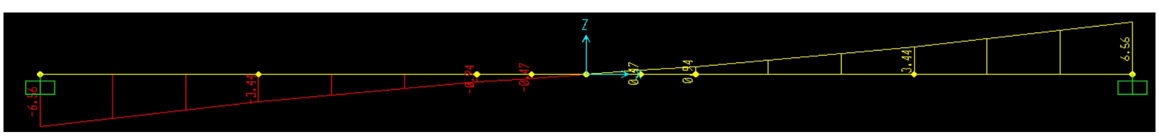

Figure 7.4.4 Shear diagram (kip) due to DL for the fixed-ends beam with uniform centroid

7.4.2 Beam with varying depth and non-uniform centroid

As it was done previously for the case with the uniform centroid, beam sections with different depths were assigned to the elements to simulate an arch beam. However, here the use of the "insertion point" tool was required to move the centroid of the second, third and fourth elements. In particular, the centroid of Section-2 was moved up 0.5 ft and that of Section-3 was shifted 1 ft upwards from their original positions. The model obtained with this procedure is displayed in Figure 7.4.5. The dotted line represents the location of the centroid of each frame section.

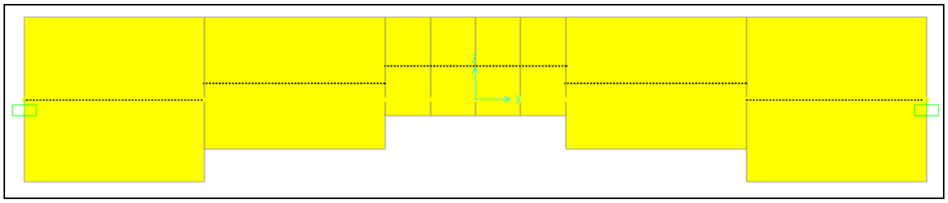

Figure 7.4.5 Fixed-ends beam with a non-uniform centroid

The beam was analyzed in 2D: only displacements along the X and Z axes and rotation about the Y axis were allowed. The deformed shape of the beam is shown in Figure 7.4.6. The maximum displacement at mid-span was -0.00256 in. The deformed shape requires an explanation: First, the apparent discontinuities at the nodes of the elements is due to the fact that the program is displaying the displacement of different points along the cross sections. Second, the maximum displacements occur at the central elements, although because of the same reason the picture may seem to indicate otherwise.

The bending moment diagram is displayed in Figure 7.4.7. The maximum moment at support was -29.08 k-ft and at mid-span was 5.86 k-ft. The maximum shear force, shown in the diagram in Figure 7.4.4 was 6.56 kip.

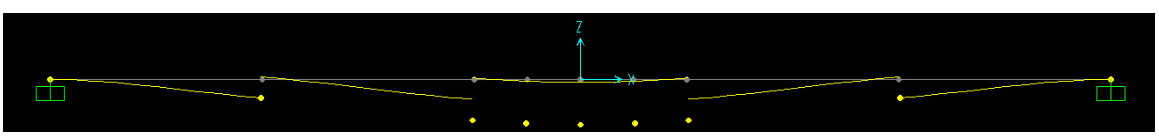

Figure 7.4.6 Displacement due to DL for the beam with fixed-ends and non-uniform centroid

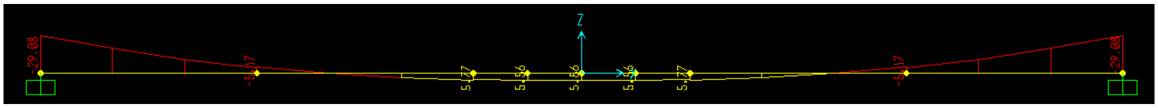

Figure 7.4.7 Moment diagram (k-ft) due to DL for the beam with fixed-ends and non-uniform centroid

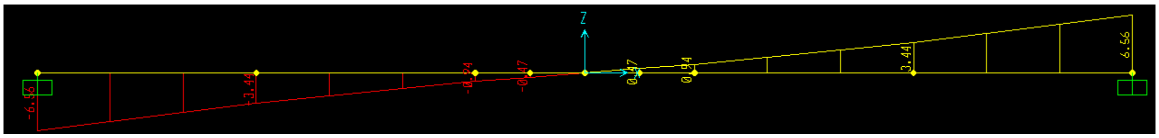

Figure 7.4.8 Shear diagram (kip) due to DL for the beam with fixed-ends and non-uniform centroid

7.4.3 Discussion of results of the statically indeterminate beam model

Table 7.4.1 presents a summary of the responses obtained with the uniform centroid and non-uniform centroid models of the statically indeterminate beam. It can be observed that there are some small differences between the results drawn from the two models. In terms of the deflection, the model with the uniform centroid is 6.9% more flexible that the non-uniform model. With regard to the positive bending moment the difference found between the models was 12.44% whereas for the negative moment the difference was 4.46%. No differences were observed for the shear force response between the two models. This demonstrates that the shear force is not affected by the position of the centroid as the flexural moment is. The natural period of the first vibration mode is 3% higher for the case with the uniform centroid compared to the one for the non-uniform centroid. This confirms that the model with the uniform centroid tends to be less rigid than the non-uniform one. It is a well known fact when one model a structure with different FEM, the more restrained is the model of the structure the greater are the natural periods because the system becomes more rigid.

Table 7.4.1 Summary of the response - Statically indeterminate beam models

Case	+Moment (k-ft)	- Moment (k-ft)	Shear (kip)	Displacement (in)	Period (sec)
Uniform Centroid	6.67	-30.44	6.56	-0.00275	0.01481
Non-uniform Centroid	5.86	-29.08	6.56	-0.00256	0.01434

7.5 Shell Elements

To determine how accurate are the results obtained from the simplified models in estimating the behavior of an arch beam, a comparison was made with the results using a shell FEM. The same beam geometry considered in previous analysis was used to create the FEM, but here the bottom arch can be accurately represented by using a fine mesh. The arch beam discretized with shell finite elements is shown in Figure 7.5.1. The span length, beam thickness and the height of the beam at the support and mid-span locations were the same for all the models. At both end edges, pin supports were used on each node to represent the fixed ends condition.

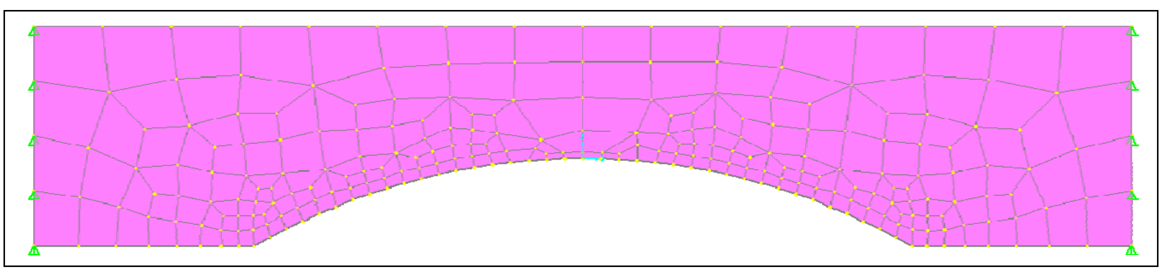

Figure 7.5.1 Shell element model

A total of 214 shell elements were used in the model which had 254 nodes. The structural behavior of the beam was analyzed considering only the beam's self weight action. The results from the FEM analysis in terms of the maximum internal forces and deflection as well as fundament natural period are summarized in Table 7.5.1. The moment and shear forces were determined by means of the "section cut" feature of SAP2000®.

Table 7.5.1 Shell element model

Case	+Moment (k-ft)	- Moment (k-ft)	Shear (kip)	Displacement (in)	Period (sec)
Shell Elements	5.66	-28.31	6.52	-0.00237	0.01337

Figure 7.5.2 shows graphically the beam deflection. The maximum value of deflection was -0.00237 and it occurred at mid-span as expected.

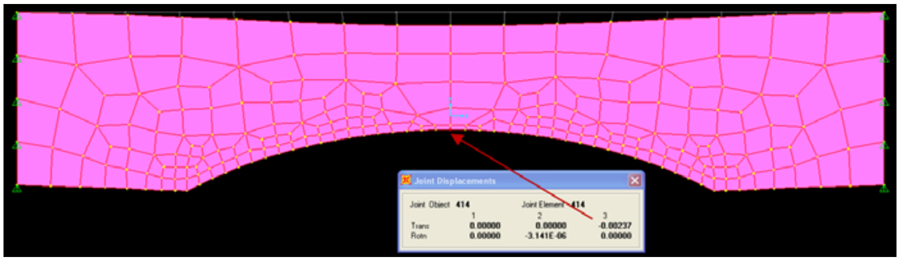

Figure 7.5.2 Beam deflection due self weight

Figure 7.5.3 and Figure 7.5.4 are examples of the negative and positive moment calculation using the “section cut” tool of SAP2000® from the stress contour diagram measured on the S_{xx} direction. The values are in the units of kips per feet in both figures. The contours in the figure show the high stress zone at top and bottom of the supports as expected.

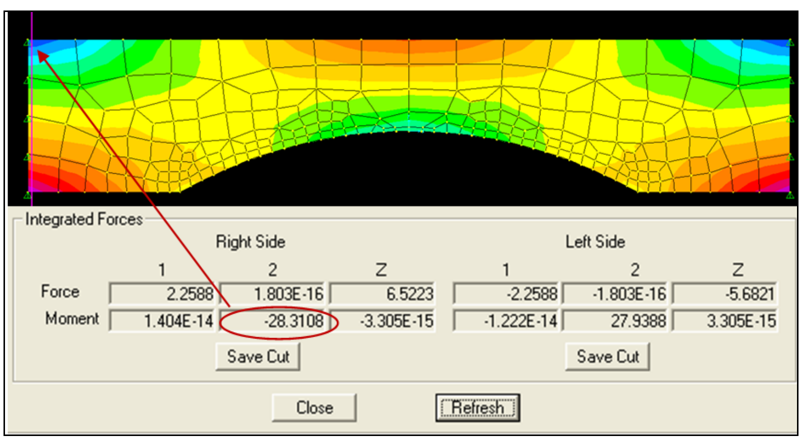

Figure 7.5.3 Negative moment on the FEM of the fixed-ends beam

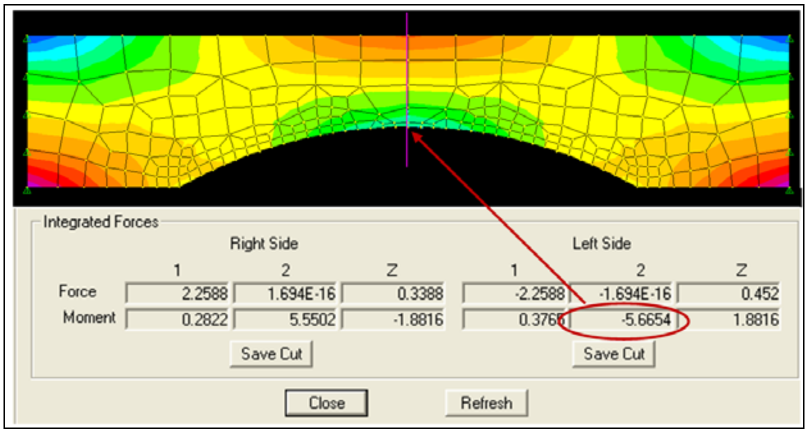

Figure 7.5.4 Positive moment on the FEM of the fixed-ends beam

By visual inspection it can be noticed the differences in the structural behavior of the prismatic beam (Figure 7.5.5) and the arch beam (Figure 7.5.4). It is interesting to compare the stress distribution in a beam with uniform section with that in the arch beam. Figure 7.5.5 displays the normal stress (S_{xx}) in a prismatic beam with the same length and maximum cross section than the arch beam. The prismatic beam has two lines of symmetry along the X and Z axes, which means that the stress values at both sides of the X axis are equal in magnitude but opposite on direction (Figure 7.5.5). Evidently this behavior does not occur on the arch beam (Figure 7.5.4.) due the variation of the section properties.

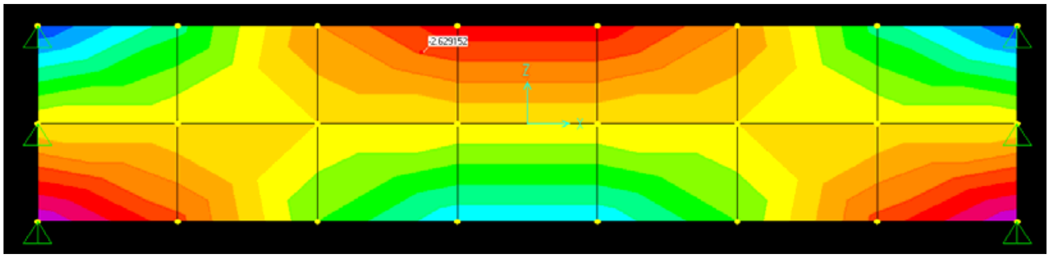

Figure 7.5.5 Stress distribution for a rectangular beam

7.6 Parametric Study Analysis

The intention in conducting this parametric study was to investigate whether there is a simpler way to analyze the behavior of arch beams. Comparing the results of the statically indeterminate beam analysis from each of the cases studied previously some important conclusions can be made. For example, the beam model that best matched the structural behavior of the shell FEM was the one with the non-uniform centroid. Table 7.6.1 summarizes the results of the different response parameters considered in the study. The results obtained from the beam model with the non-uniform centroid showed a reduction in stiffness of approximately 6.76% in comparison with the FEM with shell elements. For the negative and positive flexural moment the difference found was in the range of 2.65% to 5.3%, respectively. Observing Table 7.6.1 it can be noted that the shear forces are not significantly affected since the difference between models was less than 1%. Regarding the maximum displacement, which in both cases occurred at mid-span, a 7.42% difference was observed.

Table 7.6.1 Frame elements vs. Shell elements

Response	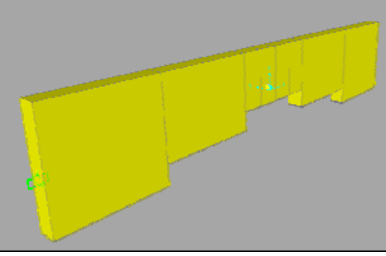	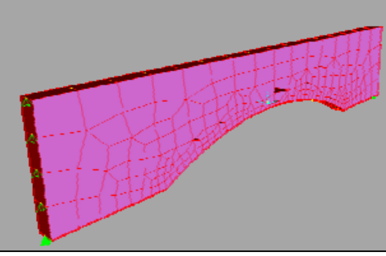
Max. displacement	-0.00256 in	-0.00237 in
Fundamental period	0.01434 sec	0.01337 sec
Negative bending moment	-29.08 k-ft	-28.31 k-ft
Positive bending moment	5.86 k-ft	5.55 k-ft
Shear force	6.56 kip	6.52 kip

The parametric study proved that the simplified frame model, which required the analysis of beams with variation in cross sectional area, can be used for future investigations. In general, a good agreement was obtained between the models.

8 CONCLUSIONS AND RECOMMENDATIONS

8.1 Summary

This thesis presented the results of a research carried out to determine the live load capacity of the Lahontan arch bridge. The bridge is 97 years old and consists of five continuous spans where each span has three cast-in-place reinforced concrete arch beams. At the time of the development of this study the bridge had been closed for almost two years due its uncertain structural conditions. Structural cracks were present on several locations along the bridge. They were documented by means of a detailed visual inspection carried out by the author.

Do to the complexity of the geometry, a finite element model (FEM) was developed using the structural analysis software SAP2000 to study in detail the behavior of the arch beams under different load scenarios. Results from the FEM showed that the use of arch beams on bridges decrease the moments and shear forces demand loads drastically in comparison with rectangular beams.

The safe live load capacity of the bridge was determined using two different rating factor methods, namely the LRF and LRFR. Both methods proved that the bridge does not have the capacity to hold the demand load of the current design and legal load vehicles.

As an alternative to the detailed FEM based on shell elements, the use of simpler frame elements was studied. The continuous variation in height of the arch beam was approximately by using several uniform elements. The fact that the neutral axis (or position of the centroid) should changes from element to element was accounted for using a feature of SAP2000.

A parametric study was carried out to verify that the frame elements can be used to study the behavior the arch beam in future studies. Results from the frame model showed a different of less than 10% in comparison with the shell FEM.

8.2 Conclusions

The main conclusions drawn from this study include:

- The variation in cross sectional area in the arch beam produces a decrease in both the negative and positive moment. For the Lahontan Bridge the gradual reduction in cross sectional area tends to decreased significantly the positive bending moment in approximately 80% compared with the negative moment. Results from the dead load analysis showed that for a continuous arch beam with a haunch lineal height ratio between 0.18-in/in to 0.20-in/in the positive moment is 20% lower and the negative moment is 53% lower than those obtained for a rectangular beam with no changes in cross sectional area. However, the shear force did not showed a significant change in behavior on the arch beam in comparison whit a beam with uniform cross sectional area.
- Due to the difference on the web width and to the amount of tension steel, the interior arch beam has 43% higher moment capacity for the negative zone, 60% for the positive zone, and 40% higher shear capacity in comparison with the exterior beam.
- The finite element model was a key tool in the study of live load capacity of the Lahontan bridge. The demands obtained from the 2D analysis using shell

elements to model the arch beams were the input values to the load rating equations.

- Both methods from AASHTO, the LRF and the LRFR established that the exterior arch beam control the bridge live load capacity. Due to the relatively low amount of longitudinal reinforcement near the support the negative moment controls over shear the rating factors. At the design inventory and operating level, both design vehicles HS20-44 and HL- 93 generated rating factors for bending moment and shear force less than 1.0. After the evaluation of the legal load vehicles, the bridge rating factors remained less than 1.0 therefore forcing the bridge to a restrictive limit weight.
- Examination of the results from the load rating analysis lead to the conclusion that the bridge was designed for a vehicle load close to the H-15 truck loading.
- The results obtained from the frame model with non-uniform centroids showed that the use of the “insertion point” tool from SAP2000 (to move the element’s centroids) produce accurate results. Therefore, it is possible in future studies to estimate the structural behavior of arch beams using a simple frame model. A reduction in stiffness of approximately 6.8% was obtained between the frame model and the shell FEM. These results were obtained by dividing the beam into 5 elements. Evidently, more accurate results can be obtained using more elements.

8.3 Recommendations for Future Work

The main recommendations for future work include the following:

- To improve the rating factors results of the bridge, an accurate assessment of the Annual Average Daily Traffic (ADTT) based on historical usage could provide a more conservative value of the load factor for the LRFR method.
- Non-destructive and destructive tests could provide accurate material properties and confirm rebar locations. Concrete coring is one method that could be used to provide actual rather than assumed properties for the concrete and steel rebars. Ground penetration radar (GPR) could be used to identify the exact position of the principal reinforcement and eliminate uncertainties in the sections used to calculate capacities.
- A diagnostic load test could be performed on the bridge using a vehicle weight lower than the suggested postings to provide a better understanding of the real behavior of the bridge and validate the FEM.

REFERENCES

AASHTO (1994). “AASHTO Manual for the Condition Evaluation of Bridges (MCEB)”, Second Edition, with revisions through 2003. Washington, D.C.

AASHTO (2002). “Standard Specifications for Highway Bridges”, 17th Edition. American Association of State Highway and Transportation Officials, Washington, D.C.

AASHTO (2003). “AASHTO Manual for Condition Evaluation and Load and Resistance Factor Rating (LRFR) of Highway Bridges”. Washington, D.C.

AASHTO (2004). “AASHTO LRFD Bridge Design Specifications”, U.S. Customary and SI Units, Third Edition, Washington, D.C.

ACI - 318 (2008). “American Concrete Institute, Building Code Requirements for Structural Concrete and Commentary”, Farmington Hills, Michigan.

Boothby, T.E. (2001). “Analysis of masonry arches and vaults”. Progress in Structural Engineering and Materials, 3, 246-256.

Boothby, T.E., and Fanning, P. (2004). "Load Rating of Masonry Arch Bridges: Refinements". *American Society of Civil Engineers* Journal, Vol. 9, No. 3, 304-307.

Chajes, M. (2002). “Load Rating of Arch Bridges”. Delaware Center for Transportation, University of Delaware, October 2002.

DelDOT (2005). “Delaware Department of Transportation Bridge Management Manual”. Second Edition. Dover, Delaware.

FHWA (1995). "Recording and Coding Guide for Structure Inventory and Appraisal of the Nation’s Bridges". FHWA-PF-96-001. Washington, D.C.

FHWA-Bridge Programs NBI Data. (2008). “Tables of Frequently Requested NBI Information, Deficient Bridges by State and Highway System”.

Garrett, P. (2007). “Analytical Load Rating of an Open-Spandrel Arch Bridge: Case Study”. *American Society of Civil Engineers* Journal, Vol. 12, No. 13, 13-20.

Halden, D. (1995). “Performance Criteria in Arch Bridge Assessment.” *Arch Bridges: Proceedings of the First International Conference on Arch Bridges,* Bolton, UK Thomas Telford, London, 439-448.

Kong, F., (1935). “Reinforced Concrete Deep Beams”, Taylor and Francis Books Inc, Van Nonstrand Reinhold, New York, USA, 2002.

Lichtenstein Consulting Engineers, Inc. (2001). “NCHRP Web Document 28: Contractor’s Final Report: Manual for Condition Evaluation and Load Rating of Highway Bridges Using Load and Resistance Factor Philosophy.” *Transportation Research Board Project No. C12-46*, Paramus, NJ.

Marefat, M.S., Ghahremani, E., and Atae, S. (2004). “Load test of a plain concrete arch railway bridge of 20-m span”. *Journal of Construction and Building Materials* , Vol. 18, 661–667.

Murdock, M., (2009). “Comparative Load Rating Study under LRFR and LFR Methodologies for Alabama Highway Bridges”, M. of Science Thesis, Auburn University, Alabama.

National Transportation and Safety Board (2008). “Collapse of I-35W Highway Bridge, Minneapolis, Minnesota”, Highway Accident Report NTSB/HAR-08/03. Washington D.C.

Nawy, E. G. (2002). "Reinforced Concrete: A Fundamental Approach", *Prentice Hall*, Fifth Edition, June 2002. Upper Saddle River, New Jersey.

Paultre, P., and Chaalial, O. (1992). “Bridge Dynamics and Dynamic Amplification Factors – a Review of Analytical and Experimental Findings.” *Canadian Journal of Civil Engineering*, Vol. 19, 260-278.

Reddy, J.N. (1988). “Mechanics of Composite Structures”. *Finite Element Analysis for Engineering Design*, Springer, Berlin, 338–359.

SAP2000, (2010). “Structural Analysis Program”, Computers and Structures, Inc., V.14.2, Berkeley, California.

U.S. Army (2002). "U.S. Army Military Nonstandard Fixed Bridging Field Manual, FM 3-34.343". Headquarters, Department of the Army, Washington, D.C.

U.S. Army Corps of Engineers, Sacramento District. (2009). "Initial Inventory Bridge Inspection Report, Lahontan Dam Spillway Bridges, Fallon, Nevada". U.S. Bureau of Reclamation, Mid-Pacific Region. Sacramento, California.

Whitney, C. S. (1942). "Plastic Theory of Reinforced Concrete Design", Transactions of the ASCE, Vol. 107, 251-326.

APPENDIX A LIVE LOAD DESCRIPTIONS

Standard AASHTO legal load and notional design vehicles will be referred to frequently in this report. The different configurations are defined as follows:

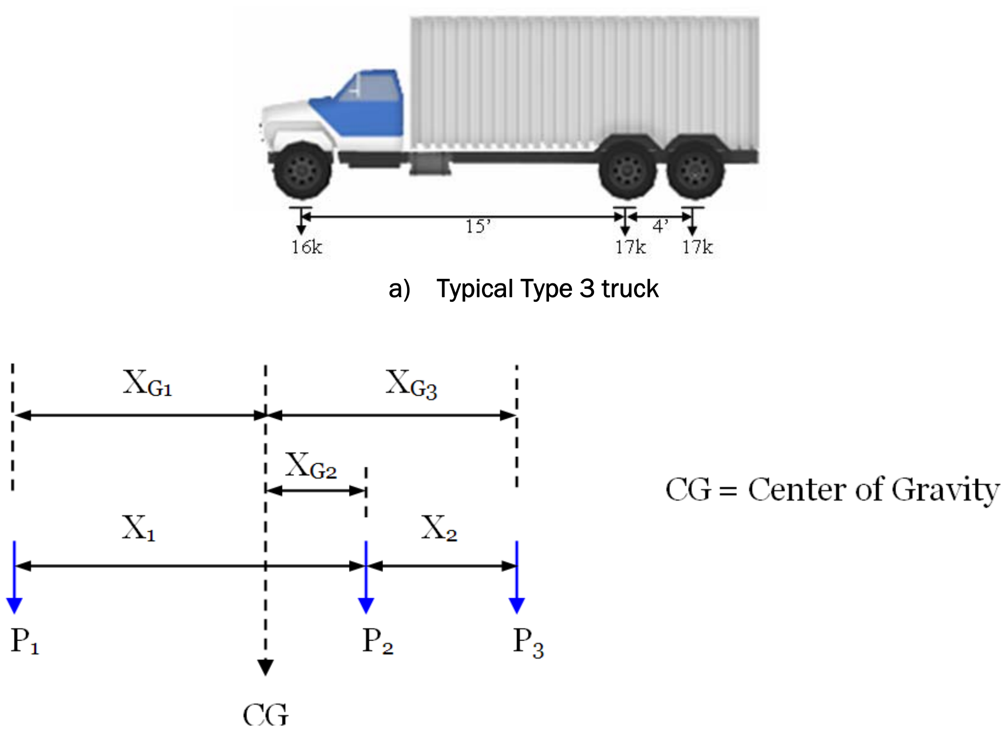

a) Typical Type 3 truck

b) Loads and dimensions for use with Table A-1

Figure A. 1 AASHTO Type 3

Table A. 1 AASHTO Type 3 - Loading & Dimensions

Loading Data – AASHTO Type 3 Total Weight = 50 kips (25 Tons)			
Axle Loads (k)	P_1	P_2	P_3
	16	17	17
Dimensions – AASHTO Type 3			
Longitudinal Spacing (ft)	X_1	X_2	
	15	4	
Distance to Center of Gravity (ft)	X_{G1}	X_{G2}	X_{G3}
	11.56	3.44	7.44

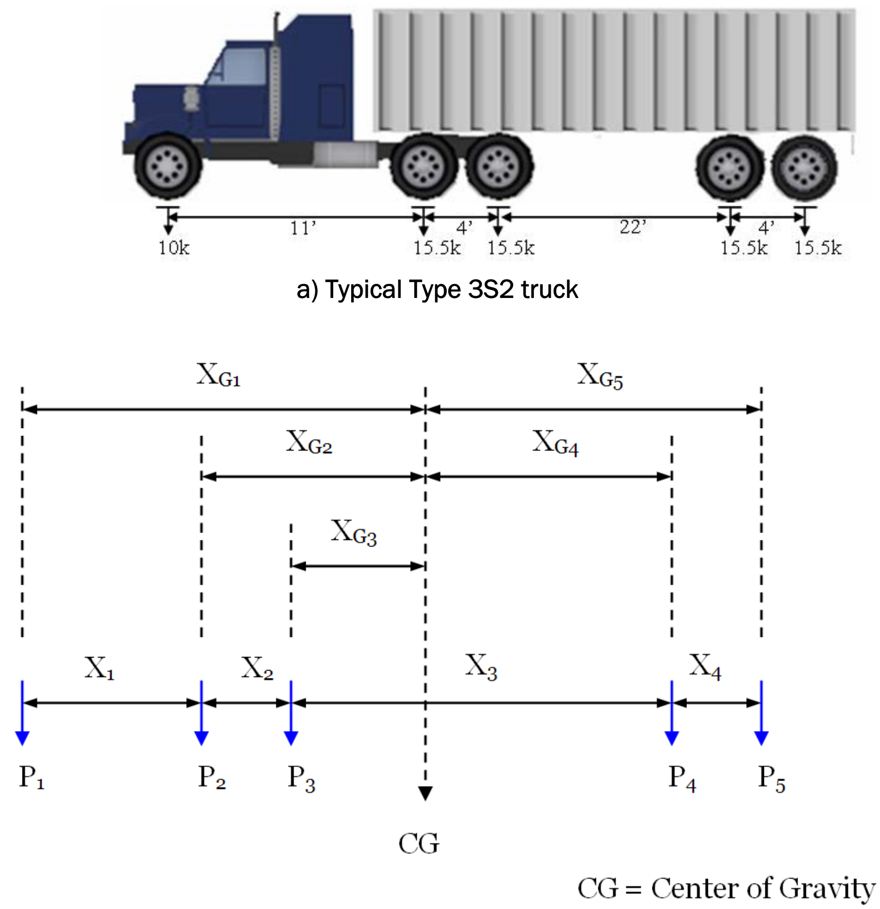

b) Loads and dimension for use with Table A-2

Figure A. 2 AASHTO Type 3S2

Table A. 2 AASHTO Type 3S2 - Loading & Dimensions

<table>
<tr><td colspan="21">Loading Data – AASHTO Type 3S2
Total Weight = 72 kips (36 Tons)</td></tr>
<tr><td rowspan="2">Axle Loads (k)</td><td colspan="4">P₁</td><td colspan="4">P₂</td><td colspan="4">P₃</td><td colspan="4">P₄</td><td colspan="4">P₅</td></tr>
<tr><td colspan="4">10</td><td colspan="4">15.5</td><td colspan="4">15.5</td><td colspan="4">15.5</td><td colspan="4">15.5</td></tr>
<tr><td colspan="21">Dimensions – AASHTO Type 3S2</td></tr>
<tr><td rowspan="2">Longitudinal Spacing (ft)</td><td colspan="5">X₁</td><td colspan="5">X₂</td><td colspan="5">X₃</td><td colspan="5">X₄</td></tr>
<tr><td colspan="5">11</td><td colspan="5">4</td><td colspan="5">22</td><td colspan="5">4</td></tr>
<tr><td rowspan="2">Distance to Center of Gravity (ft)</td><td colspan="4">X_{G1}</td><td colspan="4">X_{G2}</td><td colspan="4">X_{G3}</td><td colspan="4">X_{G4}</td><td colspan="4">X_{G5}</td></tr>
<tr><td colspan="4">22.39</td><td colspan="4">11.39</td><td colspan="4">7.39</td><td colspan="4">14.61</td><td colspan="4">18.61</td></tr>
</table>

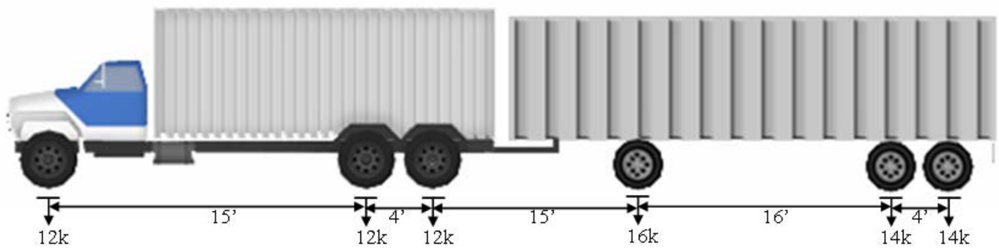

a) Typical Type 3-3 truck

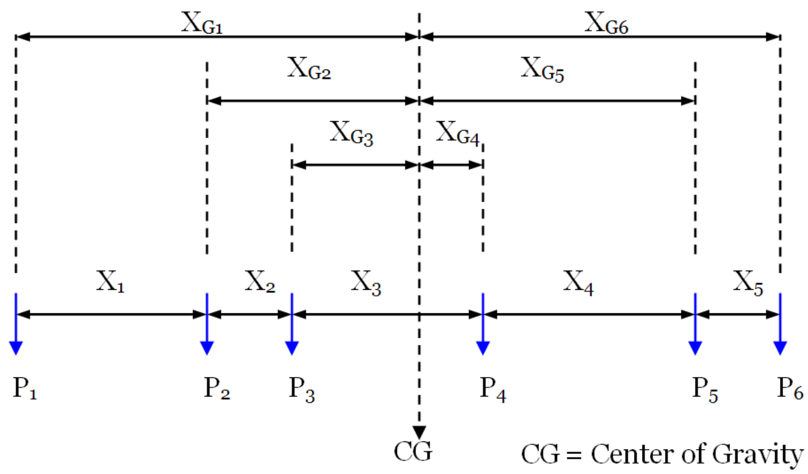

b) Loads and dimension for use with Table A-3

Figure A. 3 AASHTO - Type 3-3

Table A. 3 AASHTO Type 3-3 - Loading & Dimensions

Loading Data – AASHTO Type 3-3 Total Weight = 80 kips (40 Tons)						
Axle Loads (k)	P_1	P_2	P_3	P_4	P_5	P_6
	12	12	12	16	14	14
Dimensions – AASHTO Type 3-3						
Longitudinal Spacing (ft)	X_1	X_2	X_3	X_4	X_5	
	15	4	15	16	4	
Distance to Center of Gravity (ft)	X_{G1}	X_{G2}	X_{G3}	X_{G4}	X_{G5}	X_{G6}
	30.1	15.1	11.1	3.9	19.9	23.9

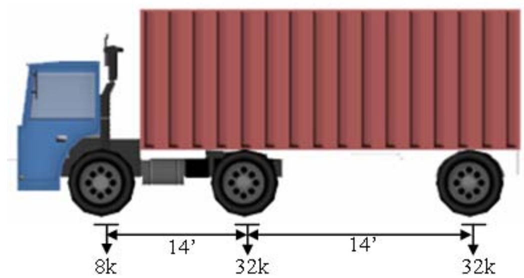

a) Typical HS20-44 truck

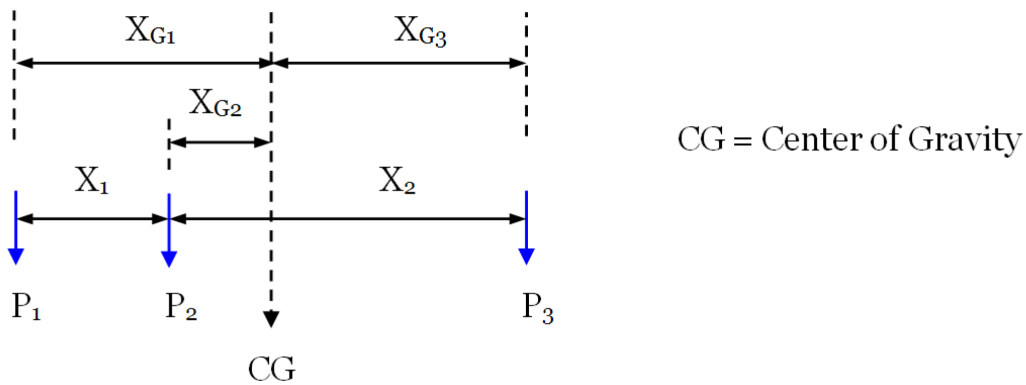

b) Loads and dimensions for use with Table A-4

Figure A. 4 AASHTO notional vehicles:HS25-44, HS20-44 & HS15-44 (1994)

Table A. 4 AASHTO HS25-44, HS20-44 & HS15-44 - Loading & Dimensions

Loading Data – AASHTO HS20-44 & HS15-44 Total Weight HS25-44 = 90 kips (45 Tons) Total Weight: HS20-44 = 72 kips (36 Tons) Total Weight: HS15-44 = 54 kips (27 Tons)						
Axle Loads (k)	P_1		P_2		P_3	
HS25-44	10		40		40	
HS20-44	8		32		32	
HS15-44	6		24		24	
Dimensions – AASHTO HS20-44 & HS15-44						
Longitudinal Spacing (ft)	X_1		$X_{2\ MIN.}$		$X_{2\ MAX.}$	
HS25-44, HS20-44 & HS15-44	14		14		30	
Distance to Center of Gravity (ft)	Minimum			Maximum		
	X_{G1}	X_{G2}	X_{G3}	X_{G1}	X_{G2}	X_{G3}
HS25-44, HS20-44 & HS15-44	18.67	4.67	9.33	25.78	11.78	18.22

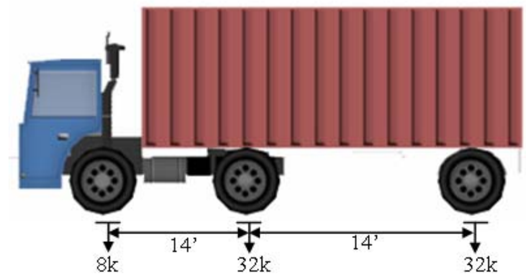

a) Typical design truck

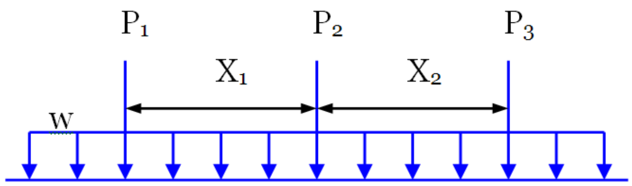

b) Loads and dimensions for use with Table A-5

Figure A. 5 HL-93 (Design Truck with Lane Load) (AASHTO 2003)

Table A. 5 HL-93 (Design Truck with Lane Load) - Loading & Dimensions (AASHTO 2003)

Loading Data – HL-93 (Design Truck with Lane Load)			
Axle Loads (k)	P_1	P_2	P_3
	8	32	32
Uniform Lane Load (klf)	0.64		
Dimensions – HL-93 (Design Truck with Lane Load)			
Longitudinal Spacing (ft)	X_1	X_2	
	14	14 to 30	

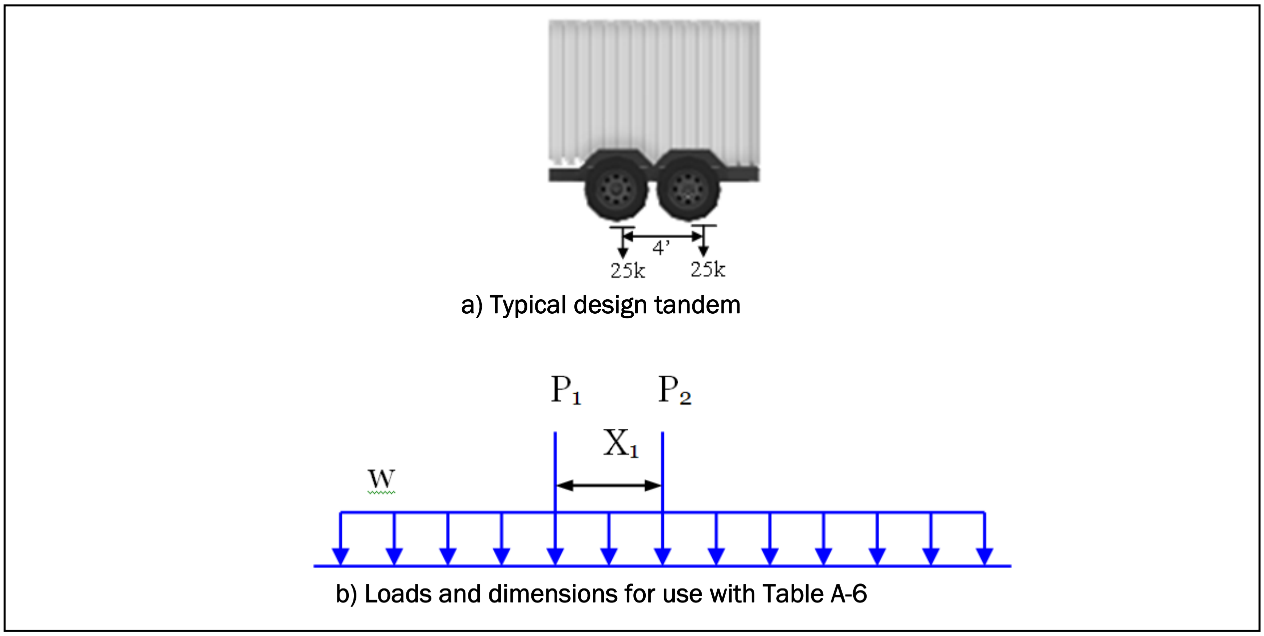

Figure A. 6 HL-93 (Design Tandem with Lane Load) (AASHTO 2003)

Table A. 6HL-93 (Design Truck with Lane Load) - Loading & Dimensions (AASHTO 2003)

Loading Data – HL-93 (Design Tandem with Lane Load)		
Axle Loads (k)	P_1	P_2
	25	25
Uniform Lane Load (klf)	0.64	
Dimensions – HL-93 (Design Tandem with Lane Load)		
Longitudinal Spacing (ft)	X_1	
	4	

APPENDIX B BRIDGE RAILING CALCULATIONS

Calculated the weight of one bridge railing per *ft* using provided drawing page 5316, November 1914, Department of the Interior United States Reclamation Service.

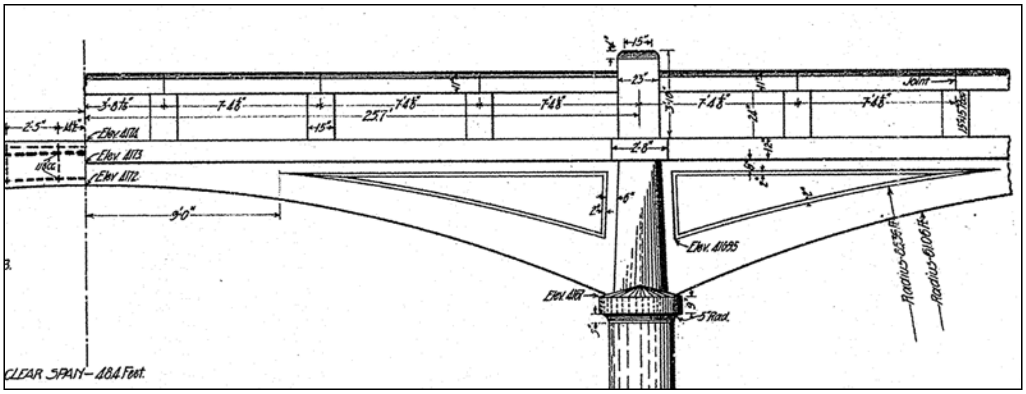

Figure B. 1Bridge Railing dimensions

Each intermediate pier and abutment has two main posts and each span has 12 intermediate posts, otherwise six per side.

$$W_{mainpost} = \frac{quantity \times V \times \gamma_{concrete}}{span\_length} = \frac{4 \times \left(\dfrac{46in \times 23in \times 23in}{12^3 \, ft^3} \right) \times 0.15 \dfrac{kips}{ft^3}}{3arch \times 51.4 ft} = 0.055 \frac{kips}{ft}$$

$$W_{post} = \frac{quantity \times V \times \gamma_{concrete}}{span\_length} = \frac{12 \times \left(\dfrac{33in \times 15in \times 15in}{12^3 \, ft^3} \right) \times 0.15 \dfrac{kips}{ft^3}}{3arch \times 51.4 ft} = 0.051 \frac{kips}{ft}$$

$$W_{rails} = quantity \times A \times \gamma_{concrete} = \frac{2}{3arch} \times \left(\frac{11in \times 15in}{12^2 \, ft^2} \right) \times 0.15 \frac{kips}{ft^3} = 0.12 \frac{kips}{ft}$$

Total for railing (including an additional 10% for bolts and clips)

$$w_{SDL} = 1.10 \left(W_{mainpost} + W_{post} + W_{rails} \right) = 1.10 \left(0.055 \frac{kips}{ft} + 0.051 \frac{kips}{ft} + 0.12 \frac{kips}{ft} \right) = 0.25 \frac{kips}{ft}$$

APPENDIX C FLEXURE AND SHEAR CAPACITY

Exterior Beam

Nominal positive moment of the exterior beam at mid span:

- Assume that all the reinforcement steel carries all tension

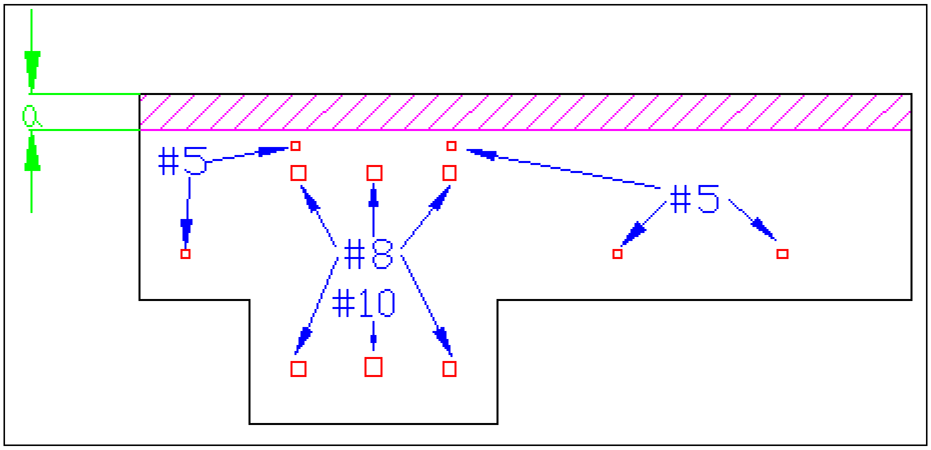

Figure C. 1 Cross Section of the exterior beam at mid-span

Assumption of all the reinforcement steel carrying all tension

Check if section is composite:

$$A_s \leq \frac{0.85 \times f'_c \times b_e \times t}{f_y}$$

$$A_s = A_{s1} + A_{s2} + A_{s3} + A_{s4} = (2\#8 + 1\#10) + 3\#8 + 3\#5 + 2\#5$$

Where:

$$A_{s\#5} = \left(\frac{5}{8}\right) in \times \left(\frac{5}{8}\right) in = 0.3906\, in^2$$

$$A_{s\#8} = \left(\frac{8}{8}\right) in \times \left(\frac{8}{8}\right) in = 1.0\, in^2$$

$$A_{s\#10} = \left(\frac{10}{8}\right) in \times \left(\frac{10}{8}\right) in = 1.5625\, in^2$$

$$A_{s1} = 2 \times 1 in^2 + 1 \times 1.5625 in^2 = 3.5625\, in^2$$

$$A_{s2} = 3 \times 1 in^2 = 3 in^2$$

$$A_{s3} = 3 \times 0.3906 in^2 = 1.1718 in^2$$

$$A_{s4} = 2 \times 0.3906 in^2 = 0.7812 in^2$$

$$A_s = 3.5625 in^2 + 3 in^2 + 1.1718 in^2 + 0.7812 in^2 = 8.5155 in^2$$

$$\frac{0.85 \times f'_c \times b_e \times t}{f_y} = \frac{0.85 \times 2.5 \frac{kips}{in^2} \times 56\, in \times 15\, in}{33 \frac{kips}{in^2}} = 54.0909\, in^2$$

Since $A_s < \frac{0.85 \times f'_c \times b_e \times t}{f_y}$, the section is composite, rectangular beam formulas are now valid.

$$T = A_s \times f_y = 8.5155 in^2 \times 33 \frac{kips}{in^2} = 281.0115\, kips$$

$$C = T \Rightarrow 0.85 \times f'_c \times b_e \times a = T \Rightarrow a = \frac{T}{0.85 \times f'_c \times b_e} = \frac{281.0115\, kips}{0.85 \times 2.5 \frac{kips}{in^2} \times 56\, in} = 2.3614\, in < 3.5\, in$$

Therefore, all the reinforcement steel carries all tension.

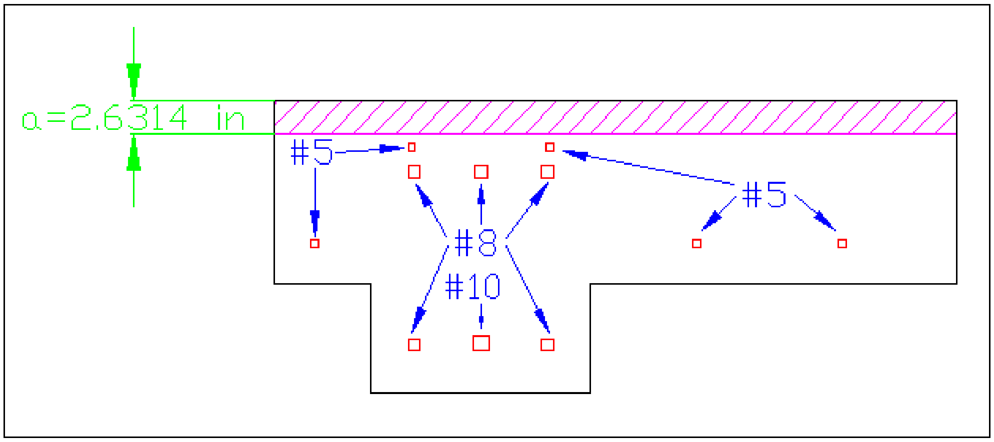

Figure C. 2 Cross section of the exterior beam at mid-span

Figure C.2 shows that the assumption of all the reinforcement steel carrying all tension was correct.

$$x = \frac{a}{\beta_1} \Rightarrow \beta_1 = 0.85 \ \ if \ f'_c \leq 4\,ksi \Rightarrow x = \frac{2.3614\ in}{0.85} = 2.7781\,in$$

$$M_n^+ = A_s \times f_y \times \left[d - \left(\frac{a}{2} \right) \right] \Rightarrow d = h - \bar{y}$$

$$\bar{y} = \frac{2 \times A_{s\#8} \times d_1 + A_{s\#10} \times d_2 + 3 \times A_{s\#8} \times d_3 + 3 \times A_{s\#5} \times d_4 + 2 \times A_{s\#5} \times d_5}{2 \times A_{s\#8} + A_{s\#10} + 3 \times A_{s\#8} + 3 \times A_{s\#5} + 2 \times A_{s\#5}}$$

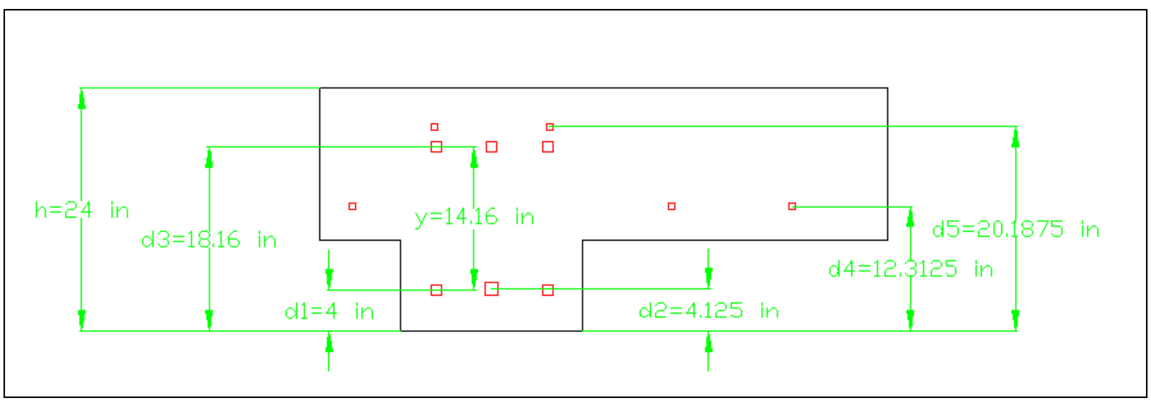

Figure C. 3 Cross section of the exterior beam at mid-span

Figure C.3 shows the distances that were needed to calculate the centroid of the reinforcement steel to calculate the positive flexural capacity.

Where:

$$d_1 = Cover\ of\ the\ bottom\ of\ the\ beam + \frac{1}{2} \times height\ of\ a\ bar\ \#8 = 3.5\,in + \frac{1}{2} \times \left(\frac{8}{8}\right) in = 4.0000\,in$$

$$d_2 = Cover\ of\ the\ bottom\ of\ the\ beam + \frac{1}{2} \times height\ of\ a\ bar\ \#10 = 3.5\,in + \frac{1}{2} \times \left(\frac{10}{8}\right) in = 4.1250\,in$$

$$d_3 = Cover\ of\ the\ bottom\ of\ the\ beam + \frac{1}{2} \times height\ of\ a\ bar\ \#8 + y$$

$$d_3 = 3.5\,in + \frac{1}{2} \times \left(\frac{8}{8}\right) in + 14.16\,in = 18.16\,in$$

$$d_4 = h - (t_s - Cover\ of\ the\ bottom\ of\ the\ slab) + \frac{1}{2} \times height\ of\ a\ bar\ \#5 = 24\,in - (15\,in - 3\,in) +$$
$$\frac{1}{2} \times \left(\frac{5}{8}\right) in = 12.3125\,in$$

$$d_5 = h - Cover\ of\ the\ top\ of\ the\ slab - \frac{1}{2} \times height\ of\ a\ bar\ \#5 = 24\,in - 3.5\,in - \frac{1}{2} \times \left(\frac{5}{8}\right) in = 20.1875\,in$$

$$\bar{y} = \frac{2 \times 1in^2 \times 4.0\,in + 1.5625\,in^2 \times 4.125\,in + 3 \times 1in^2 \times 18.16\,in + 3 \times 0.3906\,in^2 \times 12.3125\,in + 2 \times 0.3906\,in^2 \times 20.1875 \times in}{2 \times 1in^2 + 1.5625\,in^2 + 3 \times 1in^2 + 3 \times 0.3906\,in^2 + 2 \times 0.3906\,in^2} = 11.6404\,in$$

$$d = 24\,in - 11.6404\,in = 12.3596\,in$$

$$M_n^+ = 8.5155\,in^2 \times 33 \frac{kips}{in^2} \times \left[12.3596\,in - \left(\frac{2.3614\,in}{2}\right)\right] \times \frac{1\,ft}{12\,in} = 261.7833\,k - ft$$

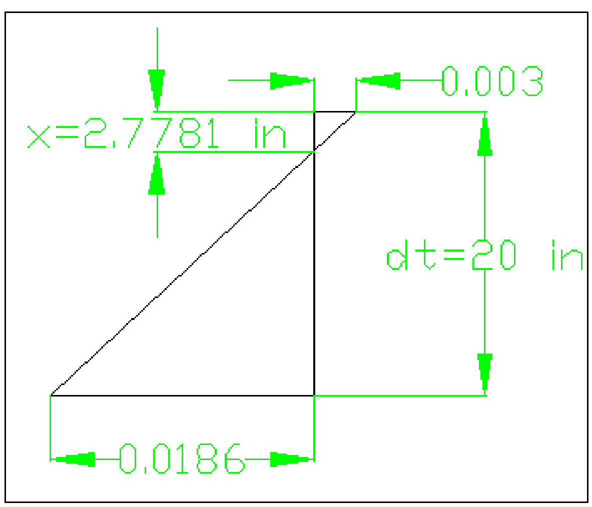

Figure C. 4 Strain diagram of the exterior beam at mid-span

$$\varepsilon_t = \varepsilon_c \times \frac{d_t - x}{x}$$

Where:

$\varepsilon_c = Ultimate\ Strain\ of\ Concrete = 0.003$

$d_t = Effective\ Depth\ of\ the\ Extreme\ Tension\ Steel$

$d_t = h - \left(Cover\ of\ the\ bottom\ of\ the\ beam + \frac{1}{2} \times height\ of\ a\ bar\ \#8 \right) = 24\,in - \left[3.5\,in + \frac{1}{2} \times \left(\frac{8}{8} \right) in \right] = 20\,in$

$\varepsilon_t = 0.003 \times \frac{20in - 2.7781in}{2.7781in} = 0.01860 \frac{in}{in} > 0.005 \frac{in}{in}, therefore,$

$Tension - controlled\ and\ \phi = 0.9$

Capacities for the load rating are:

$\phi \times M_n^+ = 0.9 \times 261.7833\,k - ft = 235.6050\,k - ft$ (LFR capacity)

$M_u^+ = 261.7833\,k - ft$ (LRFR capacity)

Nominal negative moment for the exterior beam at the edge of a pier:

Assume that the bottom layer of 3#8 reinforcement steel bars carries compression and the rest of the reinforcement steel carries all tension.

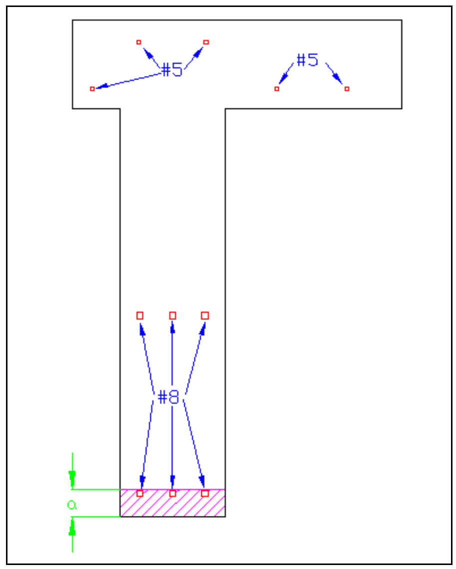

Figure C. 5 Cross Section of the exterior beam at end-span

Assume the bottom layer of 3#8 reinforcement steel carrying compression while the rest of the reinforcement steel is carrying all tension.

Check if section is composite:

$$A_s \le \frac{0.85 \times f'_c \times b_e \times t}{f_y}$$

$$A_s = A_{s1} + A_{s2} + A_{s3} = 2\#5 + 3\#5 + 3\#8$$

Where:

$$A_{s\#5} = \left(\frac{5}{8}\right) in \times \left(\frac{5}{8}\right) in = 0.3906\, in^2$$

$$A_{s\#8} = \left(\frac{8}{8}\right) in \times \left(\frac{8}{8}\right) in = 1.0\, in^2$$

$$A_{s1} = 2 \times 0.3906\, in^2 = 0.7812\, in^2$$

$$A_{s2} = 3\times 0.3906\,in^2 = 1.1718\,in^2$$

$$A_{s3} = 3\times 1\,in^2 = 3\,in^2$$

$$A_s = 0.7812\,in^2 + 1.1718\,in^2 + 3\,in^2 = 4.953\,in^2$$

$$\frac{0.85\times f'_c \times b_e \times t}{f_y} = \frac{0.85\times 2.5\frac{kips}{in^2}\times 18\,in \times 15\,in}{33\frac{kips}{in^2}} = 17.3864\,in^2$$

Since $A_s < \dfrac{0.85\times f'_c \times b_e \times t}{f_y}$, the section is composite, rectangular beam formulas are now valid.

$$T = A_s \times f_y = 4.953\,in^2 \times 33\frac{kips}{in^2} = 163.449\,kips$$

$$C = T \Rightarrow 0.85\times f'_c \times b_e \times a = T \Rightarrow a = \frac{T}{0.85\times f'_c \times b_e} = \frac{163.449\,kips}{0.85\times 2.5\frac{kips}{in^2}\times 18\,in} = 4.2732\,in > 3.5\,in$$

Therefore, the bottom layer of reinforcement steel, 3#8, carries compression, while the rest of the reinforcement steel carries all tension.

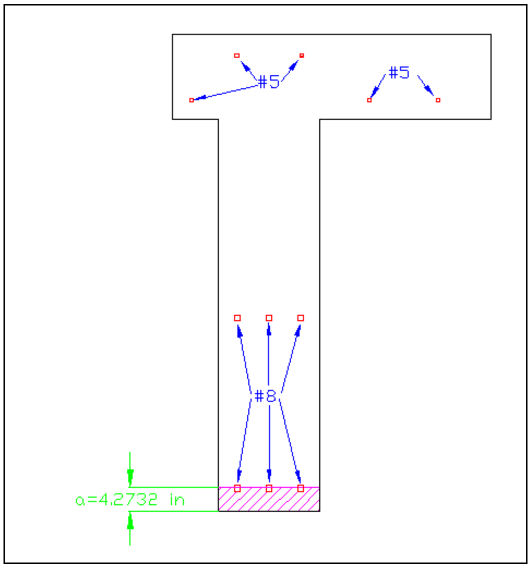

Figure C. 6 Cross section of the exterior beam at end-span with the steel rebars

Figure C.6 showing that the assumption of the bottom layer of 3#8 reinforcement steel carrying compression and the rest of the reinforcement steel carrying all tension was correct.

$$x = \frac{a}{\beta_1} \Rightarrow \beta_1 = 0.85 \;\; if \;\; f'_c \leq 4\,ksi \Rightarrow x = \frac{4.2732 \; in}{0.85} = 5.0273\,in$$

$$M_n^- = A_s \times f_y \times \left[d - \left(\frac{a}{2} \right) \right] \Rightarrow d = h - \bar{y}$$

$$\bar{y} = \frac{2 \times A_{s\#5} \times d_1 + 3 \times A_{s\#5} \times d_2 + 3 \times A_{s\#8} \times d_3}{2 \times A_{s\#5} + 3 \times A_{s\#5} + 3 \times A_{s\#8}}$$

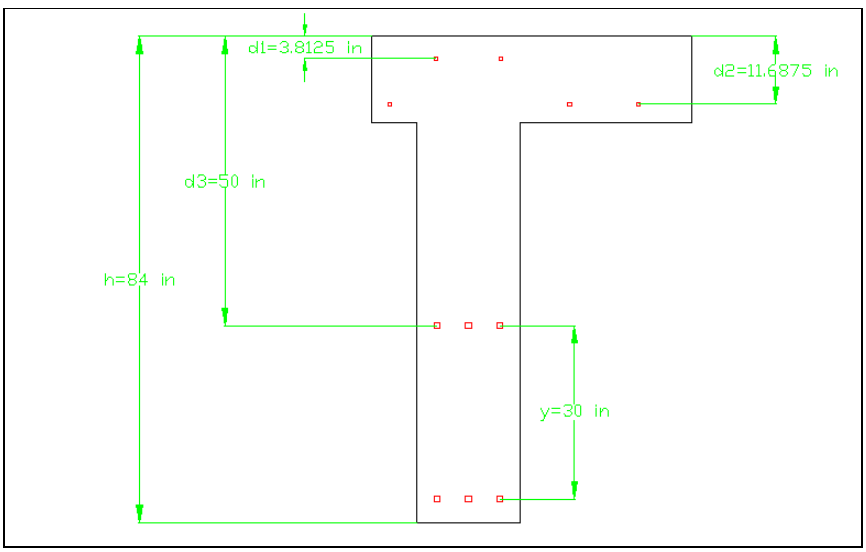

Figure C. 7 Cross section of the exterior beam at end-span, rebars locations

Figure C.7 shows the distances that were needed to calculate the centroid of the reinforcement steel to calculate the negative flexural capacity.

Where:

$$d_1 = Cover\;of\;the\;top\;of\;the\;slab + \frac{1}{2} \times height\;of\;a\;bar\;\#5 = 3.5\,in + \frac{1}{2} \times \left(\frac{5}{8} \right) in = 3.8125\,in$$

$$d_2 = t_s - Cover\ of\ the\ bottom\ of\ the\ slab - \frac{1}{2} \times height\ of\ a\ bar\ \#5 = 15\,in - 3\,in - \frac{1}{2} \times \left(\frac{5}{8}\right) in = 11.6875\,in$$

$$d_3 = h - \left(Cover\ of\ the\ bottom\ of\ the\ slab + \frac{1}{2} \times height\ of\ a\ bar\ \#8 + y \right) =$$

$$d_3 = 84\,in - \left(3.5\,in + \frac{1}{2} \times \left(\frac{8}{8}\right) in + 30\,in \right) = 50\,in$$

$$\bar{y} = \frac{2 \times 0.3906\,in^2 \times 3.8125\,in + 3 \times 0.3906\,in^2 \times 11.6875\,in + 3 \times 1\,in^2 \times 50\,in}{2 \times 0.3906\,in^2 + 3 \times 0.3906\,in^2 + 3 \times 1\,in^2} = 33.6511\,in$$

$$d = 84\,in - 33.6511\,in = 50.3489\,in$$

$$M_n^- = 4.953\,in^2 \times 33\frac{kips}{in^2} \times \left[50.3489\,in - \left(\frac{4.2732\,in}{2} \right) \right] \times \frac{1\,ft}{12\,in} = 656.6877\,k - ft$$

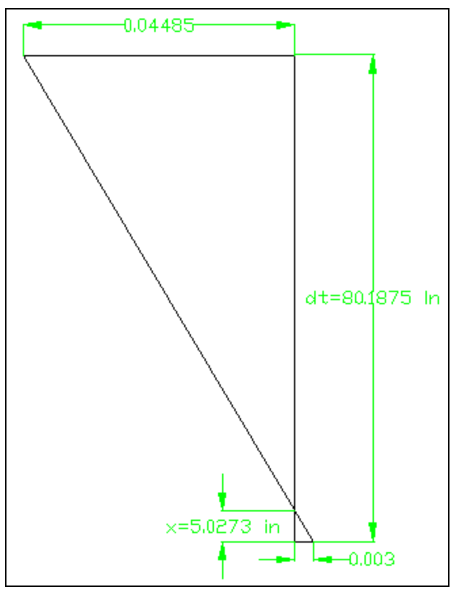

Figure C. 8 Strain diagram of the exterior beam at end-span

$$\varepsilon_t = \varepsilon_c \times \frac{d_t - x}{x}$$

Where:

$$\varepsilon_c = Ultimate\ Strain\ of\ Concrete = 0.003$$

$$d_t = Effective\ Depth\ of\ the\ Extreme\ Tension\ Steel =$$

$$h - \left(Cover\ of\ the\ bottom\ of\ the\ beam + \frac{1}{2} \times height\ of\ a\ bar\ \#5 \right) = 84\,in - \left[3.5\,in + \frac{1}{2} \times \left(\frac{5}{8} \right) in \right] = 80.1875\,in$$

$$\varepsilon_t = 0.003 \times \frac{80.1875in - 5.0273\,in}{5.0273\,in} = 0.04485 \frac{in}{in} > 0.005 \frac{in}{in},$$

$$Therfore, is\ tension - controlled\ and\ \phi = 0.9$$

Capacities for the load rating are:

$\phi \times M_n^- = 0.9 \times 656.6877\,k - ft = 591.0189\,k - ft$ (LFR capacity)

$M_u^- = 656.6877\,k - ftt$ (LRFR capacity)

LFR shear capacity at the edge section of the exterior beam

$$\phi \times V_n = \phi \times (V_c + V_s)$$

$$V_c = 2 \times \sqrt{f'_c} \times b_w \times d$$

Where:

$$d = h - \overline{y}$$

$$d = 50.34in$$

$$V_c = 2 \times \sqrt{2500 \frac{lb}{in^2}} \times 18in \times 50.34in \times \frac{1kip}{1000lb} = 90.61kips$$

$$V_s = \frac{A_v \times f_y \times d}{s}$$

Where:

$$A_v = 2 \times A_{s\#4}$$

$$A_{s\#4} = \left(\frac{4}{8}\right)in \times \left(\frac{4}{8}\right)in = 0.25in^2$$

$$A_v = 2 \times 0.25in^2 = 0.50in^2$$

$$V_s = \frac{0.50in^2 \times 33\frac{kips}{in^2} \times 50.34in}{29in} = 28.64kips$$

Capacity for the LFR is:

$$\phi \times V_n = 0.85 \times (90.61kips + 28.64kips) = 101.38kips$$

LRFD Shear capacity at the edge section of the exterior beam

Nominal shear resistance is given as:

$$V_n = \left(V_c + V_s\right)$$

For Which:

$$V_c = 0.0316 \times \beta \times \sqrt{f'_c} \times b_v \times d_v \qquad \text{(LRFD 5-68)}$$

$$V_s = \frac{A_v \times f_y \times d_v \times \cot\theta}{s} \qquad \text{(LRFD 5-69)}$$

$$\beta = 2.0 \qquad \text{(LRFD 5.8.3.4)}$$

$$\theta = 45^\circ \qquad \text{(LRFD 5.8.3.4)}$$

$$V_c = 0.0316 \times 2 \times \sqrt{2.5ksi} \times 18in \times 50.3489in = 90.56kips$$

#4 shear stirrups at 29 in. spacing are provided along the beam.

$$V_s = \frac{0.50in^2 \times 33ksi \times 50.3489in \times \cot(45)}{29in} = 28.64kips$$

LRFD design shear capacity is given by:

$$V_n = \left(90.56kips + 28.64kips\right) = 119.20kips$$

Nominal positive moment for the interior beam at the mid-span:

Assume that all reinforcement steel carries all tension

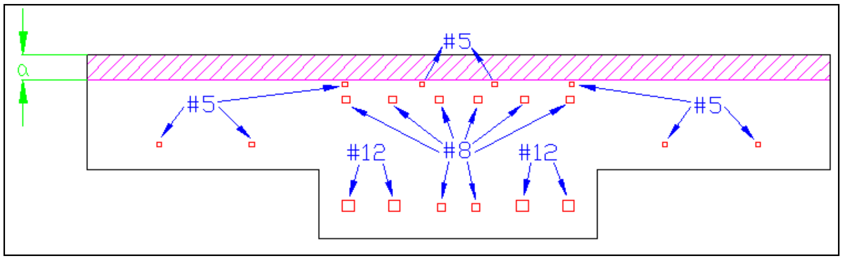

Figure C. 9 Cross Section of the interior beam at mid-span with steel rebar size

Figure C.9 shows the assumption of all the reinforcement steel carrying all tension.

Check if section is composite:

$$A_s \le \frac{0.85 \times f'_c \times b_e \times t}{f_y}$$

$$A_s = A_{s1} + A_{s2} + A_{s3} + A_{s4} = (4\#12 + 2\#8) + 6\#8 + 4\#5 + 4\#5$$

Where:

$$A_{s\#5} = \left(\frac{5}{8}\right) in \times \left(\frac{5}{8}\right) in = 0.3906\, in^2$$

$$A_{s\#8} = \left(\frac{8}{8}\right) in \times \left(\frac{8}{8}\right) in = 1.0\, in^2$$

$$A_{s\#12} = \left(\frac{12}{8}\right) in \times \left(\frac{12}{8}\right) in = 2.25\, in^2$$

$$A_{s1} = 4 \times 2.25\, in^2 + 2 \times 1\, in^2 = 11\, in^2$$

$$A_{s2} = 6 \times 1\, in^2 = 6\, in^2$$

$$A_{s3} = 4 \times 0.3906\, in^2 = 1.5624\, in^2$$

$$A_{s4} = 4 \times 0.3906\, in^2 = 1.5624\, in^2$$

$$A_s = 11\,in^2 + 6\,in^2 + 1.5624\,in^2 + 1.5624\,in^2 = 20.1248\,in^2$$

$$\frac{0.85 \times f'_c \times b_e \times t}{f_y} = \frac{0.85 \times 2.5\frac{kips}{in^2} \times 96\,in \times 15\,in}{33\frac{kips}{in^2}} = 92.7273\,in^2$$

Since $A_s < \dfrac{0.85 \times f'_c \times b_e \times t}{f_y}$, the section is composite, rectangular beam formulas are now valid.

$$T = A_s \times f_y = 20.1248\,in^2 \times 33\frac{kips}{in^2} = 664.1184\,kips$$

$$C = T \Rightarrow 0.85 \times f'_c \times b_e \times a = T \Rightarrow a = \frac{T}{0.85 \times f'_c \times b_e} = \frac{664.1184\,kips}{0.85 \times 2.5\frac{kips}{in^2} \times 96\,in} = 3.2555\,in < 3.5\,in$$

Therefore, all the reinforcement steel carries all tension.

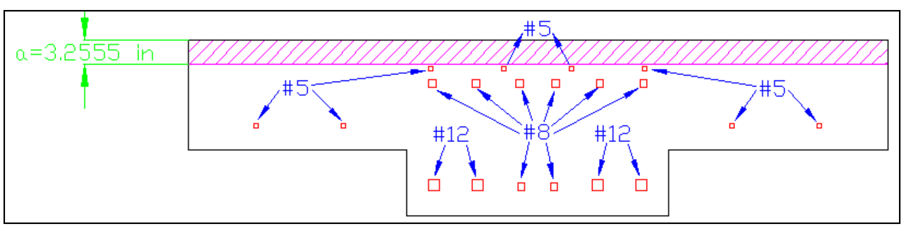

Figure C. 10 Cross section of the interior beam at mid-span showing the compression zone

Figure C.10 shows that the assumption of all the reinforcement steel carrying all tension was correct.

$$x = \frac{a}{\beta_1} \Rightarrow \beta_1 = 0.85 \;\; if \;\; f'_c \le 4\,ksi \Rightarrow x = \frac{3.2555\;in}{0.85} = 3.83\,in$$

$$M_n^+ = A_s \times f_y \times \left[d - \left(\frac{a}{2}\right)\right] \Rightarrow d = h - \bar{y}$$

$$\bar{y} = \frac{4 \times A_{s\#12} \times d_1 + 2 \times A_{s\#8} \times d_2 + 6 \times A_{s\#8} \times d_3 + 4 \times A_{s\#5} \times d_4 + 4 \times A_{s\#5} \times d_5}{4 \times A_{s\#12} + 2 \times A_{s\#8} + 6 \times A_{s\#8} + 4 \times A_{s\#5} + 4 \times A_{s\#5}}$$

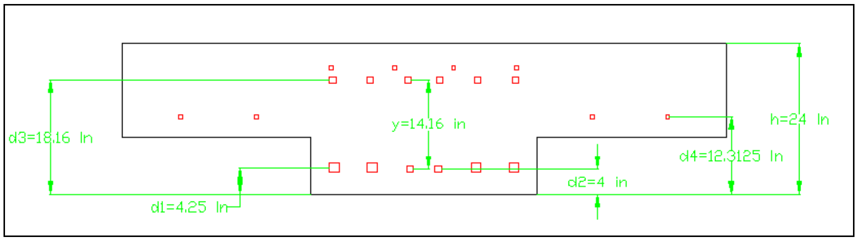

Figure C. 11 Cross section of the interior beam at mid-span steel rebar locations

Figure C.11 shows the distances that were needed to calculate the centroid of the reinforcement steel for use in calculating the positive flexural capacity.

Where:

$$d_1 = Cover\ of\ the\ bottom\ of\ the\ beam + \frac{1}{2} \times height\ of\ a\ bar\ \#12 = 3.5\,in + \frac{1}{2} \times \left(\frac{12}{8}\right) in = 4.2500\,in$$

$$d_2 = Cover\ of\ the\ bottom\ of\ the\ beam + \frac{1}{2} \times height\ of\ a\ bar\ \#8 = 3.5\,in + \frac{1}{2} \times \left(\frac{8}{8}\right) in = 4.0000\,in$$

$$d_3 = Cover\ of\ the\ bottom\ of\ the\ beam + \frac{1}{2} \times height\ of\ a\ bar\ \#8 + y$$

$$d_3 = 3.5\,in + \frac{1}{2} \times \left(\frac{8}{8}\right) in + 14.16\,in = 18.1600\,in$$

$$d_4 = h - (t_s + Cover\ of\ the\ bottom\ of\ the\ slab) + \frac{1}{2} \times height\ of\ a\ bar\ \#5 = 24\,in - (15\,in - 3\,in) + \frac{1}{2} \times \left(\frac{5}{8}\right) in = 12.3125\,in$$

$$d_5 = h - Cover\ of\ the\ top\ of\ the\ slab - \frac{1}{2} \times height\ of\ a\ bar\ \#5 = 24\,in - 3.5\,in - \frac{1}{2} \times \left(\frac{5}{8}\right) in = 20.1875\,in$$

$$\bar{y} = \frac{4 \times 2.25\,in^2 \times 4.25\,in + 2 \times 1\,in^2 \times 4.00\,in + 6 \times 1\,in^2 \times 18.16\,in + 4 \times 0.3906\,in^2 \times 12.3125\,in + 4 \times 0.3906\,in^2 \times 20.1875\,in}{4 \times 2.25\,in^2 + 2 \times 1\,in^2 + 6 \times 1\,in^2 + 4 \times 0.3906\,in^2 + 4 \times 0.3906\,in^2} = 10.2355\,in$$

$$d = 24\,in - 10.2355\,in = 13.7645\,in$$

$$M_n^+ = 20.1248\,in^2 \times 33\frac{kips}{in^2} \times \left[13.7645\,in - \left(\frac{3.2555\,in}{2}\right)\right] \times \frac{1\,ft}{12\,in} = 671.6866\,k - ft$$

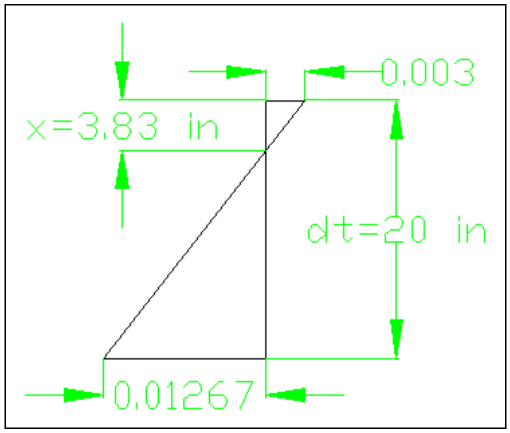

Figure C. 12 Strain diagram of the interior beam at mid-span

$$\varepsilon_t = \varepsilon_c \times \frac{d_t - x}{x}$$

Where:

$\varepsilon_c = Ultimate\ Strain\ of\ Concrete = 0.003$

$d_t = Effective\ Depth\ of\ the\ Extreme\ Tension\ Steel =$

$h - \left(Cover\ of\ the\ bottom\ of\ the\ beam + \frac{1}{2} \times height\ of\ a\ bar \right) = 24\,in - \left[3.5\,in + \frac{1}{2} \times \left(\frac{8}{8} \right) in \right] = 20\,in$

$\varepsilon_t = 0.003 \times \frac{20in - 3.83\,in}{3.83\,in} = 0.01267 \frac{in}{in} > 0.005 \frac{in}{in},$

$Therefore, is\ tension - controlled\ and\ \phi = 0.9$

Capacities for the load rating are:

$\phi \times M_n^+ = 0.9 \times 671.6866\,k - ft = 604.5179\,k - ft$ (LFR capacity)

$M_u^+ = 671.6866\,k - ft$ (LRFR capacity)

Nominal negative moment for the interior beam at the edge location:

Assume that the bottom layer of 4#12 and 2#8 reinforcement steel bars carries compression and the rest of the reinforcement steel carries all tension.

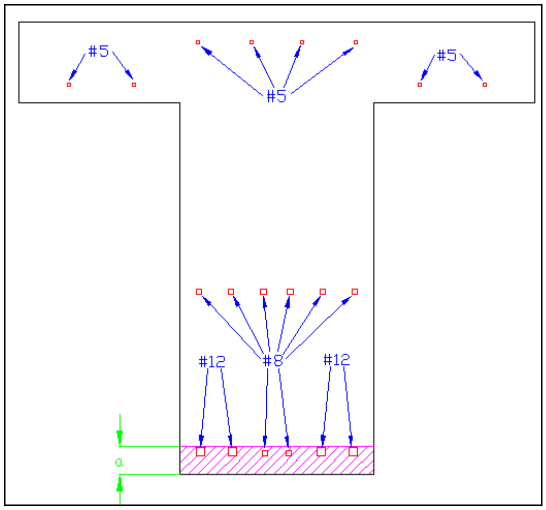

Figure C. 13 Cross Section of the interior beam at end-span with the steel rebar size

Assume the bottom layer of 4#12 and 2#8 reinforcement steel is carrying compression while the rest of the reinforcement steel is carrying all tension, Figure C.13.

Check if section is composite:

$$A_s \leq \frac{0.85 \times f'_c \times b_e \times t}{f_y}$$

$$A_s = A_{s1} + A_{s2} + A_{s3} = 4\#5 + 4\#5 + 6\#8$$

Where:

$$A_{s\#5} = \left(\frac{5}{8}\right) in \times \left(\frac{5}{8}\right) in = 0.3906\, in^2$$

$$A_{s\#8} = \left(\frac{8}{8}\right) in \times \left(\frac{8}{8}\right) in = 1.0\, in^2$$

$$A_{s1} = 4 \times 0.3906\, in^2 = 1.5624\, in^2$$

$A_{s2} = 4 \times 0.3906\, in^2 = 1.5624\, in^2$

$A_{s3} = 6 \times 1\, in^2 = 6\, in^2$

$A_s = 1.5624\, in^2 + 1.5624\, in^2 + 6\, in^2 9.1248\, in^2$

$$\frac{0.85 \times f'_c \times b_e \times t}{f_y} = \frac{0.85 \times 2.5 \frac{kips}{in^2} \times 36\, in \times 15\, in}{33 \frac{kips}{in^2}} = 34.7727\, in^2$$

Since $A_s < \dfrac{0.85 \times f'_c \times b_e \times t}{f_y}$, the section is composite, rectangular beam formulas are now valid.

$$T = A_s \times f_y = 9.1248 in^2 \times 33 \frac{kips}{in^2} = 301.1184\, kips$$

$$C = T \Rightarrow 0.85 \times f'_c \times b_e \times a = T \Rightarrow a = \frac{T}{0.85 \times f'_c \times b_e} = \frac{301.1184\, kips}{0.85 \times 2.5 \frac{kips}{in^2} \times 36\, in} = 3.9362\, in > 3.5\, in$$

Therefore, the bottom layer of reinforcement steel, 4#12 and 2#8, carries compression, while the rest of the reinforcement steel carries all tension.

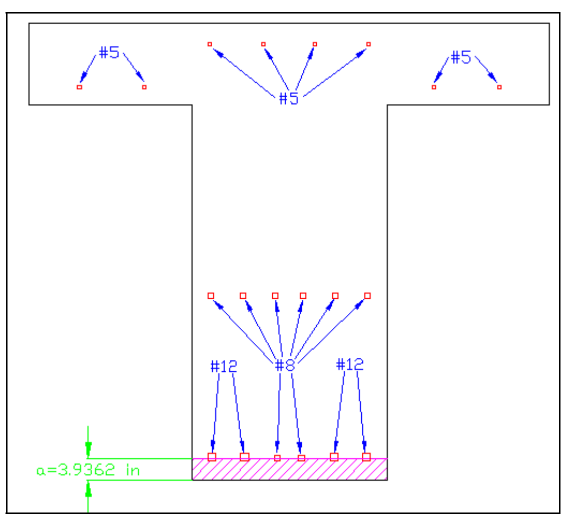

Figure C. 14 Cross section of the interior beam at end-span

Figure C.14 shows that the assumption of the bottom layer of 4#12 and 2#8 reinforcement steel carrying compression and the rest of the reinforcement steel carrying all tension was correct.

$$x = \frac{a}{\beta_1} \Rightarrow \beta_1 = 0.85 \;\; if \;\; f'_c \leq 4\,ksi \Rightarrow x = \frac{3.9362\;in}{0.85} = 4.6308\,in$$

$$M_n^- = A_s \times f_y \times \left[d - \left(\frac{a}{2} \right) \right] \Rightarrow d = h - \bar{y}$$

$$\bar{y} = \frac{4 \times A_{s\#5} \times d_1 + 4 \times A_{s\#5} \times d_2 + 6 \times A_{s\#8} \times d_3}{4 \times A_{s\#5} + 4 \times A_{s\#5} + 6 \times A_{s\#8}}$$

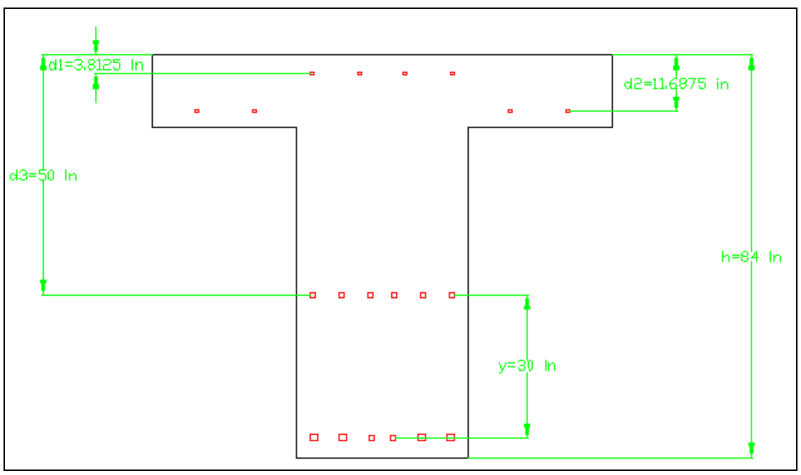

Figure C. 15 Cross section of the interior beam at end-span, steel rebars location

Figure C.15 shows the distances that were needed to calculate the centroid of the reinforcement steel for use in calculating the negative flexural capacity.

Where:

$$d_1 = Cover\; of\; the\, top\; of\; the\; slab + \frac{1}{2} \times height\; of\; a\, bar\, \#5 = 3.5\,in + \frac{1}{2} \times \left(\frac{5}{8} \right) in = 3.8125\,in$$

$$d_2 = t_s - Cover\ of\ the\ bottom\ of\ the\ slab - \frac{1}{2} \times height\ of\ a\ bar\ \#5 = 15\,in - 3\,in - \frac{1}{2} \times \left(\frac{5}{8}\right) in = 11.6875\,in$$

$$d_3 = h - \left(Cover\ of\ the\ bottom\ of\ the\ slab + \frac{1}{2} \times height\ of\ a\ bar\ \#8 + y \right)$$

$$d_3 = 84\,in - \left(3.5\,in + \frac{1}{2} \times \left(\frac{8}{8}\right) in + 30\,in \right) = 50\,in$$

$$\bar{y} = \frac{4 \times 0.3906\,in^2 \times 3.8125\,in + 4 \times 0.3906\,in^2 \times 11.6875\,in + 6 \times 1\,in^2 \times 50\,in}{4 \times 0.3906\,in^2 + 4 \times 0.3906\,in^2 + 6 \times 1\,in^2} = 35.5314\,in$$

$$d = 84\,in - 35.5314\,in = 48.4686\,in$$

$$M_n^- = 9.1248\,in^2 \times 33 \frac{kips}{in^2} \times \left[48.4686\,in - \left(\frac{3.9362\,in}{2} \right) \right] \times \frac{1\,ft}{12\,in} = 1166.8463\,k - ft$$

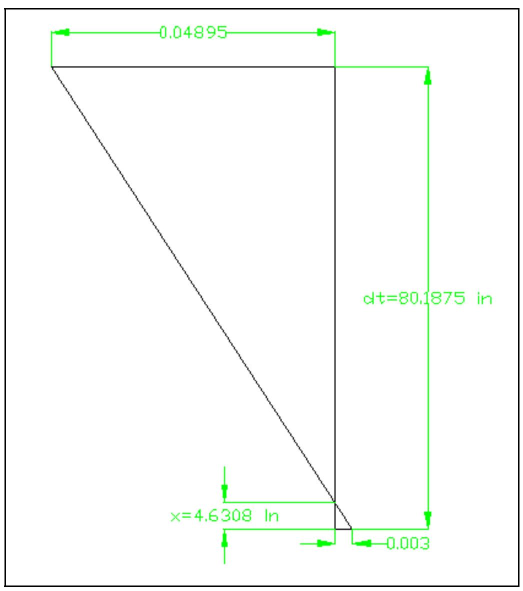

Figure C. 16 Strain diagram of the interior beam at mid-span.

$$\varepsilon_t = \varepsilon_c \times \frac{d_t - x}{x}$$

Where:

$$\varepsilon_c = Ultimate\ Strain\ of\ Concrete = 0.003$$
$$d_t = Effective\ Depth\ of\ the\ Extreme\ Tension\ Steel =$$
$$h - \left(Cover\ of\ the\ bottom\ of\ the\ beam + \frac{1}{2} \times height\ of\ a\ bar\right) = 84\,in - \left[3.5\,in + \frac{1}{2} \times \left(\frac{5}{8}\right) in\right] = 80.1875\,in$$
$$\varepsilon_t = 0.003 \times \frac{80.1875\,in - 4.6308\,in}{4.6308\,in} = 0.04895\frac{in}{in} > 0.005\frac{in}{in},$$
$$Therefore, is\ tension - coontrolled\ and\ \phi = 0.9$$

Capacities for the load rating are:

$\phi \times M_n^- = 0.9 \times 1166.8463\,k - ft = 1050.1617\,k - ft$ (LFR capacity)

$M_u^- = 1166.8463\,k - ft$ (LRFR capacity)

LFR Nominal shear capacity of the interior beam at the edge:

$$\phi \times V_n = \phi \times (V_c + V_s)$$

$$V_c = 2 \times \sqrt{f'_c} \times b_w \times d$$

Where:

$$d = h - \bar{y}$$

$$d = 48.46 in$$

$$V_c = 2 \times \sqrt{2500 \frac{lb}{in^2}} \times 36 in \times 48.469 in \times \frac{1 kip}{1000 lb} = 174.456 kips$$

$$V_s = \frac{A_v \times f_y \times d}{s}$$

Where:

$$A_v = 2 \times A_{s\#4}$$

$$A_{s\#4} = \left(\frac{4}{8}\right) in \times \left(\frac{4}{8}\right) in = 0.25 in^2$$

$$A_v = 2 \times 0.25 in^2 = 0.50 in^2$$

$$V_s = \frac{0.50 in^2 \times 33 \frac{kips}{in^2} \times 48.469 in}{29 in} = 27.57 kips$$

LFR design shear capacity is given by:

$$\phi \times V_n = 0.85 \times (174.456 kips + 27.57 kips) = 171.72 kips$$

LRFD Shear capacity at the edge section of the interior beam

Nominal shear resistance is given as:

$$V_n = \left(V_c + V_s\right)$$

For Which:

$$V_c = 0.0316 \times \beta \times \sqrt{f'_c} \times b_v \times d_v \qquad \text{(LRFD 5-68)}$$

$$V_s = \frac{A_v \times f_y \times d_v \times \cot\theta}{s} \qquad \text{(LRFD 5-69)}$$

$$\beta = 2.0 \qquad \text{(LRFD 5.8.3.4)}$$

$$\theta = 45^\circ \qquad \text{(LRFD 5.8.3.4)}$$

$$V_c = 0.0316 \times 2 \times \sqrt{2.5\,ksi} \times 36in \times 48.469in = 174.36kips$$

#4 shear stirrups at 29 in. spacing are provided along the beam.

$$V_s = \frac{0.50in^2 \times 33ksi \times 48.469in \times \cot(45)}{29in} = 27.57kips$$

LRFD design shear capacity is given by:

$$V_n = \left(174.36kips + 27.57kips\right) = 201.90kips$$

APPENDIX D RATING FACTOR EXAMPLE

The nomenclatures used in the load rating factor example are as follows.

- Capacity of the beam section – C
  - M_n, M_u
  - V_n, V_u
- Dead load – D
  - M_{DL}
  - V_{LL}
- Live load – L
  - M_{LL}
  - V_{LL}
- Rating Factor result – RF

Load factor (LFR) rating equation

$$RF = \frac{C - A_1 \times D}{A_2 \times L}$$

Where:

$$C = Capacity\ of\ the\ beam$$

$$A_1 = Dead\ Load\ Factor \begin{pmatrix} 1.3\ for\ Operating\ and\ Inventory \\ 1\ for\ Allowable\ Stress \end{pmatrix}$$

$$D = Dead\ Load$$

$$A_2 = LiveLoadFactor \begin{pmatrix} 1.3\ for\ Operating; \\ 2.17\ for\ Inventory \end{pmatrix}$$

$$L = Live\ Load$$

LFR method: Exterior Beam

Load Rating for the exterior beam at 1/3 of the mid-span length using the HS-20 design vehicle.

<u>Negative Moment:</u>

$$C = \phi \times M_n^- = 359.8497\,k - ft$$

$$D = M_{DL}^- = 164.88\,k - ft$$

$$L = M_{LL}^- = 143.5\,k - ft$$

For the Operating Level rating:

$$RF = \frac{359.8497\,k - ft - (1.3 \times 164.88\,k - ft)}{1.3 \times 143.5\,k - ft} = 0.78$$

For the Inventory Level rating:

$$RF = \frac{359.8497\,k - ft - (1.3 \times 164.88\,k - ft)}{2.17 \times 143.5\,k - ft} = 0.47$$

Shear Force

$$C = \phi \times V_n = 63.408\,k$$

$$D = V_{DL} = 21.42\,k$$

$$L = V_{LL} = 21.6252\,k$$

For the Operating Level rating:

$$RF = \frac{63.408\,k - (1.3 \times 21.42\,k)}{1.3 \times 21.6252\,k} = 1.27$$

For the Inventory Level rating:

$$RF = \frac{63.408\,k - (1.3 \times 21.42\,k)}{2.17 \times 21.6252\,k} = 0.76$$

LFR method: Exterior Beam

Load Rating for the exterior beam at 2/3 of the mid-span length using the HS-20 design vehicle.

Positive Moment:

$$C = \phi \times M_n^+ = 285.3778k - ft$$

$$D = M_{DL}^+ = 40.11k - ft$$

$$L = M_{LL}^- = 63.2901k - ft$$

For the Operating Level rating:

$$RF = \frac{285.3778k - ft - (1.3 \times 40.11k - ft)}{1.3 \times 63.2901k - ft} = 2.83$$

For the Inventory Level rating:

$$RF = \frac{285.3778k - ft - (1.3 \times 40.11k - ft)}{2.17 \times 63.2901k - ft} = 1.69$$

Shear Force

$$C = \phi \times V_n = 31.412k$$

$$D = V_{DL} = 11.89k$$

$$L = V_{LL} = 16.8205k$$

For the Operating Level rating:

$$RF = \frac{31.412k - (1.3 \times 11.89k)}{1.3 \times 16.8205k} = 0.73$$

For the Inventory Level rating:

$$RF = \frac{31.412k - (1.3 \times 11.89k)}{2.17 \times 16.8205k} = 0.44$$

LFR method: Interior Beam

Load Rating for the interior beam at the edge using the HS-20 design vehicle.

<u>Negative Moment:</u>

$$C = \phi \times M_n^- = 1050.1617\,k - ft$$

$$D = M_{DL}^- = 618.49\,k - ft$$

$$L = M_{LL}^- = 443.12k - ft$$

For the Operating Level rating:

$$RF = \frac{1050.1617\,k - ft - (1.3 \times 618.49\,k - ft)}{1.3 \times 443.12\,k - ft} = 0.43$$

For the Inventory Level rating:

$$RF = \frac{1050.1617\,k - ft - (1.3 \times 618.49\,k - ft)}{2.17 \times 443.12\,k - ft} = 0.26$$

<u>Shear:</u>

$$C = \phi \times V_n = 171.73\,k$$

$$D = V_{DL} = 59.26\,k$$

$$L = V_{LL} = 44.5836\,k$$

For the Operating Level rating:

$$RF = \frac{171.73\,k - (1.3 \times 59.26\,k)}{1.3 \times 44.5836\,k} = 1.63$$

For the Inventory Level rating:

$$RF = \frac{171.73\,k - (1.3 \times 59.26\,k)}{2.17 \times 44.5836\,k} = 0.98$$

LFR method: Interior Beam

Load Rating for the interior beam at mid-span using the HS-20 design vehicle.

Positive Moment:

$$C = \phi \times M_n^+ = 604.5179\,k - ft$$

$$D = M_{DL}^+ = 114.34\,k - ft$$

$$L = M_{LL}^+ = 156.507\,k - ft$$

For the Operating Level rating:

$$RF = \frac{604.5179\,k - ft - (1.3 \times 114.34\,k - ft)}{1.3 \times 156.507\,k - ft} = 2.24$$

For the Inventory Level rating:

$$RF = \frac{604.5179\,k - ft - (1.3 \times 114.34\,k - ft)}{2.17 \times 156.507\,k - ft} = 1.34$$

Load Rating for the interior beam at 1/3 of the mid-span length using the HS-20 design vehicle.

LFR method: Interior Beam

Negative Moment:

$$C = \phi \times M_n^- = 653.5594\,k - ft$$

$$D = M_{DL}^- = 288.44\,k - ft$$

$$L = M_{LL}^- = 243.33\,k - ft$$

For the Operating Level rating:

$$RF = \frac{653.5594\,k - ft - (1.3 \times 288.44\,k - ft)}{1.3 \times 243.33\,k - ft} = 0.88$$

For the Inventory Level rating:

$$RF = \frac{653.5594\,k - ft - (1.3 \times 288.44k - ft)}{2.17 \times 243.33\,k - ft} = 0.53$$

<u>Shear:</u>

$$C = \phi \times V_n = 109.523\,k$$

$$D = V_{DL} = 37.15\,k$$

$$L = V_{LL} = 36.6687\,k$$

For the Operating Level rating:

$$RF = \frac{109.523\,k - (1.3 \times 37.15\,k)}{1.3 \times 36.6687\,k} = 1.28$$

For the Inventory Level rating:

$$RF = \frac{109.523\,k - (1.3 \times 37.15\,k)}{2.17 \times 36.6687\,k} = 0.77$$

LFR method: Interior Beam

Load Rating for the interior beam at 2/3 of the mid-span length using the HS-20 design vehicle.

Positive Moment:

$$C = \phi \times M_n^- = 826.6705 k - ft$$

$$D = M_{DL}^- = 66.81 k - ft$$

$$L = M_{LL}^- = 107.318 k - ft$$

For the Operating Level rating:

$$RF = \frac{826.6705 k - ft - (1.3 \times 66.81 k - ft)}{1.3 \times 107.318 k - ft} = 5.30$$

For the Inventory Level rating:

$$RF = \frac{826.6705 k - ft - (1.3 \times 66.81 k - ft)}{2.17 \times 107.318 k - ft} = 3.17$$

Shear:

$$C = \phi \times V_n = 64.564 k$$

$$D = V_{DL} = 20.22 k$$

From **Error! Reference source not found.**,

$$L = V_{LL} = 28.5218 k$$

For the Operating Level rating:

$$RF = \frac{64.564 k - (1.3 \times 20.22 k)}{1.3 \times 28.5218 k} = 1.03$$

For the Inventory Level rating:

$$RF = \frac{64.564 k - (1.3 \times 20.22 k)}{2.17 \times 28.5218 k} = 0.62$$

Load and Resistance Factor Rating (LRFR) equation

LRFD:

$$RF = \frac{C - \gamma_D \times D}{\gamma_L \times L}$$

Where:

$$C = Capacity\ of\ the\ beam$$
$$\gamma_D = Dead\ Load\ Factor(1.25\ for\ Operating\ and\ Inventory\ on\ both\ Legal\ Loads\ and\ HL-93)$$
$$D = Dead\ Load$$
$$\gamma_L = LiveLoadFactor \begin{pmatrix} 1.35\ for\ Operating\ on\ HL-93 \\ 1.75\ for\ Inventory\ on\ HL-93 \\ 1.80\ on\ Legal\ Loads \end{pmatrix}$$
$$L = Live\ Load$$

LRFR method: Exterior Beam

Load Rating for the exterior beam at the edge using the HL-93 design vehicle.

HL-93

Negative Moment:

$$C = M_n^- = 656.689\, k - ft$$

Applying the conditions and reduction factors

$$C = \phi_c \phi_s \phi \times M_n^- = 0.85 \times 1.0 \times 0.9 \times 656.689\, k - ft = 502.37k - ft$$

$$D = M_{DL}^- = 354.28\, k - ft$$

$$L = M_{LL}^- = 399.22\, k - ft$$

For the Operating Level rating:

$$RF = \frac{502.37\, k - ft - (1.25 \times 354.28\, k - ft)}{1.35 \times 399.22\, k - ft} = 0.11$$

For the Inventory Level rating:

$$RF = \frac{502.37k - ft - (1.25 \times 354.28\,k - ft)}{1.75 \times 399.22\,k - ft} = 0.09$$

Shear:,

$$C = V_n = 119.209\,k$$

Applying the conditions and reduction factors

$$C = \phi_c \phi_s \phi \times V_n = 0.85 \times 1.0 \times 0.9 \times 119.209k = 91.20\,k$$

$$D = V_{DL} = 33.68\,k$$

$$L = V_{LL} = 38.07\,k$$

For the Operating Level rating:

$$RF = \frac{91.20\,k - (1.25 \times 33.68\,k)}{1.35 \times 38.07\,k} = 0.96$$

For the Inventory Level rating:

$$RF = \frac{91.20\,k - (1.25 \times 33.68\,k)}{1.75 \times 38.07\,k} = 0.74$$

Since the HL-93 load rating is less than 1 for the negative moment, it is necessary perform the analysis using the Legal Load vehicles.

Using the Type 3 (Legal Load): Exterior Beam

Negative Moment:

$$C = M_n^- = 656.689\,k - ft$$

Applying the conditions and reduction factors

$$C = \phi_c \phi_s \phi \times M_n^- = 0.85 \times 1.0 \times 0.9 \times 656.689\,k - ft = 502.37k - ft$$

$$D = M_{DL}^- = 354.28k - ft$$

$L = M_{LL}^{-} = 201.56k - ft$

$$RF = \frac{502.37k - ft - (1.25 \times 354.28k - ft)}{1.80 \times 201.56k - ft} = 0.16$$

Shear:

$C = V_n = 119.209k$

Applying the conditions and reduction factors

$C = \phi_c \phi_s \phi \times V_n = 0.85 \times 1.0 \times 0.9 \times 119.209k = 91.20k$

$D = V_{DL} = 33.68k$

$L = V_{LL} = 19.8636k$

$$RF = \frac{91.20k - (1.25 \times 33.68k)}{1.80 \times 19.8636k} = 1.37$$

LRFR method: Exterior Beam

Load Rating for the exterior beam at the Mid-span using the HL-93 design vehicle.

HL-93

Positive Moment:

$C = M_n^{+} = 261.777k - ft$

Applying the conditions and reduction factors

$C = \phi_c \phi_s \phi \times M_n = 0.85 \times 1.0 \times 0.9 \times 261.777k - ft = 200.26k - ft$

$D = M_{DL}^{+} = 69.10k - ft$

$L = M_{LL}^{-} = 127.66k - ft$

For the Operating Level rating:

$$RF = \frac{200.26k - ft - (1.25 \times 69.10k - ft)}{1.35 \times 127.66k - ft} = 0.66$$

For the Inventory Level rating:

$$RF = \frac{200.26\,k - ft - (1.25 \times 69.10\,k - ft)}{1.75 \times 127.66\,k - ft} = 0.51$$

Since the HL-93 load rating is less than 1 for the positive moment, it is necessary perform the analysis using the Legal Load vehicles.

Using the Type 3 (Legal Load):

Positive Moment:

$C = M_n^+ = 261.777\,k - ft$

Applying the conditions and reduction factors

$C = \phi_c \phi_s \phi \times M_n = 0.85 \times 1.0 \times 0.9 \times 261.777k - ft = 200.26\,k - ft$

$D = M_{DL}^+ = 69.10\,k - ft$

$L = M_{LL}^- = 73.1269\,k - ft$

$$RF = \frac{200.26\,k - ft - (1.25 \times 69.10\,k - ft)}{1.80 \times 73.1269\,k - ft} = 0.87$$

LRFR method: Exterior Beam

Load Rating for the exterior beam at 1/3 of the mid-span length using the HL-93 design vehicle.

HL-93:

Negative Moment:

$C = M_n^- = 399.83\,k - ft$

Applying the conditions and reduction factors

$C = \phi_c \phi_s \phi \times M_n = 0.85 \times 1.0 \times 0.9 \times 399.83k - ft = 305.23\,k - ft$

$D = M_{DL}^- = 164.88\,k - ft$

$L = M_{LL}^- = 212.14\,k - ft$

For the Operating Level rating:

$$RF = \frac{305.23\,k - ft - (1.25 \times 164.88\,k - ft)}{1.35 \times 212.14\,k - ft} = 0.35$$

For the Inventory Level rating:

$$RF = \frac{305.23k - ft - (1.25 \times 164.88\,k - ft)}{1.75 \times 212.14\,k - ft} = 0.27$$

<u>Shear:</u>

$$C = V_n = 74.557\,k$$

Applying the conditions and reduction factors

$$C = \phi_c \phi_s \phi \times V_n = 0.85 \times 1.0 \times 0.9 \times 74.557k = 57.04\,k$$

$$D = V_{DL} = 21.42\,k$$

$$L = V_{LL} = 30.02\,k$$

For the Operating Level rating:

$$RF = \frac{57.04k - (1.25 \times 21.42\,k)}{1.35 \times 30.02k} = 0.75$$

For the Inventory Level rating:

$$RF = \frac{57.04\,k - (1.25 \times 21.42\,k)}{1.75 \times 30.02k} = 0.58$$

Since the HL-93 load rating is less than 1 for the negative moment, it is necessary perform the analysis using the Legal Load vehicles.

Using the Type 3 (Legal Load):

<u>Negative Moment:</u>

$$C = M_n^- = 399.83\,k - ft$$

Applying the conditions and reduction factors

$$C = \phi_c \phi_s \phi \times M_n = 0.85 \times 1.0 \times 0.9 \times 399.83k - ft = 305.23\,k - ft$$

$$D = M_{DL}^- = 164.88\,k - ft$$

$$L = M_{LL}^- = 115.52k - ft$$

$$RF = \frac{305.23k - ft - (1.25 \times 164.88k - ft)}{1.80 \times 115.52k - ft} = 0.48$$

Shear:

$C = V_n = 74.557k$

Applying the conditions and reduction factors

$C = \phi_c \phi_s \phi \times V_n = 0.85 \times 1.0 \times 0.9 \times 74.557 = 57.04k$,

$D = V_{DL} = 21.42k$

$L = V_{LL} = 16.7205k$

$$RF = \frac{57.05k - (1.25 \times 21.42k)}{1.80 \times 16.7205k} = 1.00$$

LRFR method: Exterior Beam

Load Rating for the exterior beam at 2/3 of the mid-span length using the HL-93 design vehicle.

HL-93:

Positive Moment:

$C = M_n^+ = 317.011k - ft$

Applying the conditions and reduction factors

$C = \phi_c \phi_s \phi \times M_n = 0.85 \times 1.0 \times 0.9 \times 317.011k - ft = 242.51k - ft$

$D = M_{DL}^+ = 40.11k - ft$

$L = M_{LL}^+ = 79.94k - ft$

For the Operating Level rating:

$$RF = \frac{242.51k - ft - (1.25 \times 40.11k - ft)}{1.35 \times 79.94k - ft} = 1.78$$

For the Inventory Level rating:

$$RF = \frac{242.51k - ft - (1.25 \times 40.11k - ft)}{1.75 \times 79.94k - ft} = 1.38$$

<u>Shear:</u>

$$C = V_n = 36.935k$$

Applying the conditions and reduction factors

$$C = \phi_c \phi_s \phi \times V_n = 0.85 \times 1.0 \times 0.9 \times 36.935k = 28.255k$$

$$D = V_{DL} = 11.89k$$

$$L = V_{LL} = 22.16k$$

For the Operating Level rating:

$$RF = \frac{28.25k - (1.25 \times 11.89k)}{1.35 \times 22.16k} = 0.45$$

For the Inventory Level rating:

$$RF = \frac{28.25k - (1.25 \times 11.89k)}{1.75 \times 22.16k} = 0.35$$

Since the HL-93 load rating is less than 1 for the positive moment, it is necessary to perform the analysis using the Legal Load vehicles.

Using the Type 3 (Legal Load): Exterior Beam

<u>Positive Moment:</u>

$$C = M_n^+ = 317.011k - ft$$

Applying the conditions and reduction factors

$$C = \phi_c \phi_s \phi \times M_n = 0.85 \times 1.0 \times 0.9 \times 317.011k - ft = 242.51k - ft$$

$$D = M_{DL}^+ = 40.11k - ft$$

$$L = M_{LL}^{+} = 44.5589\,k - ft$$

$$RF = \frac{242.51\,k - ft - (1.25 \times 40.11\,k - ft)}{1.80 \times 44.5589\,k - ft} = 2.40$$

<u>Shear:</u>

$$C = V_n = 36.935\,k$$

Applying the conditions and reduction factors

$$C = \phi_c \phi_s \phi \times V_n = 0.85 \times 1.0 \times 0.9 \times 36.935k = 28.255k$$

$$D = V_{DL} = 11.89\,k$$

$$L = V_{LL} = 16.4718\,k$$

$$RF = \frac{28.255\,k - (1.25 \times 11.89\,k)}{1.80 \times 16.4718k} = 0.45$$

LRFR method: Interior Beam

Load Rating for the interior beam at the edge using the HL-93 design vehicle.

HL-93

<u>Negative Moment:</u>

$$C = M_n^{-} = 1166.84\,k - ft$$

Applying the conditions and reduction factors

$$C = \phi_c \phi_s \phi \times M_n = 0.85 \times 1.0 \times 0.9 \times 1166.84k - ft = 892.633k - ft$$

$$D = M_{DL}^{-} = 618.49\,k - ft$$

$$L = M_{LL}^{-} = 676.93\,k - ft$$

For the Operating Level rating:

$$RF = \frac{892.633\,k - ft - (1.25 \times 618.49\,k - ft)}{1.35 \times 676.93\,k - ft} = 0.13$$

For the Inventory Level rating:

$$RF = \frac{892.633\,k - ft - (1.25 \times 618.49\,k - ft)}{1.75 \times 676.93\,k - ft} = 0.10$$

<u>Shear:</u>

$$C = V_n = 201.902k$$

Applying the conditions and reduction factors

$$C = \phi_c \phi_s \phi \times V_n = 0.85 \times 1.0 \times 0.9 \times 201.902k = 154.46k$$

$$D = V_{DL} = 59.26k$$

$$L = V_{LL} = 64.56\,k$$

For the Operating Level rating:

$$RF = \frac{154.46\,k - (1.25 \times 59.26\,k)}{1.35 \times 64.56\,k} = 0.92$$

For the Inventory Level rating:

$$RF = \frac{154.46\,k - (1.25 \times 59.26\,k)}{1.75 \times 64.56\,k} = 0.71$$

Since the HL-93 load rating is less than 1 for the negative moment, it is necessary to perform the analysis using the Legal Load vehicles.

Using the Type 3 (Legal Load): Interior Beam

<u>Negative Moment:</u>

$$C = M_n^- = 1166.84\,k - ft$$

Applying the conditions and reduction factors

$$C = \phi_c \phi_s \phi \times M_n = 0.85 \times 1.0 \times 0.9 \times 1166.84k - ft = 892.633k - ft$$

$$D = M_{DL}^- = 618.49\,k - ft$$

$L = M_{LL}^{-} = 341.78k - ft$

$$RF = \frac{892.633k - ft - (1.25 \times 618.49k - ft)}{1.80 \times 341.78k - ft} = 0.19$$

Shear:

$C = V_n = 201.902k$

Applying the conditions and reduction factors

$C = \phi_c \phi_s \phi \times V_n = 0.85 \times 1.0 \times 0.9 \times 201.902k = 154.46k$

$D = V_{DL} = 59.26k$

$L = V_{LL} = 33.6818k$

$$RF = \frac{154.46k - (1.25 \times 59.26k)}{1.80 \times 33.6818k} = 1.33$$

LRFR method: Interior Beam

Load Rating for the interior beam at the mid-span using the HL-93 design vehicle.

HL-93

Positive Moment:

$C = M_n^{+} = 671.688k - ft$

Applying the conditions and reduction factors

$C = \phi_c \phi_s \phi \times M_n = 0.85 \times 1.0 \times 0.9 \times 671.688k - ft = 513.841k - ft$

$D = M_{DL}^{+} = 114.34k - ft$

$L = M_{LL}^{-} = 216.46k - ft$

For the Operating Level rating:

$$RF = \frac{513.841k - ft - (1.25 \times 114.34k - ft)}{1.35 \times 216.46k - ft} = 1.27$$

For the Inventory Level rating:

$$RF = \frac{513.841k - ft - (1.25 \times 114.34k - ft)}{1.75 \times 216.46k - ft} = 0.98$$

Since the HL-93 load rating is less than 1 for the positive moment, it is necessary to perform the analysis using the Legal Load vehicles.

Using the Type 3 (Legal Load): Interior Beam

Positive Moment:

$$C = M_n^+ = 671.688k - ft$$

Applying the conditions and reduction factors

$$C = \phi_c \phi_s \phi \times M_n = 0.85 \times 1.0 \times 0.9 \times 671.688k - ft = 513.841k - ft$$

$$D = M_{DL}^+ = 114.34k - ft$$

$$L = M_{LL}^- = 123.998k - ft$$

$$RF = \frac{513.841k - ft - (1.25 \times 114.34k - ft)}{1.80 \times 123.998k - ft} = 1.66$$

LRFR method: Interior Beam

Load Rating for the interior beam at 1/3 of the mid-span length using the HL-93 design vehicle.

Negative Moment:

$$C = M_n^- = 726.178k - ft$$

Applying the conditions and reduction factors

$$C = \phi_c \phi_s \phi \times M_n = 0.85 \times 1.0 \times 0.9 \times 726.178k - ft = 555.526k - ft$$

$$D = M_{DL}^{-} = 288.44\,k - ft$$

$$L = M_{LL}^{-} = 359.71\,k - ft$$

For the Operating Level rating:

$$RF = \frac{555.53k - ft - (1.25 \times 288.44\,k - ft)}{1.35 \times 359.71\,k - ft} = 0.40$$

For the Inventory Level rating:

$$RF = \frac{555.53\,k - ft - (1.25 \times 288.44\,k - ft)}{1.75 \times 359.71\,k - ft} = 0.31$$

<u>Shear:</u>

$$C = V_n = 128.771k$$

Applying the conditions and reduction factors

$$C = \phi_c \phi_s \phi \times V_n = 0.85 \times 1.0 \times 0.9 \times 128.771k = 98.51k$$

$$D = V_{DL} = 37.15k$$

$$L = V_{LL} = 50.91\,k$$

For the Operating Level rating:

$$RF = \frac{98.51\,k - (1.25 \times 37.15\,k)}{1.35 \times 50.91\,k} = 0.76$$

For the Inventory Level rating:

$$RF = \frac{98.51\,k - (1.25 \times 37.15\,k)}{1.75 \times 50.91\,k} = 0.58$$

Since the HL-93 load rating is less than 1 for the negative moment, it is necessary to perform the analysis using the Legal Load vehicles.

Using the Type 3 (Legal Load): Interior Beam

Negative Moment:

$$C = M_n^- = 726.178\,k - ft$$

Applying the conditions and reduction factors

$$C = \phi_c \phi_s \phi \times M_n = 0.85 \times 1.0 \times 0.9 \times 726.178k - ft = 555.526k - ft$$

$$D = M_{DL}^- = 288.44\,k - ft$$

$$L = M_{LL}^- = 195.89\,k - ft$$

$$RF = \frac{555.526\,k - ft - (1.25 \times 288.44\,k - ft)}{1.80 \times 195.89k - ft} = 0.55$$

Shear:

$$C = V_n = 128.771k$$

Applying the conditions and reduction factors

$$C = \phi_c \phi_s \phi \times V_n = 0.85 \times 1.0 \times 0.9 \times 128.771k = 98.51k$$

$$D = V_{DL} = 37.15\,k$$

$$L = V_{LL} = 28.3521k$$

$$RF = \frac{98.15\,k - (1.25 \times 37.15\,k)}{1.80 \times 28.3521\,k} = 1..02$$

LRFR method: Interior Beam

Load Rating for the interior beam at 2/3 of the mid-span length using the HL-93 design vehicle.

HL-93:

<u>Positive Moment:</u>

$$C = M_n^+ = 918.522\,k - ft$$

Applying the conditions and reduction factors

$$C = \phi_c \phi_s \phi \times M_n = 0.85 \times 1.0 \times 0.9 \times 918.552k - ft = 702.67k - ft$$

$$D = M_{DL}^+ = 66.81k - ft$$

$$L = M_{LL}^+ = 135.55k - ft$$

For the Operating Level rating:

$$RF = \frac{702.67\,k - ft - (1.25 \times 66.81\,k - ft)}{1.35 \times 135.55\,k - ft} = 3.38$$

For the Inventory Level rating:

$$RF = \frac{702.67\,k - ft - (1.25 \times 66.81\,k - ft)}{1.75 \times 135.55\,k - ft} = 2.61$$

Shear:

$C = V_n = 75.911k$

Applying the conditions and reduction factors

$C = \phi_c \phi_s \phi \times V_n = 0.85 \times 1.0 \times 0.9 \times 75.911k = 58.07k$

$D = V_{DL} = 20.22\,k$

$L = V_{LL} = 37.59\,k$

For the Operating Level rating:

$$RF = \frac{58.07\,k - (1.25 \times 20.22\,k)}{1.35 \times 37.59\,k} = 0.65$$

For the Inventory Level rating:

$$RF = \frac{58.07\,k - (1.25 \times 20.22\,k)}{1.75 \times 37.59\,k} = 0.50$$

Since the HL-93 load rating is less than 1 for the positive moment, it is necessary to perform the analysis using the Legal Load vehicles.

Using the Type 3 (Legal Load): Interior Beam

Positive Moment:

$$C = M_n^+ = 918.522\, k - ft$$

Applying the conditions and reduction factors

$$C = \phi_c \phi_s \phi \times M_n = 0.85 \times 1.0 \times 0.9 \times 918.552k - ft = 702.67k - ft$$

$$D = M_{DL}^+ = 66.81\, k - ft$$

$$L = M_{LL}^+ = 75.5564\, k - ft$$

$$RF = \frac{702.67\, k - ft - (1.25 \times 66.81\, k - ft)}{1.80 \times 75.5564\, k - ft} = 4.55$$

Shear:

From **Error! Reference source not found.**,

$$C = V_n = 75.911\, k$$

Applying the conditions and reduction factors

$$C = \phi_c \phi_s \phi \times V_n = 0.85 \times 1.0 \times 0.9 \times 75.911k = 58.07k$$

$$D = V_{DL} = 20.22\, k$$

$$L = V_{LL} = 22.8436\, k$$

$$RF = \frac{58.07\, k - (1.25 \times 20.22\, k)}{1.80 \times 22.8436\, k} = 0.80$$

APPENDIX E BRIDGE DESIGN DRAWINGS

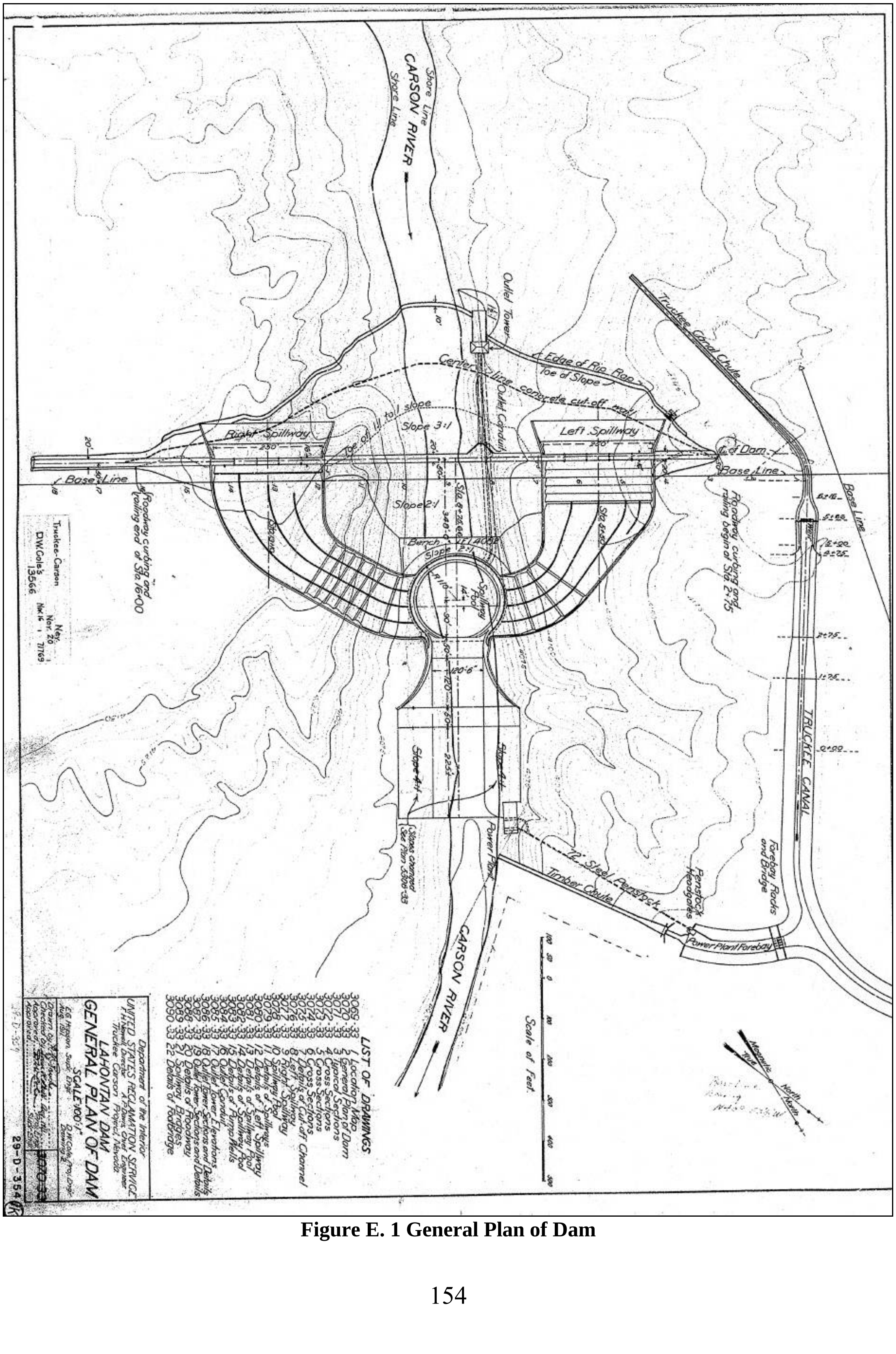

Figure E. 1 General Plan of Dam

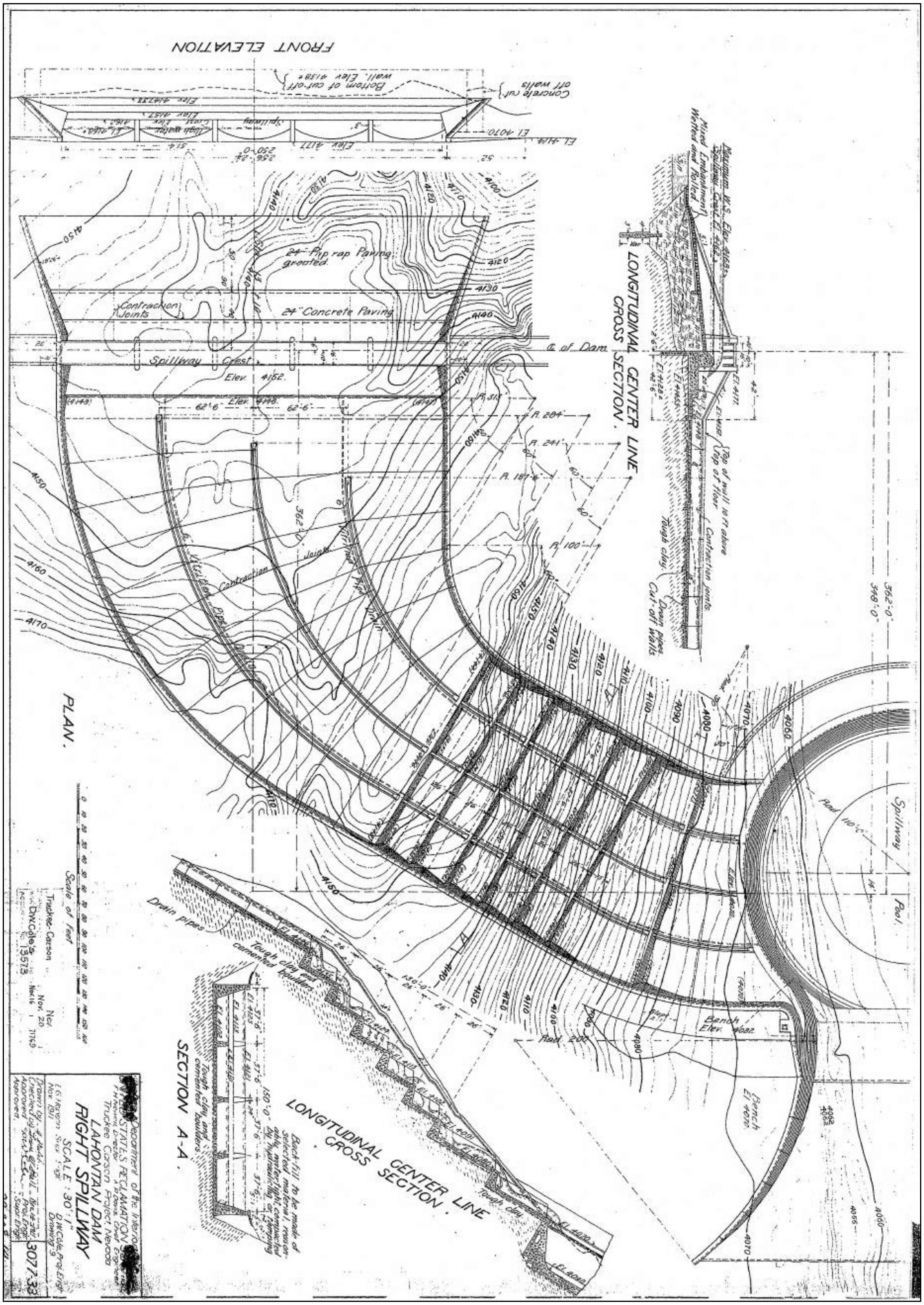

Figure E. 2 Lahontan Dam Right Spillway

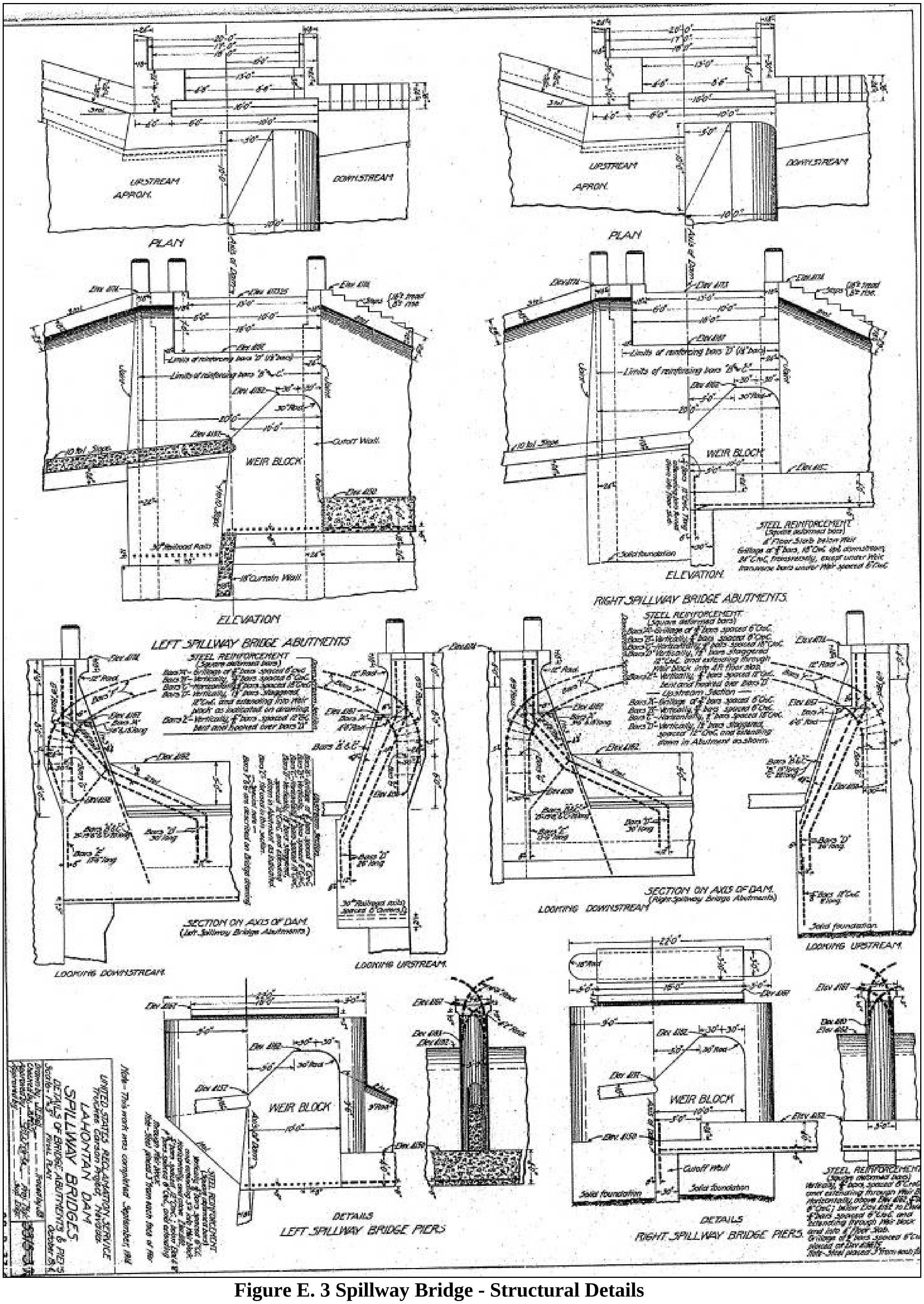

Figure E. 3 Spillway Bridge - Structural Details

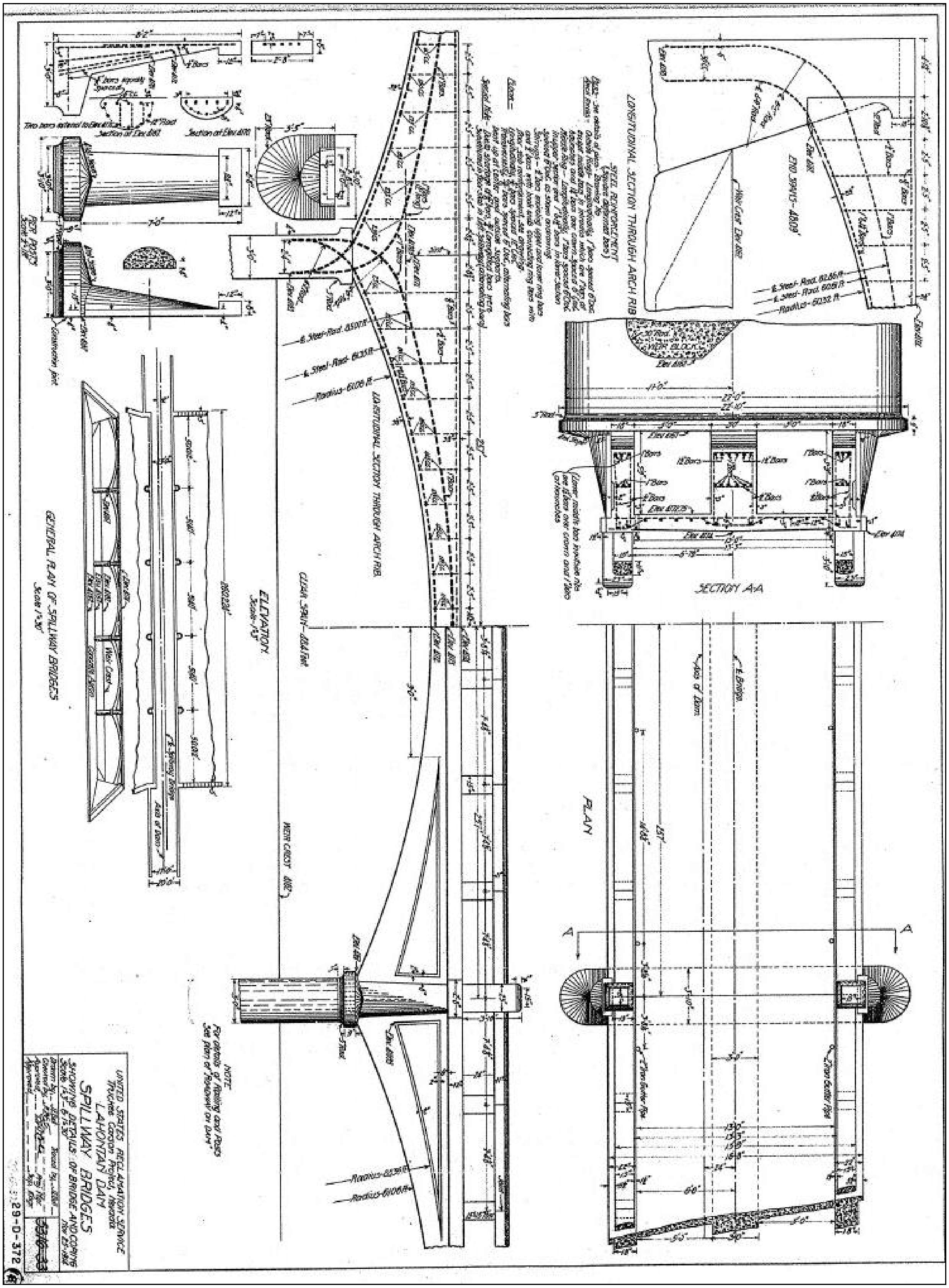

Figure E. 4 Spillway Bridge - Structural Details II